This is to certify that the
dissertation entitled

The Analysis Of Dynamic Stress And Plastic Wave Propagation In The Taylor Impact Test

presented by

Gong Song

has been accepted towards fulfillment
of the requirements for the

Ph.D degree in Mechanical Engineering

Dr. Lin
Major Professor's Signature

Feb. 10, 2006
Date

The Analysis Of Dynamic Stress And Plastic Wave Propagation In The Taylor Impact Test

By

Gong Song

A DISSERTATION

Submitted to
Michigan State University
in partial fulfillment of the requirements
for the degree of

DOCTOR OF PHILOSOPHY

Department of Mechanical Engineering

2006

ABSTRACT

The Analysis of Dynamic Stress and Plastic Wave Propagation in the Taylor Impact Test

By

Gong Song

This thesis investigates the propagation of plastic wave in a projectile of the Taylor Impact Test. The theories of plastic wave propagation, RI theory and RD theory, are used to analyze the Taylor Impact Test. A complete method (theoretical investigation, experimental and measurement and numerical analysis) of computing the dynamic stresses in the projectile is developed. The yielding dynamic stress and the shape curves of the projectile after impact are used to verify our theoretical investigation. Three phases model of the Taylor Impact Test, a new constitutive equation (RI theory) and the Modified Malvern model (RD theory) in the Taylor Impact Test are proposed. The determination of the maximum dynamic stress and the characteristics of the plastic wave propagation are included.

In order to verify the proposed constitutive equation and model, the Taylor Impact Tests are performed with three different materials (Aluminum, Copper and Steel) and impact velocities, and numerical analysis is carried out. The experimental and numerical analysis results indicate that the conclusions from our theoretical investigation match experimental and numerical analysis results well.

Dedicated to my father, mother,

wife Xiao-Cui and son Guan-Long

ACKNOWLEDGEMENT

I would like to acknowledge my sincere thanks to all my committee members for their serving on my committee and making contribution to this investigation. In particular, I would like to express my deepest gratitude to Prof. D. Liu who advises me during the whole course of this investigation. Also, I would like to express my deepest thanks to Professor Zhou, Dr.Tsai, Professor Kwon and Professor Lee from whom I have received valuable advice and suggestions. The pioneers in the area of plastic wave propagation are gratefully acknowledged for their prominent theoretical work and excellent experimental results. I wish to thank many professors of the University of Alabama who helped me in my student career in one way or another. Finally, I want to express my deep thanks to everyone who has helped my in my study and life.

TABLE OF CONTENTS

LIST OF TABLE

LIST OF FIGURES

CHAPTER 1

INTRODUCTION

Impact dynamics is one important area in engineering practice. It covers subjects from aerospace and automotive crashworthiness to human body health and military applications.

In aerospace, research in impact dynamics is performed to develop techniques capable of predicting the dynamic behavior of aerospace structures and to devise advanced control techniques aimed to improve the performance of the structures. There is currently an increasing demand for dynamic, stress analyses; material behavior; and constitutive equations of metal materials. For example, rotor containment design is not yet an exact science and it currently depends mainly on empirical methods and extensive testing. The requirement to produce a safe design while at the same time reducing development cost and time in order to be competitive in the aero-engine market is of paramount importance. When engineers use the supercomputer to simulate non-linear numerical modeling of an aircraft frame to investigate the distribution of the dynamic stress in the frame, this work needs the help of impact dynamics.

In the automotive industry, because of the rapid growth of crashworthiness as a stand-along, engineering subject; there is a need for impact dynamics devoted to the crash behavior of structures and materials, body structures, and energy-absorbing systems subject to sudden dynamic loading. This includes side-impact protection, analysis of frontal collisions, structural crashworthiness simulation of the rear-end collision of small cars, prediction of energy absorption capability of composite materials, and more.

In bio-mechanics, people use the research results of impact dynamics to investigate the fracture in long bones, head injury and protection, injury mechanisms and criteria for the human feet and ankle under axial impact loads, and the simulation of head/neck dynamic responses under impact loading. These research activities are now called impact bio-mechanics.

Another application of impact dynamics is in the military. The modern battlefield is an increasingly dynamic and complex environment that requires weapons with increased agility and speed with strong ability to penetrate armor plate. These requirements provide challenges to the warhead or penetrator design. One challenge is that the engagement conditions translate to high, strain rates in the order of 10^6 1/s. In such an environment, the ability for a material to not fracture is challenged. In the case of a warhead/ penetrator, its ability to perform its function (kill the target) is compromised if a material fails. In order to design such a warhead/penetrator with material that can maintain its integrity under such loading conditions, the failure process and dynamic stress distribution, and the dynamic yield strength of a material must be understood. This is exactly the task of impact dynamics.

1.1 Literature Reviews

1.1.1 Development of Theories

A. Strain Rate Independent Theory (RI Theory)

In the 1930s, as one of the first pioneers in the study of plastic wave propagation, Donnell [1] introduced the first scheme for treating the wave propagation in a media beyond the Hooke's law. Although the focus of Donnell's research was not directly aimed at plastic wave propagation, a formula expressing the velocity of wave propagation

was developed

$$C_p = \sqrt{\frac{1}{\rho}\frac{d\sigma}{d\varepsilon}} \qquad (1.1)$$

where σ is stress, ε is strain, ρ is density, and C_p is the velocity of a plastic wave.

The systematic studies of plastic, wave propagation from the aspects of theory and testing of metallic materials, such as copper and aluminum, began in 1940. The studies were motivated in light of developments of armor-piercing shells and plates, and were performed independently by von Karman and Duwez [2], Taylor [3] and Rakhmatulin [4]. The difference among their studies was essentially based on the choice of coordinate systems. Von Karman used a Lagrangian coordinate system while Taylor used an Eulerian, coordinate system. Today their studies are known as the classical plastic wave propagation theory by some researchers or the strain rate independent (RI) theory by most researchers.

There were two assumptions in the RI theory.

1) The stress σ was only a function of strain ε, i.e. $\sigma = \sigma(\varepsilon)$.

2) The curve of stress versus strain was concave toward the strain.

Under these assumptions, the following one-dimensional, wave equation was formulated:

$$\rho\frac{\partial^2 u}{\partial t^2} = \frac{d\sigma}{d\varepsilon}\frac{\partial^2 u}{\partial x^2} \qquad (1.2)$$

where $u = u(x,t)$ is displacement, x is coordinate and t is time.

After the strain rate independent (RI) theory was proposed, some studies were conducted by Duwez and Clark [5], Campell [6], Johnson, Wood and Clark [7] from 1946 through 1953 to further examine the plastic wave propagation. Their studies could

be divided into two groups. The first group verified the existence of the plastic wave through the comparison between theoretical analyses and experimental investigations. The second group investigated the physical nature of plastic wave propagation, as in the relationships of wave velocity vs. time and stress vs. time. All these studies concluded that plastic wave propagation did exist and the RI theory was basically correct, although some predictions from the RI theory did not totally match with the experimental results at the impacted end.

B. Strain Rate Dependent Theory (RD Theory)

By the time the RI theory was proposed, the strain rate dependent (RD) theory though not aiming at plastic wave propagation had already been established. In 1909, Ludwik [8] proposed a logarithmic function among the stress, strain, and strain rate

$$\sigma = \sigma_1(\varepsilon) + K \ln \dot{\varepsilon}$$

where $\sigma_1(\varepsilon)$ is the stress of strain ε when strain rate $\dot{\varepsilon}$ is unity. The factor K was a function of strain. Prandtl [8] reached the same conclusion with the use of a physical theory of plastic flow. Meanwhile, a power law was proposed by Prandtl

$$\sigma = \sigma_1(\varepsilon)\dot{\varepsilon}^n$$

where n could be a function of stress.

In 1950, Sokolovsky [9] and Malvern [10] also proposed the strain rate dependent theory for studying plastic wave propagation. They suggested that the effects of visco-plasticity should be considered in the study of plastic wave propagation. Their theories could be expressed by the following stress, strain, and strain-rate relation

$$\sigma = \sigma(\varepsilon, \dot{\varepsilon})$$

Based on Newton's second law, the equation for plastic wave propagation could be written as

$$\rho\frac{\partial^2 u}{\partial t^2}=\frac{\partial\sigma}{\partial\varepsilon}\frac{\partial^2 u}{\partial x^2}+\frac{\partial\sigma}{\partial\dot{\varepsilon}}\frac{\partial^3 u}{\partial x^2\partial t} \tag{1.3}$$

where $\dot{\varepsilon}$ is strain rate.

Malvern proposed the following stress-strain rate relation:

$$\sigma=\sigma_0+k\dot{\varepsilon} \tag{1.4}$$

where σ_0 represents for the static stress-strain relation and k is a constant. With the use of the equation of motion and the strain-displacement relation

$$\frac{\partial\sigma}{\partial x}=\rho\frac{\partial v}{\partial t} \tag{1.5}$$

$$\frac{\partial\sigma}{\partial x}=\rho\frac{\partial v}{\partial t} \tag{1.6}$$

where v is particle velocity, the following constitutive relationship could be obtained:

$$E\dot{\varepsilon}=\dot{\sigma}+k[\sigma-f(\varepsilon)] \tag{1.7}$$

where E is Young's modulus, $f(\varepsilon)$ is a strain function obtained from a hardened aluminum alloy, $\dot{\varepsilon}$ is strain rate, and $\dot{\sigma}$ is stress rate.

Sokolovsky proposed the following stress-strain-strain-rate relation to model dynamic behavior of materials:

$$\sigma=\sigma(\varepsilon)+\ln(1+b\dot{\varepsilon}) \tag{1.8}$$

where $\sigma(\varepsilon)$ is a quasi-static stress-strain relation, dot denotes time and b is a constant. Substituting Equation (1.8) into Equations (1.5) and (1.6), yields

$$E\dot{\varepsilon}=\dot{\sigma}+g(\sigma,\varepsilon) \tag{1.9}$$

where $g(\sigma,\varepsilon)$ is a stress-strain function.

Although the two types of theories, the RI theory and the RD theory, were

proposed for studying plastic wave propagation, either the RI theory or the RD theory alone could not explain all experimental results. In fact, the experimental results seemed to indicate that strain rate should not be neglected completely and there existed a strain plateau around the impacted surface [9,10,11]. The RD theory could not explain the existence of the plateau, while RI theory could. The RI theory agreed with the experimental results in the region away from the impact surface while the RD theory did not.

C. Plasticity-Viscoplasticity Theory

From 1962 through 1968, Simmons, Hauser and Dorn [18], and Lubliner and Valathur [19] proposed a generalized plasticity-viscoplasticity theory. According to the theory, the strain rate independent theory (RI) could be classified as the plasticity theory and the strain rate dependent theory (RD) could be classified as the viscoplasticity theory. That is, the strain rate independent theory (RI) did not consider the viscous effect of the materials while the strain rate dependent theory (RD) did. For viscid ductile materials, the RD theory agreed with experimental results better than the RI theory. For less viscid ductile materials, the RI theory agreed with experimental results better than the RD theory. This plasticity-viscoplasticity theory was supported by the experiments from Kolsky and Dough [14] and Lindholm [15]. For pure aluminum and pure copper, the RD theory agreed with the experiments better than the RI theory. For aluminum alloys, the RI theory agreed with the experimental results better than the RD theory.

A model was proposed by Lublinear [19] as follows:

$$\dot{\varepsilon} = p(\sigma,\varepsilon)\dot{\sigma} + q(\sigma,\varepsilon) \qquad (1.10)$$

where the function $p(\sigma,\varepsilon)$ and $q(\sigma,\varepsilon)$ governed the instantaneous and non-instantaneous response respectively.

D. Stress-Strain Relations

The relationship between the stress and the strain in the impacted materials was always a primary interest in the study of plastic wave propagation. In 1968, Bell [20] proposed the following stress-strain relation based on nearly 600 experiments covering 2200 individual tests and 27 types of solids reported in the literature over a period of 45 years

$$\sigma = \left(\frac{2}{3}\right)^{\frac{r}{2}} \mu(0) B_0 \left(1 - \frac{T}{T_m}\right) (\varepsilon - \varepsilon_b)^{\frac{1}{2}}$$

where B_0 is a dimensionless universal constant, i.e. $B_0 = 0.028$, $\mu(0)$ is the shear modulus at zero point; $r = 1, 2, 3, \ldots$ is the finite deformation mode, and ε_b is the parabola intercept upon the strain abscissa of the particular deformation mode of interest ($\varepsilon_b = 0$ for the initial finite deformation mode). T is testing temperature and T_m is melting temperature.

1.1.2 Development of Experimental Techniques

A. Experimental Measurements

In order to further identify the above usefulness of the RI theory and the RD theory, Bell [11--13] developed a diffraction grating method to measure the strain in rods made of aluminum and copper impacted by a constant velocity. His findings could be summarized as follows:

1) The RI theory could not completely agree with the experimental results in the zone close to the impact end. However, it could be applied to the rod in the zone away from the impact end. On the contrary, the RD theory could be applied to the rod in the zone close to the impact end but away from it.

2) After impact, a non-dispersive shock wave was inaugurated in a location approximately equal to one-quarter of the diameter of the rods and then developed into a dispersive, plastic-wave front.

3) The dispersive, plastic wave developed into two wave fronts. The first wave front was associated with the deviatoric component of the dynamic stress and was called the shear wave. The second wave front was associated with the hydrostatic component of the dynamic stress and was called the longitudinal wave. The longitudinal wave was developed much more slowly than the shear wave.

4) The deviatoric stress was about 2/3 of the dynamic stress while the hydrostatic stress was about 1/3 of the dynamic stress.

5) The initial non-dispersive shock wave first developed the shear wave and then the longitudinal wave. The shear wave and the longitudinal wave each contained approximately one-half the initial kinetic energy.

6) The von Karman critical velocity was found to be about 48.5 ft/sec for aluminum and 73 ft/sec for copper.

In 1964, Kolsky and Dough [14] studied wave propagation in short bars made of pure aluminum, pure copper, and an aluminum alloy. They found no appreciable strain rate dependence for the aluminum alloy. For pure aluminum and pure copper, the strain rate dependent theory had reasonable agreement. In 1964, Lindholm [15], in a series of tests in which short specimens (aspect ratio of length to diameter ranging from 0.2 to 2.0) made of pure aluminum were subjected to strain cycling at various strain rates, showed that the RD theory agreed better with the experimental results than the RI theory. These experiments indicated that both the aspect ratio and material characteristics played important roles in the strain rate effect.

Malvern and Huffington [16], Gillich and Ewing [17], and Bell [13] conducted many experiments attempting to directly measure the profiles of strain vs. time and velocity vs. time. They found that the velocity of the plastic wave propagation was a constant for each strain and the strain rate did not affect the velocity of plastic wave propagation very much. That is to say, the influence of strain rate could be neglected in the zone away from the impact end.

B. Split Hopkinson's Pressure Bar and Plate Impact

Split Hopkinson's pressure bars (SHPB) were used in the studying of plastic wave propagation investigation. Karnes [21] and Bertholf and Karnes [22] showed that the length-to-diameter ratio of the specimens used in the SHPB tests should be around 0.3, and that both the faces of the specimens should be lubricated to reduce friction.

In the 1970s, the experimental investigation of plastic wave propagation turned to develop the plate impact technique. Because the longitudinal dimension of plate specimen, i.e. the thickness, was small plate specimens were more suitable for the investigation of strain rate effect than thicker specimens used in SPHB. Clifton[23,24] found that high strain rates could cause thermal disturbance in the plate specimens due to the elevated temperature around the impacted surface, hence, the effect of strain rate could influence the plastic wave propagation. This conclusion seemed to agree with Bell's conclusion [12,13].

C. Taylor Impact Test

In the 1940s, Taylor devised a method to estimate the dynamic strength of materials. Due to World War II, this work was not published until the late 1940s [32,33]. Now this test is called Taylor Impact Test, or Taylor test. The Taylor Test consisted of

firing a solid cylinder of the material against a rigid target. The dynamic flow stress of the cylinder could be estimated from the deformed cylinder by measuring the overall length of the un-deformed section. One of the assumptions in the Taylor Test was that the rear of the cylinder undergoes constant deceleration. Today, this test has being investigated by many people and military labs. For example, Wilkins and Guinan in 1973 [34] used computer simulation to compute the dynamic stress of the material and found the final position of the plastic wave front inside the cylinder differed from the one resulting from the surface deformation evaluation of the cylinder used by Taylor. In 1985, Kuscher [35] experimentally proved the theory of Taylor, using a laser velocity interferometer, the so-called VISAR. The front-side movement of the cylinder and the plastic-wave-front movement can be seen, along with the velocity, which decreases exponentially. The propagation of the elastic wave traveling in between the plastic wave and the rear end of the cylinder is also proved. Now the Taylor test has not been used for its original purpose of obtaining dynamic-yield stresses of the materials. It has come into its own usage for checking constitutive equations by comparing the shapes of the deformed cylinders with the predictions from the constitutive equations.

Since the 1990s, the investigation about the Taylor impact test has made progress in theoretical model, numerical simulation and experimental methods.

In theoretical investigation, J.W.House, J.C.Lewis, P.P.Gills and L.L.Wilson [36] in 1995 modified the Jones and co-authors' works. This paper introduced approximation for the Jones' model. The author used the experiments to verify their results in aluminum, copper, and steel. In 1997 and 1998, W.K.Rule, S.E.Jones, J.A.Drinkard and L.L.Wilson [37,38] revised the Johnson-Cook model in the term of strain rate. This

model was used in four materials (aluminum, copper, iron, and steel). In the papers, they proposed a theoretical analysis for the linearity and several important parameters. These parameters were used to determine the state of stress at strain rates exceeding 10^4 (1/s). A numerical integration method was used to obtain the parameters for the revised Johnson-Cook model. Essentially, this method considered the effect of thermal energy and the concept optimization. In 2001, Guoxing Lu, Bin Wang, and Tieguang Zhang [39,40] modified the original Taylor impact model for porous materials. Calculations were made for porous materials with a relative density that was a linear function of compressive strain. The final length of the projectile after impact was plotted against the density, impact velocity, and the dynamic yielding stress. The experimental results with bronze and iron were presented for the static and dynamic stresses of porous metals.

R.L.Woodward, N.M.Burman, and B.J.Baxter in 1994 [41] presented the experimental method of using Taylor impact test with a Hopkinson bar as a target to record the load/time data for an aluminum alloy. The elastic deformation and plastic deformation were checked. In 1999, C.G.Lamontage, G.N.Manuelpillai, E.A.Taylor, and R.C.Tennyson [42] reported the results of a hypervelocity (5km/s) oblique impact test (35 and 45 degrees) which were performed on carbon fiber/Peek composite specimens using the light gas gun. In 2001, E.A.Taylor [43] investigated the numerical simulation of the impact of hollow shaped charge jet projectiles onto stuffed, Whipple-bumper shielding using AUTODYN-2D and AUTODYN-3D. A total of 56 simulations were carried out. J.D.Yatteau, G.W.Recht, R.H.Zernow, and K.T.Edquist in 2001 [44] described the experiments to record deformation profiles versus time in metallic rods subjected to transverse ballistic impact (materials: tungsten alloy, alloy steel, titanium and copper).

The deformation profiles were analyzed to determine transverse plastic deformation wave speeds. The rod materials were also subjected to Taylor impact tests to measure the static tensile and dynamic yielding strengths and longitudinal wave speeds. In 2004, I.Rohr, H.Nahme, and K.Thomas [45] described the behavior of 35NiCrMoV109 high strength steel over a wide range of strain rates for numerical simulations of dynamic events. The low, strain-rate, tensile tests and a numerical stress state were carried out. These data were linked to high, strain-rate data from a novel modified Taylor impact test using VISAR technique and data from planar, plate-impact tests. A material model and an equation of state were developed. The enhanced model was made by comparing the measured and calculated VISAR signals.

1.1.3 Development of Computational Methods

In the 1980s, finite element methods and other computer-based methods, such as LS-DYNA and Pam & Trade, were developed to study structural crashworthiness. The models of the materials included in the software packages consisting of both the RD theory and the RI theory. For instance, the Johnson-Cook model was a model of the RD theory while the power law plasticity model was a model of the RI theory. Many other models are given in Appendix C.

Nicholas [25] in 1981 pointed out that there appeared to be no theoretical basis for the RD models. In other words, the model was not unique. Besides, there was no basis to claim that other models could not be proposed for the investigation of plastic wave propagation. It was not expected to propose a model based on some experimental results to model all effects due to strain rate. Even if one model could be generally accepted, the methodology for determining the empirical constants might not be straightforward.

In 1987, Jones [26] proposed a two-phase theory, which was later developed into a three-phase theory [27], to study Taylor's test. According to Jones, the deformation of copper in the Taylor test could be characterized by three phases of behavior. In the beginning, denoted by phase I, the behavior was dominated by a shock-wave front. This was followed by a steady motion of plastic wave front, denoted by phase II. In phase III, the deceleration of the plastic wave front occurred. Jones' study showed that the plastic wave front entered phase II from phase I about 10 μs after the impact of a 30-caliber, copper rod by 4340 steel anvils. His study also showed that there was a decay of the function of strain rate vs. time. Jones' study further supported Bell's conclusions that the strain rate dependent theory did not seem to be applicable for the zone beyond the first diameter of the rods from the impact ends.

In 1991, Khan [28] and Hsiao used electrical resistance strain gages to investigate both small-amplitude and large-amplitude plastic wave propagation in fully annealed 1100 aluminum subjected to axi-symmetric free projectile impact. The results showed that the dynamic behavior of the material could be described by the strain rate independent theory for large-amplitude plastic wave propagation if elastic strain and strain rate sensitivity were negligible. On the contrary, the material response appeared to be strain rate sensitive for small-amplitude plastic wave propagation if elastic strain was not negligible when compared to plastic strain.

In 1997, Maudlin, Foster, and Jones [29] used a continuum mechanics code to analyze the plastic wave propagation in the Taylor test. They found that the use of the strain rate dependent Johnson-Cook model [29], the MTS flow stress mode [29], and the thermodynamic response with the Mie-Grunisen equation-of-state [29] could not capture

the plastic wave propagation in annealed and hardened copper. They also found the velocity of the plastic wave propagation became slow as the strain decreased.

In 1998, Wright [30] used the three-dimensional, nonlinear continuum to investigate the plastic wave propagation in a circular rod with the effects of radial inertia and radial shear. His investigation showed that the RI theory (von Karman-Taylor theory) should hold eventually at a large distance from the impact end of a bar where the radial effects had decayed essentially to zero. This distance could be several tens of radii from the impact end before the von Karman-Taylor solution became a good approximation. Alternatively, if the axial loading at the impact end was slow enough and the wave front could be distributed over the time axis, the radial shear was always small and the von Karman-Taylor theory (the RI theory) would be valid throughout the analysis. In 2000, Rusinek and Klepaczko [31] reported the critical impact velocity value in the steel sheet with the help of finite element code ABAQUS. Their conclusion was consistent with von Karman-Taylor's theory and Bell's experiments.

1.2 Statement of Problem

From the foregoing review, it can be seen that impact dynamics is a discipline of studying material responses under impact loading. Being different from the static loading, dynamic loading such as impact loading causes instantaneous wave propagation. Hence, wave propagation is a branch of this discipline for studying waves, elastic as well as plastic, propagating in impacted materials such as rods and plates. When the impact velocity becomes high, the elastic wave propagation is usually neglected and only plastic wave propagation is considered. Although the study of plastic wave propagation has made significant progress in the past six decades, some fundamental problems still

remain open and hinder the development of impact dynamics to some extent. This deserves some attention.

The purpose of this thesis is to study the plastic wave propagation and constitutive equation of the materials in the Taylor test.

Taylor impact tests are specially designed to exploit the inertia of a test specimen to produce very high loading rates that is used to study a large deformation, high strain (50 %) and high strain rate behavior of materials. It consisted of firing a short rod of the material against a rigid anvil or wall and making measurements on the rod before and after. During the deformation of the specimen, the plastic deformation and fracture will take place and a plastic wave will propagate. So the Taylor test is suited very well to investigate and study constitutive equation of materials, the nonlinear response of materials and structures, fundamental theoretical analyses and dynamic materials characterization. Typical applications include armor and anti-armor, penetration mechanics, physical security, demilitarization, safety studies, accident post-mortem analyses, containment studies, transient loads, structural response analyses, and computational modeling of materials.

The approach is first to use the two types of plastic-wave theory, the strain rate independent theory (RI) and the strain rate dependent theory (RD) to investigate the plastic wave propagation. The theoretical results from the plastic wave propagation are then used to investigate the distributions of the dynamic stress and dynamic strain of the projectiles in the Taylor test.

1.3 Organization

This thesis starts with a historical literature review on plastic wave propagation in Chapter 1. It is followed by the investigation of the fundamental equations of plastic wave propagation in Chapter 2.

In Chapter 2, a constitutive equation is proposed based on VISAR experimental results. Using this constitutive equation, an analytical solution of one-dimensional, plastic wave equation derived from RI theory is obtained under the condition of constant velocity impact. Using this solution, the propagation of the plastic wave can be described.

Based on the theoretical results obtained in Chapter 2, the model of three phases theory in the Taylor test is proposed in Chapter 3. Using this model, the propagation of the plastic wave of four kinds of material (6061-T6 Aluminum, 145-Hard-H02 Copper, 6061-T6511 Aluminum, and C1045 Steel) in the Taylor tests for different impact velocities are investigated and the dynamic stress, dynamic strain and the velocity of the propagation of the plastic wave are calculated. According to the three phases model, there exists a mushroom shapes in the projectiles after impact. This conclusion is verified by the four experimental results.

In Chapter 4, eight constitutive equations from RI theory and RD theory are used to investigate the propagation of the plastic wave in the Taylor tests. The results indicate that the conclusions from these constitutive equations cannot match the experimental phenomena well.

In Chapter 5, the one-dimensional plastic wave of RD theory is investigated. The investigation includes the plateau of RD theory, the characteristic equation of the plastic

wave propagation and numerical analyses (Eulerian method and Hartree method) along the characteristic curves. The results indicate that there exists a plateau for RD theory. The propagation of the plastic wave can be computed by the numerical methods along the characteristic curves.

It is shown in Chapter 6 that the Modified Molvern model is used to numerically compute the propagation of the plastic wave (RD theory) in the Taylor test for material 6061-T6511. Both the Eulerian method and the Hartree method are used, separately. The computed results indicate that the Eulerian method is simple but not accurate; the Hartree method is complicated but possesses better convergence.

Finally, in Chapter 7, what was done in this investigation is summarized and some recommendations for future works are made.

CHAPTER 2

FUNDAMENTAL EQUATIONS FOR PLASTIC WAVE PROPAGATION

2.1 Material Deformation and Plastic Wave Propagation

The impact process is a very complex phenomenon. One of the important characteristics of the impact process is its short duration. Experimental results have indicated that the impacted object during the impact process is deformed both elastically and plastically and with thermal energy change. In this investigation, the thermal energy is not considered. Experimental results have also shown that the elastic deformation occurs prior to the plastic deformation under high-velocity impact. The amount of the deformation is dependent on the amount of energy absorbed by the impacted object. Corresponding to the elastic deformation (linear as well as non-linear), two types of elastic waves (linear and non-linear) are formed and propagate in the impacted object.

From the elastic theory for isotropic materials, there are two types of waves in solids: longitudinal (or dilatational) wave and transverse (or distortional, or shear) waves. The longitudinal waves are those in which the particles move in the same direction as the wave propagation. The transverse waves are those in which the particles move in the direction normal to the wave propagation. In the meanwhile, elastic waves may propagate on the surface of a solid. Two types of surface waves, the Rayleigh wave and Love wave, have been investigated extensively. Rayleigh waves decay exponentially with the depth from the surface to the interior of the medium and move only in two dimensions. They propagate more slowly than other types of elastic waves. Love waves are induced by material mismatch, e.g. a layer of material that possesses one set of

physical constants overlies another layer of the material that possesses a different set of physical constants. As the intensity of the impact force increases, the material is driven beyond its elastic limit and becomes a plastic deformation, resulting in two waves propagating in the solid: an elastic wave and a much slower but more intensive plastic wave. In addition, if the characteristics of the medium are such that the velocity of propagation of large disturbances is greater than that of smaller ones, the stress pulse develops a steeper and steeper front when propagating through the medium. In this way, a shock wave is formed. Shock waves can also be formed if the impact velocity exceeds the wave velocity in the material. In this thesis, only plastic wave propagation is considered.

A plastic wave is formed and propagated in the impacted object following the plastic deformation. The plastic wave is a kind of nonlinear wave. Compared with the plastic deformation from high-velocity impact, the magnitude of elastic deformation is much smaller. Hence the elastic waves can be neglected in the investigating of wave propagation under high-velocity impacts. In this thesis, the high-velocity impact is defined as the impact velocity which results in plastic deformation.

Historically, most research activities on plastic wave propagation dealt with long bars. According to experimental [13] and theoretical investigations [1,2], the plastic waves were not formed at the impacted face; instead they were inaugurated at a distance away from the impacted face. The plastic wave propagation causes plastic deformation and sharp changes of stress and strain in the impacted object. The stress and the strain are called dynamic stress and dynamic strain in this investigation. The propagation can be described by a governing equation based on assumptions concerning the relationship

among stress, strain and strain rate. There are two major approaches for the propagation of plastic wave: the strain rate independent theory (RI) and the strain rate dependent theory (RD).

2.2 Theories of Plastic Wave Propagation

2.2.1 Strain Rate Independent Theory (RI)

The strain rate independent theory assumes that a stress σ is only a function of strain ε when plastic wave propagates in a solid. The relation between stress and strain can be written as $\sigma = \sigma(\varepsilon)$ and the curve between them has been formed to be concave toward the axis of strain for most solids.

The equation of plastic wave propagation can be derived from Newton's second law. Without the loss of generality, only one-dimensional motion is considered. The governing equation can then be expressed as

$$\rho \frac{\partial^2 u}{\partial t^2} = \frac{d\sigma}{d\varepsilon} \frac{\partial \varepsilon}{\partial x} \qquad (2.1)$$

where σ is stress, ε is strain, ρ is mass density, t is time, u is displacement, and x is displacement.

2.2.2 Strain Rate Dependent Theory (RD)

Two strain rate dependent theories were proposed independently by Solovsky [9] in 1949 and by Malvern [10] in 1950. These theories consider stress as a function of strain ε and strain rate $\dot{\varepsilon}$, i,e.

$$\sigma = \sigma(\varepsilon, \dot{\varepsilon})$$

From Newton's second law, without loss of generality, the following one-dimensional motion in x direction can be formatted:

$$\rho \frac{\partial^2 u}{\partial t^2} = \frac{\partial \sigma}{\partial \varepsilon}\frac{\partial \varepsilon}{\partial x} + \frac{\partial \sigma}{\partial \dot{\varepsilon}}\frac{\partial \dot{\varepsilon}}{\partial x} \qquad (2.2)$$

2.2.3 Comparison of the Two Theories

As mentioned above, the problems involving plastic wave propagation in metals and ductile materials can be analyzed based on two types of hypotheses: the strain rate independent theory (RI) and the strain rate dependent theory (RD). From the point of view of Simmons [18] and Lubliner [19], the strain rate independent theory is associated with plasticity theory while the strain rate dependent theory is associated with visco-plastic theory.

For less viscid ductile materials, the strain rate independent theory seems to agree with experimental results, e.g., the strain rate independent theory agreed better with the experimental results for aluminum alloy in the experiments conducted by Kolsky and Dutch [14] and Lindholm [15]. For viscid ductile materials, the strain rate dependent theory seems to agree better with the experimental results for aluminum and copper. Because the viscosity of materials is dependent on temperature and the elevated temperature mainly appears around the impacted face under the high velocity impact [22], the effect of strain rate (viscosity effect) should only influence the plastic wave propagation around the impacted face. This result is strongly supported by Bell's experiment [13]. From Bell's experiment, the strain rate independent theory of plastic wave propagation was feasible in annealed aluminum and copper with a distance approximately equal to the diameter from the impacted surface. Further experiments [4] showed that this conclusion is applicable for zinc, lead, magnesium, nickel, and 70-30 α-brass. In addition, Jones' experimental result [26] also concluded that the strain rate

dependent theory was not applicable after the first diameter from the impact face if the ratio of length to diameter was greater than 5. It should be noted that the RD theory is referred to $\sigma = \sigma(\varepsilon, \dot{\varepsilon})$ and the wave equation. Many models based on the RD theory have been proposed. However, they cannot completely represent the RD theory. From the RD theory, the stress is a function of strain and strain rate, Equation (2.2) tells us that the effect of strain rate influences the plastic wave propagation by term of $\frac{\partial \sigma}{\partial \dot{\varepsilon}}$. If the strain rate is a constant, say c_ε, then $\sigma = \sigma(\varepsilon, c_\varepsilon)$. This means that $\frac{\partial \sigma}{\partial \dot{\varepsilon}}$ is zero and Equation (2.2) will become Equation (2.1). That is, the RI theory is a special case of the RD theory.

2.3 Equation of One-Dimensional Plastic Wave

Assume that a bar extending from $x = 0$ to $x = L$. The endpoint, $x = 0$, of the bar is suddenly impacted with a constant velocity V_0, as shown in Figure 2.1. The relation $\sigma = \sigma(\varepsilon, \dot{\varepsilon})$ holds only for the initial deformation of the material of the rod beyond the elastic limit. The lateral contraction of the material and the inertia effects are neglected.

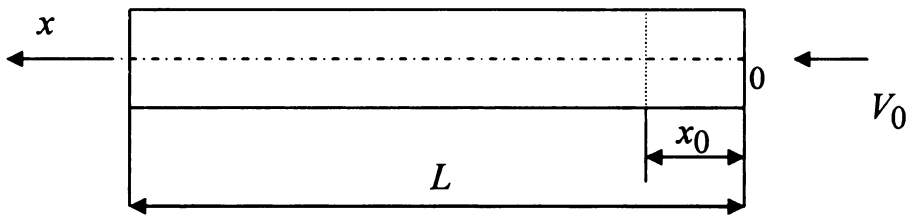

Figure 2.1 Impact Diagram

Recall Equation (2.2) and use $\varepsilon = \frac{\partial u}{\partial x}$ and $\dot{\varepsilon} = \frac{\partial^2 u}{\partial x \partial t}$, then

$$\rho \frac{\partial^2 u}{\partial t^2} = \frac{\partial \sigma}{\partial \varepsilon} \frac{\partial^2 u}{\partial x^2} + \frac{\partial \sigma}{\partial \dot{\varepsilon}} \frac{\partial^3 u}{\partial x^2 \partial t} \qquad (2.3)$$

where u is the displacement function of an element in the longitudinal direction, i .e, $u = u(x,t)$.

If the strain rate is not considered, the equation of plastic wave propagation, Equation (2.3), can be reduced to Equation (2.1)

$$\rho \frac{\partial^2 u}{\partial t^2} = \frac{d\sigma}{d\varepsilon} \frac{\partial^2 u}{\partial x^2}$$

This is a plastic-wave equation of RI theory in Lagrangian coordinate system. This equation was first proposed by von Karman in 1942. It is usually called the von Karman plastic-wave equation. When the deformation of the materials is within the elastic range, $\frac{d\sigma}{d\varepsilon} = E$, where E is Young's modulus. Equation (2.1) becomes a linear elastic wave equation

$$\rho \frac{\partial^2 u}{\partial t^2} = E \frac{\partial^2 u}{\partial x^2}$$

Apparently, the linear, elastic-wave equation is a special case of a nonlinear, plastic-wave equation.

2.4 A Solution of the One-Dimensional Plastic-Wave Equation

When a bar with length L is impacted by a constant velocity V_0 at $x = 0$, the constitutive equation of a material (the relation between the stress σ and the strain ε) can be expressed as $\sigma = \sigma(\varepsilon)$. In 1985, Kuscher used his VISAR test to prove that the plastic wave propagates exponentially in the projectile. Based on this experimental

result, a constitutional equation is proposed as follows:

$$\sigma = \frac{\rho C_2}{2}[e^{\frac{2(\varepsilon - C_1)}{C_2}}] \qquad (2.4)$$

where C_1 and C_2 are constants. Based on Newton's second law, the plastic wave equation can be written as follows:

$$\rho \frac{\partial^2 u}{\partial t^2} = \frac{d\sigma}{d\varepsilon} \frac{\partial^2 u}{\partial x^2} \qquad (2.5)$$

and subjected to the following boundary conditions:

$$u(x_0, t_0) = h_d;$$

$$\frac{\partial u(x_0, t_0)}{\partial t} = V_0;$$

$$u(L, t_p) = 0.$$

where $u(x,t)$ is the displacement function, x is position, t is time, t_p is the plastic wave propagation time and ρ is the density. x_0 and t_0 are constants. Using the substitution, $\xi = \frac{x}{t}$, then ε can be considered as a function of ξ, i.e. $\varepsilon = f(\xi)$.

According to the experimental results obtained by Bell, a plastic wave is inaugurated at a distance, i.e. at $x = x_0 > 0$ ($t = t_0 > 0$). So, the computation of displacement should begin from $x = x_0$. That is, the coordinate original point is set at $x = x_0$. It yields

$$u(x,t) = \int_0^x \frac{\partial u(y,t)}{\partial y} dy = \int_0^x f(\frac{y}{t}) dy = t \int_0^\xi f(\eta) d\eta \qquad (2.6)$$

where $\eta = \frac{y}{t}$, $dy = td\eta$.

Take the derivative for the above Equation, it gives

$$\frac{\partial u}{\partial x} = \frac{\partial u}{\partial \xi}\frac{\partial \xi}{\partial x} = \frac{1}{t}\frac{\partial u}{\partial \xi};$$

$$\frac{\partial^2 u}{\partial x^2} = \frac{\partial}{\partial \xi}(\frac{1}{t}\frac{\partial u}{\partial \xi})\frac{\partial \xi}{\partial x} = \frac{1}{t}f'(\xi) \qquad (2.7)$$

$$\frac{\partial u}{\partial t} = \int_0^{\xi} f(\eta)d\eta - \xi f(\xi)$$

$$\frac{\partial^2 u}{\partial t^2} = \frac{\xi^2}{t}f'(\xi) \qquad (2.8)$$

Take Equations (2.7) and (2.8) into Equation (2.5), then

$$\rho\frac{\xi^2 f'(\xi)}{t} = \frac{d\sigma}{d\varepsilon}\frac{f'(\xi)}{t} \qquad (2.9)$$

From Equation (2.9), we have

$$f'(\xi) = 0 \qquad (2.10)$$

Or $$\xi^2 = \frac{1}{\rho}\frac{d\sigma}{d\varepsilon} \qquad (2.11)$$

From (2.10), we know that $f(\xi) =$ constant, c_1. That is, the strain is a constant. From the experimental results, this solution is in the interval of $0 \le x < x_0$.

From Equations (2.11) and (2.4), we have that

$$\xi^2 = \frac{1}{\rho}\rho e^{\frac{2(\varepsilon - C_1)}{C_2}} \qquad (2.12)$$

$$\Rightarrow \quad \varepsilon = C_1 + C_2 \ln \xi$$

$$\Rightarrow \quad f(\xi) = C_1 + C_2 \ln \xi \qquad (2.13)$$

Taking Equation (2.13) into Equation (2.14), then we have

$$u(x,t) = \int_0^x \frac{\partial u(y,t)}{\partial x} dy = t \int_0^{\xi} f(\eta) d\eta$$

$$= t \int_0^{\xi} [C_1 + C_2 \ln \eta] d\eta = C_1 x + C_2 x (\ln \frac{x}{t} - 1) \qquad (2.14)$$

where $0 < t_0 \le t \le t_p$, $x_0 \le x \le L - L_e$. L_e is a constant.

Notice that Equation (2.14) is from the coordinate original point setting at $x = x_0$. If the coordinate original is set at the impact end, ξ_0 is the velocity of the plastic wave for $x < x_0$, then

$$u(x,t) = C_1 x + C_2 x (\ln \frac{x}{t} - 1) + t \int_0^{\xi 0} c_1 d\xi$$

$$= C_1 x + C_2 x (\ln \frac{x}{t} - 1) + C_3 t \qquad (2.15)$$

where C_1, C_2 and C_3 are constants and will be determined by the boundary condition.

From Equation (2.12), it gives the velocity of the plastic wave propagation as follows:

$$C_p = e^{\frac{\varepsilon - C_1}{C_2}} \qquad (2.16)$$

This conclusion matches the experimental result of VISAR test.

CHAPTER 3

APPLICATION OF PLASTIC WAVE PROPAGATION THEORY IN TAYLOR IMPACT TEST

In the 1940s, Taylor [32,33] conducted a test of a projectile at constant, high-velocity impact against a rigid wall. The test involved the determining of the dynamic yielding stress of the material. Since then, the Taylor test has become a very useful method to verify the dynamic behavior of materials. Many researchers have carried out the same tests to analyze the propagation of a plastic wave and determine the dynamic yielding stress of the materials. In 1971, Wilkins and Guinan[34] used the Taylor test to determine the dynamic yielding stress of the materials. In 1997, Jones [26,27] proposed his three phases model to investigate the propagation of plastic wave in the projectile. His works are very significant for recent investigations of the Taylor test. However, the theory of plastic wave propagation and the shape curves of the projectile after impact to has not been used to verify theoretical investigation. In this chapter, the theory of plastic wave propagation, RI theory, is used to analyze the Taylor test. The shape curves and dynamic yielding stresses of the projectiles are used to verify our investigation. It includes the determining of dynamic, yielding stress; the characteristics of the plastic wave propagation; and the constitutive equation proposed by us.

This chapter consists of two parts. In the first part, a new model is proposed to describe the Taylor test. RI theory is used to analyze the propagation of the plastic wave in the projectile. At the same time, a constitutive equation is proposed. In the second part, in order to verify our theoretical investigation, three Taylor tests are carried out for Aluminum 6061-T6511, Copper 145-Hard-H02, and Steel C1045. The comparisons

between the shape curves and the dynamic yielding stresses of the projectiles predicted by the constitutive equation and experimental result show good agreement. The experimental results support our theoretical investigation.

3.1 Three Phases Model

Consider that a cylindrical projectile with length L and radius r_0 impacts a rigid wall at a constant velocity V_0, shown in Figure 3.1. We depict the process of deformation as a sequence of elastic and plastic wave propagation into the projectile. Here only a linear, elastic wave and a plastic wave are considered. At the moment of impacting the wall, the elastic, compression wave and the plastic, compression wave are formed in the projectile, separately. Because the elastic, compression wave is formed first and then the plastic, compression wave ensues, the elastic, compression wave propagates in the projectile until it reaches the back end of the projectile and reflects there. Because the back end is free of stress, the elastic, compression wave is reflected into tensile wave. When this elastic, tensile wave returns toward the plastic, compression wave, it interacts with plastic, compression wave. Suppose that this marks the end of the plastic, deformation process. When the elastic, tensile wave meets the plastic, compression wave, the elastic stress from the elastic, tensile wave is less than plastic stress from the plastic compression wave. From Newton's second law, the elastic wave is reflected again as an elastic compression wave, moves back, and so on. Because of the effect of friction in the material, the elastic wave will oscillate and disappear. In this paper, a tensile stress is defined as negative one and a compression wave is defined as positive stress to follow the tradition of studying impact dynamics. According to many

experimental results and theoretical investigation from the references, a new model is proposed, shown in Figure 3.2 and Figure 3.3. That is, the projectile can be divided into two regions and three phases:

Plastic Region:

a. First Phase: In this phase, the plastic wave is non-dispersive. The strain is constant and near to the impact end. The density is ρ_{p1}. **The shape of the projectile is concave** in transverse direction after impact. Before impact, the length is h. After impact, the length is h_d. The plastic dispersive wave would be inaugurated at $x = h$. Physically, the first phase is called the plastic plateau.

b. Second Phase: In this phase, the plastic wave is dispersive. The strain, stress and the velocity of the plastic wave are decreased. The density is ρ. **The shape of the projectile is convex** in transverse direction after impact. Physically, that is the so-called shape of a mushroom. Before impact, the length is $L - L_e - h$. After impact, the length is L_p.

Elastic Region:

c. Third Phase: In this phase, the elastic wave oscillates and disappears after impact as friction in the material. The density is ρ_e. Before impact, the length is L_e. After impact, the length is still L_e. The shape of the projectile remains a straight line.

In this paper, the investigation is concentrated on the plastic wave. So, the first phase and second phase are mainly discussed.

3.2 Theory

Suppose a constitutive equation between the plastic stress σ and strain ε is $\sigma = \sigma(\varepsilon)$ (RI theory) in the projectile, the transverse wave is neglected. The density does not change after impact. Then, from Newton's second law, the plastic wave equation in the Lagrangian form is

$$\rho \frac{\partial^2 u}{\partial t^2} = \frac{d\sigma}{d\varepsilon} \frac{\partial^2 u}{\partial x^2} \qquad (3.1)$$

where $u = u(x,t)$ is displacement function, x is displacement and t is time. We want to investigate the propagation of the plastic wave under the condition of constant velocity propagation.

3.2.1 First Phase

Because the impact velocity is assumed as constant, then the von Karman's boundary condition

$$u(0,t) = V_0 t$$

and a linear solution [2] can be used to the first phase, that is

$$u(x,t) = V_0(t + \frac{x}{c_1}), \quad 0 \le t \le t_h, \; 0 \le x \le h \qquad (3.2)$$

where c_1 is a constant and t_h is the time interval from the beginning of material deformation to the end.

Suppose ε_{p1} is the plastic strain and v_{p1} is the velocity of the particle in the first phase. Then from Equation (3.2), it gives

$$\varepsilon_{p1} = \frac{\partial u}{\partial x} = \frac{V_0}{c_1} \qquad (3.3)$$

$$v_{pl} = \frac{\partial u}{\partial t} = V_0 \qquad (3.4)$$

From Equation (3.3) and Equation (3.4), the plastic strain and the velocity of the particle are constants in the first phase, then the propagation of plastic wave is constant. c_1 can be obtained from Equation (3.3) after V_0 is known and ε_{pl} is measured.

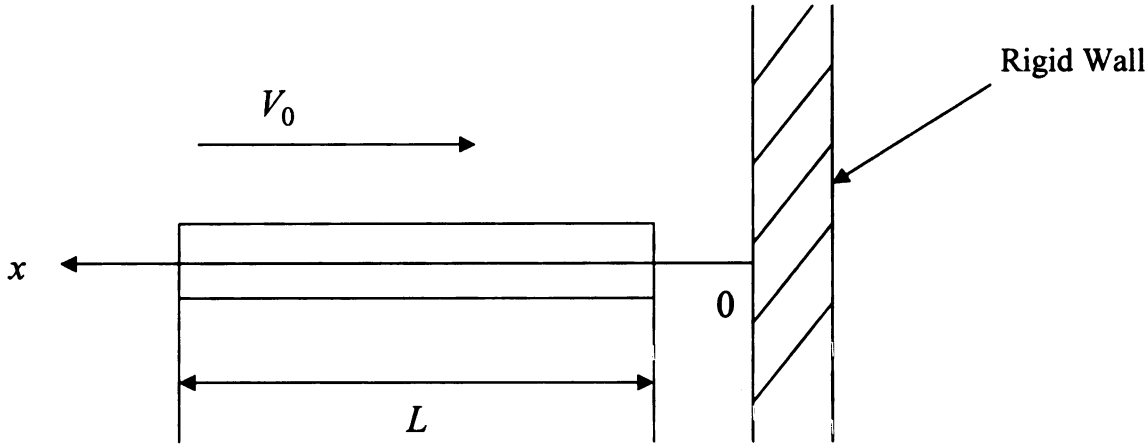

Figure 3.1 Before Impact

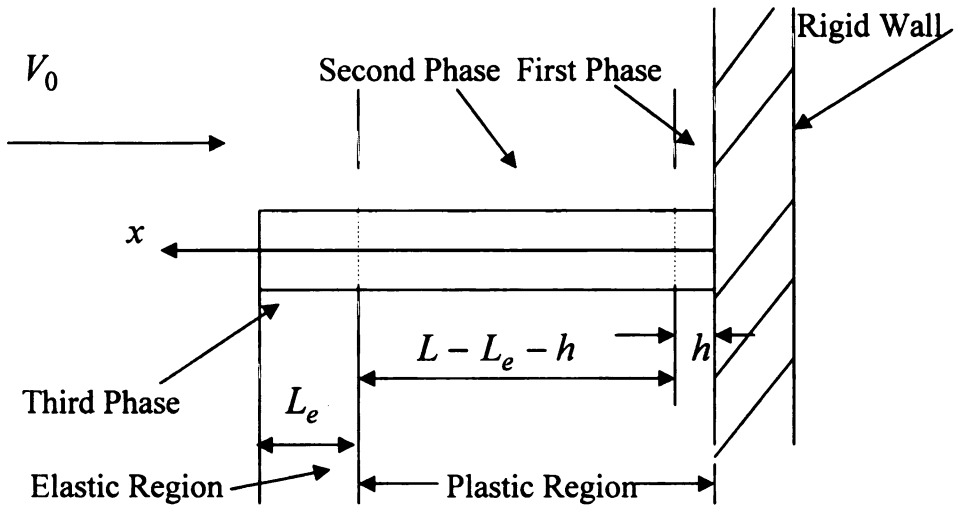

Figure 3.2 At the Moment of Impact

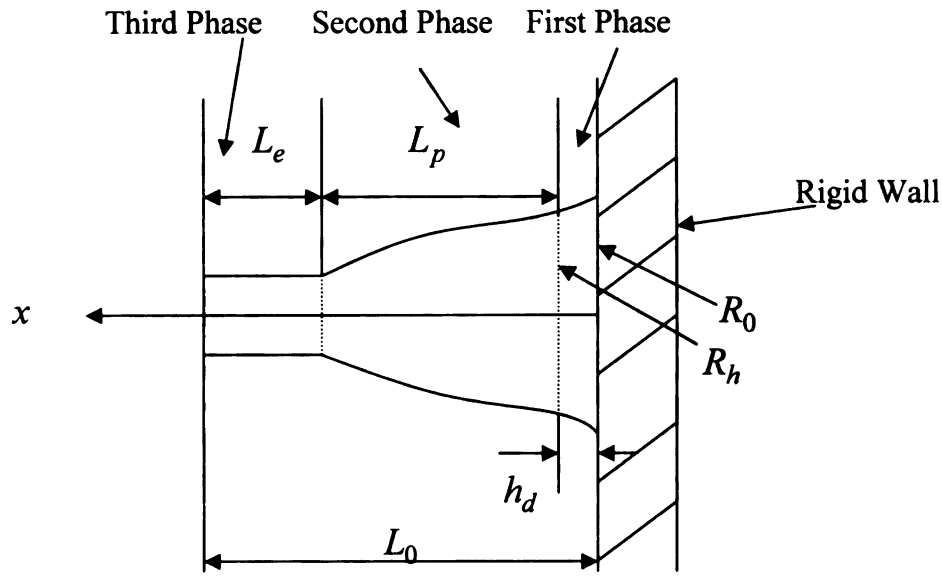

Figure 3.3 After Impact

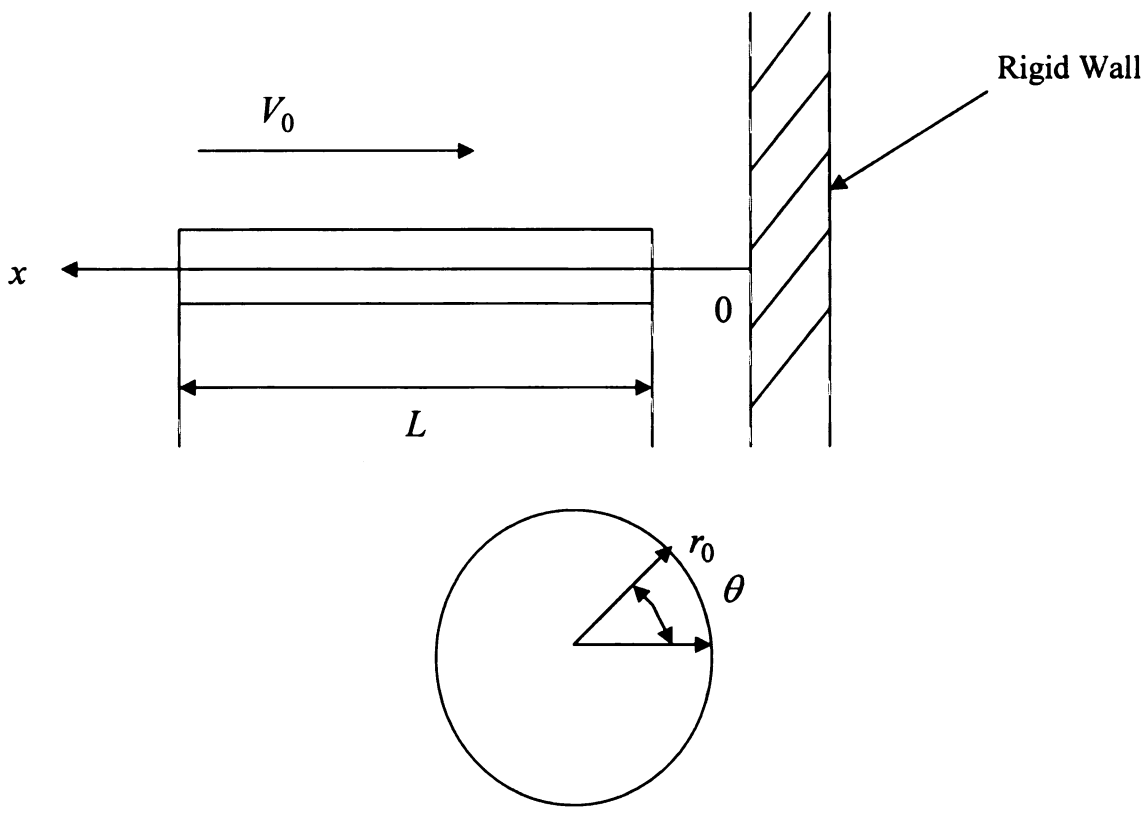

Figure 3.4 Cross Section of Projectile

In order to use Equation (3.2) to describe the propagation of the plastic wave, t_h must be known. Notice ($t + \frac{x}{c_1}$) in Equation (3.2) is a concept of time. Let $\tau = t + \frac{x}{c_1}$. Then we have

$$u(x,t) = V_0 \tau, \qquad 0 \le \tau \le t_h \qquad (3.5)$$

That is, τ can be divided into two parts: deformation of the material, $\frac{x}{c_1}$ and pure time, t.

As we know, the impact process is very complicated. Here, it is assumed that the impact process can be divided into two sub-processes: pure-impact process and deformation process.

We define that the pure-impact process is the process of impact taking place. The time of the pure impact process takes time t_{pure}. In this sub-process, no deformation takes place. The deformation process is the process of deformation of the material. In this sub-process, only the deformation of the material takes place; impact does not take place. It takes time t_{deform}. Because the pure impact process takes place first, and then the deformation process begins. The time of the impact process should be equal to the sum of the times of the pure impact process and the deformation process. And during the impact, the total time, t_0, can be calculated as follows:

$$t_0 = t_{pure} + t_{deform} \qquad (3.6)$$

Because in the first phase the velocity of the particle is a constant, that is to say, a

particle moves uniformly for a distance h with velocity V_0 from the impact end. According to Newton's first law, the sum of the total forces applied to the particle in the first phase should be zero. That is to say, when the particle moves uniformly for a distance h, the impact force is always applied to the particle. According to Bell's experiments [13], beyond h, the velocity of particle is not a constant. So, it can be concluded that the impact force is no longer applied to the particle. Based on this analysis, the time of material deformation, t_h, is equal to t_{deform} and can be calculated as follows:

$$t_h = t_{deform} = \frac{h}{V_0} \tag{3.7}$$

that is, after $t_h = \frac{h}{V_0}$, the deformation of material ends.

From the above analysis, we give two conditions at $x = h$ and $t = t_h$ as follows:

$$u(h,t_h) = h_d \tag{3.8}$$

$$\frac{\partial u}{\partial t}(h,t_h) = V_0 \tag{3.9}$$

where h_d is the length of h after impact.

3.2.2 The Shape Curve of the Projectile

Suppose the radius of the projectile is r_0 or the diameter is D_1 before impact. Taking a polar coordinate at the centerline of the projectile, x is along the centerline, shown in Figure 3.4. In order to describe the shape curve of the projectile after impact, we must relate r with x, that is, to find $r = r(x)$. In order to do so, let us use the plastic incompressibility [Zukas,25]

$$d\varepsilon_r + d\varepsilon_\theta + d\varepsilon_x = 0 \qquad (3.10)$$

where ε_r and ε_θ are the strain along r and θ, and ε_x is the plastic strain along x axis. Noticing that for the centerline of the geometry, the transverse strain increment $d\varepsilon_r$ and $d\varepsilon_\theta$ are equal [Maudlin, 29],

$$d\varepsilon_r = d\varepsilon_\theta \qquad (3.11)$$

From Equation (3.11), Equation (3.10) can be written as

$$2d\varepsilon_r = -d\varepsilon_x$$

Taking integration for the above equation, we have

$$\varepsilon_r = -\frac{\varepsilon_x}{2} + C_q$$

where C_q is an integrative constant. Assume when $\varepsilon_r = 0$, $C_q = 0$. Then, we have

$$\varepsilon_r = -\frac{\varepsilon_x}{2} \qquad (3.12)$$

Because the radial strain ε_r is defined as

$$\varepsilon_r = \frac{dr}{r} \qquad (3.13)$$

combining Equation (3.12) and Equation (3.13), we have

$$\frac{dr}{r} = -\frac{1}{2}\varepsilon_x \qquad (3.14)$$

Equation (3.14) gives the relationship between x and r. Now we are going to use Equation (3.14) to get the shape curve of the projectile in the plastic region after impact.

3.2.3 The Shape Curve of the Projectile In the First Phase

Since in this phase the strain is a constant, we take integration for both sides of Equation (3.14)

$$\frac{dr}{r} = -\frac{1}{2}\varepsilon_x$$

$$\Rightarrow \quad \frac{dr}{r} = -\frac{1}{2}\frac{\partial u}{\partial x}$$

$$\Rightarrow \quad \int_{r_0}^{r} d\ln r = -\frac{1}{2}\int_0^x \frac{\partial u}{\partial x} dx$$

$$\Rightarrow \quad \ln r - \ln r_0 = -\frac{u(x,t)}{2} + u(0,t)$$

According to the von Karman boundary condition, when $x = 0$ and $t = 0$, it gives $u(0,0) = 0$. So we have

$$r = B_0 e^{-\frac{u(x,t)}{2}} \qquad (3.15)$$

where B_0 is a constant.

From Equation (3.15), we have

$$r = B_0 e^{-\frac{u(x,t)}{2}}$$
$$= B_0 e^{-\frac{V_0 \tau}{2}}$$

Suppose that after impact R_0 is the radius of the projectile at $\tau = 0$ and $x = 0$, and R_h is the radius of the projectile at $\tau = t^*$, then we have

$$\tau = 0, \quad r = R_0;$$
$$\tau = t^*, \quad r = R_h;$$

Take the above conditions back into Equation (3.15), then we have

$$R_0 = B_0 \tag{3.16}$$

$$R_h = B_0 e^{-\frac{V_0 t^*}{2}} \tag{3.17}$$

Solving the above equations, it gives

$$t^* = \frac{2}{V_0} \ln \frac{R_0}{R_h} \tag{3.18}$$

So we have

$$r = R_0 e^{-\frac{V_0}{2}\tau}, \qquad 0 \le \tau \le t^*, \quad 0 \le x \le h \tag{3.19}$$

Notice that the movement of the particle is uniform in this region, we have

$$\tau = \frac{x}{h} t^* = \frac{x}{h} \frac{2}{V_0} \ln \frac{R_0}{R_h}$$

Then, Equation (3.19) can be rewritten as

$$r = R_0 e^{-\frac{V_0}{2}\tau} = R_0 r^{-\frac{V_0}{2}(\frac{x}{h}\frac{2}{V_0}\ln\frac{R_0}{R_h})} = R_0 e^{-\frac{x}{h}\ln\frac{R_0}{R_h}}$$

$$\Rightarrow \quad r = R_0 e^{-\frac{x}{h}\ln\frac{R_0}{R_h}}, \qquad 0 \le x \le h \tag{3.20}$$

The shape curve of the projectile in the first sub-region can be described by Equation (3.20) after impact.

Taking a derivative twice for x to Equation (3.20), it gives

$$r'' = \frac{R_0}{h^2} (\ln \frac{R_0}{R_h})^2 e^{-\frac{x}{h}\ln\frac{R_0}{R_h}}$$

Because the second derivative is greater than zero, the shape of the projectile is

concave. Using the rule of plastic incompressibility, h can be calculated from Equation (3.20) and h_d

$$\pi r_0^2 h = \pi \int_0^{h_d} R_0^2 e^{-\frac{2x}{h}\ln\frac{R_0}{R_h}} dx$$

Solve this equation, it gives

$$h = -\frac{2\ln\frac{R_h}{R_0}}{\ln[1-\frac{2r_0^2}{R_0^2}\ln(\frac{R_h}{R_0})]} h_d \qquad (3.20\text{-}1)$$

3.2.4 Plastic Wave Propagation in the Second Phase

3.2.4.1 Condition of Constant Velocity Propagation

At $x = h$ and $t = t_h$, the plastic wave enters the second phase from the first phase. Consider the propagation of the plastic wave is constant velocity during the plastic wave propagates in the second phase, that is, the velocity of the plastic wave, C_p, satisfies

$$C_p = \frac{x}{t} \qquad (3.21)$$

According to von Karman [2] and Taylor's derivations [3], the velocity of the plastic wave in Equation (3.1) should satisfy

$$C_p^2 = \frac{1}{\rho}\frac{d\sigma}{d\varepsilon} \qquad (3.22)$$

Combing Equation (3.21) and Equation (3.22), it gives the condition of constant velocity propagation

$$\frac{x^2}{t^2} = \frac{1}{\rho}\frac{d\sigma}{d\varepsilon} \tag{3.23}$$

3.2.4.2 A Solution of Plastic Wave Equation

In Chapter 2, a constitutive equation is proposed as follows when the plastic wave propagates in the second phase:

$$\sigma = \frac{\rho C_2}{2} e^{\frac{2(\varepsilon + C_1)}{C_2}} \tag{3.24}$$

And the solution of Equation (3.1) is that

$$u(x,t) = C_1 x + C_2 x(\ln\frac{x}{t} - 1) + C_3 t \tag{3.25}$$

where C_1, C_2 and C_3 are constants and will be determined by boundary conditions. In order to determine three constants, three boundary conditions are needed. Because we have two boundary conditions already, Equations (3.8) and (3.9), another one is needed. At the interface of the second phase and the third phase, we have a boundary condition as follows:

$$u(L - L_e, t_p) = (L - L_0) - (h - h_d) \tag{3.26}$$

Suppose that after impact the time when the plastic wave reaches the interface of the second and third phase is t_p. The time when the elastic wave propagates in the projectile and reaches the interface after reflecting at the back end is t_e. Then t_e should be equal to t_p approximately, that is

$$t_e = t_p \tag{3.27}$$

If the velocity of the elastic wave propagation is C_e, $C_e = \sqrt{\frac{E}{\rho}}$, where ρ_e is the density of projectile and E is Young's modulus, then it is easy to calculate t_e as follows:

$$t_e = \frac{L + L_e}{C_e} = \frac{L + L_e}{\sqrt{\frac{E}{\rho}}} \qquad (3.28)$$

So, from Equations (3.27) and (3.28), we have

$$t_p = \frac{L + L_e}{\sqrt{\frac{E}{\rho}}} \qquad (3.29)$$

Now, we assume the displacement function $u(x,t)$ and the velocity of the particles are continuous when the plastic wave enters the second phase from the first phase. Then we have the following three boundary conditions, Equations (3.8), (3.9) and (3.26), to solve the three integrative constants in Equation (3.25). Taking the three boundary conditions into Equation (3.25), then we have

$$C_1 h + C_2 h(\ln\frac{h}{t_h} - 1) + C_3 t_h = h_d \qquad (3.30)$$

$$-\frac{C_2 h}{t_h} + C_3 = V_0 \qquad (3.31)$$

$$C_1(L - L_e) + C_2(L - L_e)(\ln\frac{L - L_e}{t_p} - 1) + C_3 t_p = (L - L_0) - (h - h_d) \qquad (3.32)$$

Write the above three equations as a matrix form

$$\begin{bmatrix} h & h(\ln\frac{h}{t_h}-1) & t_h \\ 0 & -\frac{h}{t_h} & 1 \\ L-L_e & (L-L_e)(\ln\frac{L-L_e}{t_p}-1) & t_p \end{bmatrix}\begin{bmatrix} C_1 \\ C_2 \\ C_3 \end{bmatrix}=\begin{bmatrix} h_d \\ V_0 \\ (L-L_0)-(h-h_d) \end{bmatrix} \tag{3.33}$$

Because L_0, L_e and h_d are measurable, V_0, E, ρ and L are given. t_p, t_h can be calculated. If h is known, the three integrative constants can be calculated.

3.2.4.3 The Shape Curve of the Projectile in the Second Phase

Because in the second phase, ε_x is a function of x and t, Equation (3.25) can be used directly in Equation (3.14), that is

$$\frac{dr}{r} = -\frac{1}{2}\varepsilon_x = -\frac{1}{2}(C_1 + C_2 \ln\frac{x}{t})$$

$$\Rightarrow \quad dr = -\frac{r}{2}(C_1 + C_2 \ln\frac{x}{t})$$

Since r_0 is the radius of the projectile before impact, then after impact, the radius r can be written as

$$r = r_0 + r_0|dr|$$

$$= r_0(1+|dr|)$$

$$= r_0(1 + \frac{C_1}{2} + \frac{C_2}{2}\ln\frac{x}{t})$$

$$\Rightarrow \qquad r = r_0(1 + \frac{C_1}{2} + \frac{C_2}{2}\ln\frac{x}{t}) \qquad (3.34)$$

or $$D = D_1(1 + \frac{C_1}{2} + \frac{C_2}{2}\ln\frac{x}{t}) \qquad (3.35)$$

where D_1 is the diameter of the projectile before impact. D is the diameter of the projectile after impact. The shape curve of the projectile in the second phase can be described by Equation(3.34) or Equation (3.44) after impact. Taking derivative twice for x to Equation (3.34), it gives $r'' = -\frac{r_0 C_2}{2x^2}$. Because the second derivative is less than zero, the shape of the projectile is convex.

Using Equation (3.20), Equation (3.34) and considering the third phase of the projectile, the shape curve of the whole projectile can be drawn as follows:

First Phase: $r = R_0 e^{-\frac{x}{h}\ln\frac{R_0}{R_h}}, \qquad 0 \le x \le h$

Second Phase: $r = r_0(1 + \frac{C_1}{2} + \frac{C_2}{2}\ln\frac{x}{t}), \; h \le x \le L - L_e, \; t_h \le t \le t_p$

or $$D = D_1(1 + \frac{C_1}{2} + \frac{C_2}{2}\ln\frac{x}{t})$$

Third Phase: $r = r_0, \qquad L - L_e \le x \le L$

The above formulas indicate that in the first phase, the shape curve of the projectile is concave. In the second phase, the shape curve is convex, like the mushroom. In the third phase, the shape curve is a straight line.

3.3 Three Taylor Impact Tests

Three Taylor impact tests were carried out to verify the theoretical analysis at the Impact Dynamics Lab of the Department of Mechanical Engineering, Michigan State University. The test data and figures of the projectiles are shown in Figure. Projectile-1-Aluminum 6061-T6511, Figure. Projectile-2-Copper 145-Hard-H02 and Figure. Projectile-3-Steel C1045. The measured test data are shown in Table-Experimental Data-1-Aluminum 6061-T6511, Table-Experimental Data-2-Copper 145-Hard-H02 and Table-Experimental Data 3-Steel C1045. All tables can be seen in Section 3.5. Three figures only show the plastic region of the projectile after impact. The parameters of projectiles can be seen in Section 3.4.

From the test data and three figures, there exist two phases in every projectile. For the projectile of Aluminum 6061-T6511, the first phase's length is 0.299 cm. The length of the second phase is 3.4282 cm. The length of the third phase is 4.12 cm. In the first phase, the shape curve of the projectile after impact is concave. In the second phase, the shape curve of the projectile after impact is convex. For the projectile of Copper 145-hard-H02, the first phase's length is 0.32 cm. The length of the second phase is 2.60 cm. The length of the third phase is 6.788 cm. In the first phase, the shape curve of the projectile after impact is concave. In the second phase, the shape curve of the projectile after impact is convex.

For the projectile of Steel C1045, the first phase's length is 0.24 cm. The length of the second phase is 2.1532 cm. The length of the third phase is 4.422 cm. In the first phase, the shape curve of the projectile after impact is concave. In the second phase, the

shape curve of the projectile after impact is convex. These three tests support firmly our theoretical model and investigation.

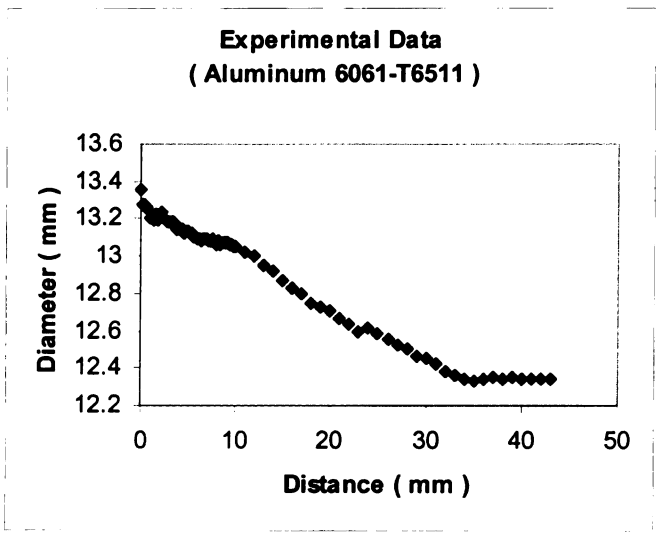

Figure. 3-Projectile-1 –Aluminum 6061-T6511

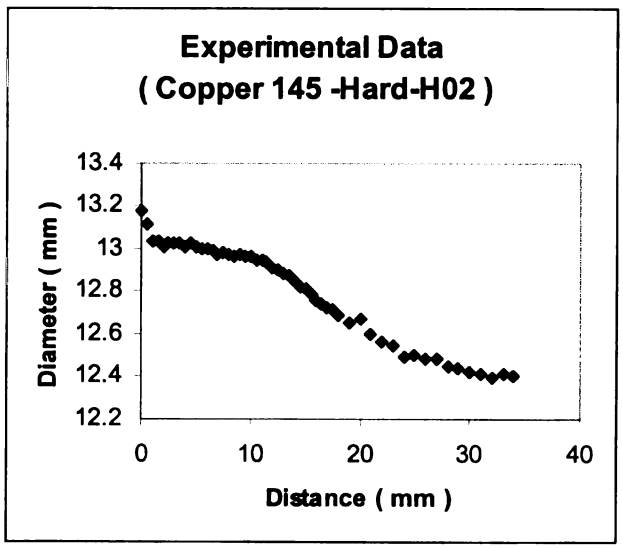

Figure.3-Projectile-2 -Copper 145-Hard-H02

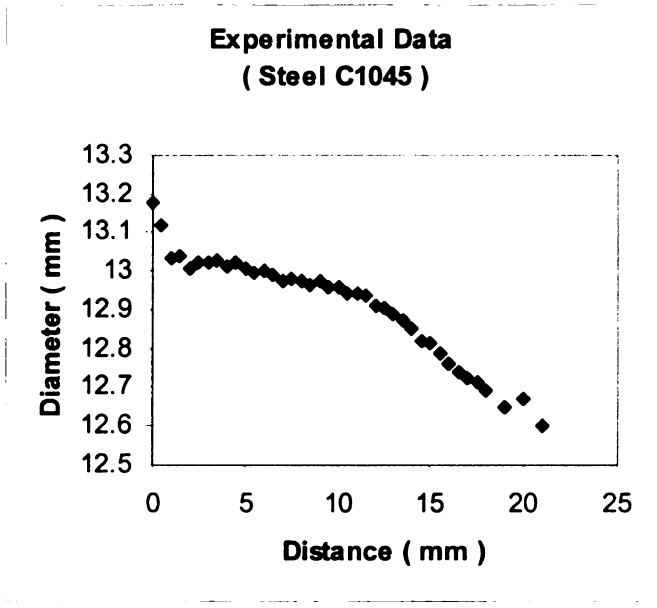

Figure.3-Projectile-3- Steel C1045

3.4 Computation And Discussion

3.4.1 Material: Aluminum 6061-T6511

The physical and measured parameters, geometrical parameters, and computed parameters of the projectile are as follows:

Density: ρ=2700 kg/m^3
Static Yield Stress: $\sigma_s = 275MPa$
Young Modulus: $E = 69 \times 10^9 N/m^2$
Elastic Wave Velocity: $C_e = 5055m/s$
Impact Velocity: $V_0 = 93m/s$
Original Length: $L = 7.8232cm$
Final Length: $L_0 = 7.5727cm$
$L_p = 3.4282cm$
$L_e = 4.12cm$
Projectile Diameter: $D_1 = 1.22936cm$
Measured $h = 0.275cm$, Computed $h = 0.299cm$
$h_d = 0.2565cm$, $2R_h = 1.3195cm$, $2R_0 = .1335cm$
$\Delta L = (L - L_0) - (h - h_d) = 0.269cm$
$t_p = (L + L_e)/C_e = 23.63 \times 10^{-6} s$
$t_h = h/V_0 = 29.55 \times 10^{-6} s$

In the first phase, the radius of projectile is obtained from Equation (3.20)

$$r = 0.6968e^{-0.37\frac{x}{h}}, \qquad 0 \le x \le 0.299\ cm$$

Table 3.4.1.1 shows the measured values of r and theoretically computed values of r. Figure 3.4.1.1 shows the theoretical values and the actual values. The series 1 represents the computed theoretical curve and the series 2 represents the measured curve. In order to calculate the dynamic stress in this phase, the Johnson-Cook model is used. According to analysis in the first phase, the velocity of the particle is a constant. This is then an adiabatic phase. The thermal effect can be omitted. Because the strain is a constant, 0.148, the effect of the strain rate is not considered. So the Johnson-Cook model can be written a $\sigma = (A + B\varepsilon^n)$, where $A = 275$ MPa, $B = 426$ MPa and $n = 0.34$. From the computed strain and the above model, the dynamic stress in the first phase of Aluminum 6061-T6511 can be computed as shown in Table 3.4.1.1.1. The relationship of stress σ_{p1} and x is shown in Figure 3.4.1.1.1

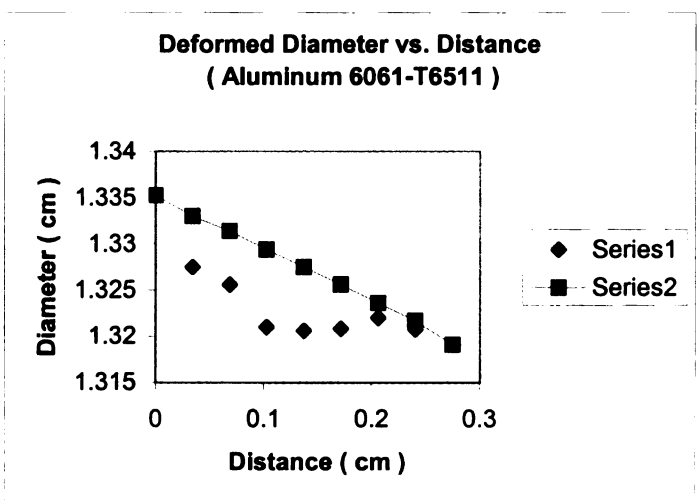

Figure 3.4.1.1 Deformed Diameter vs. Distance (Aluminum)

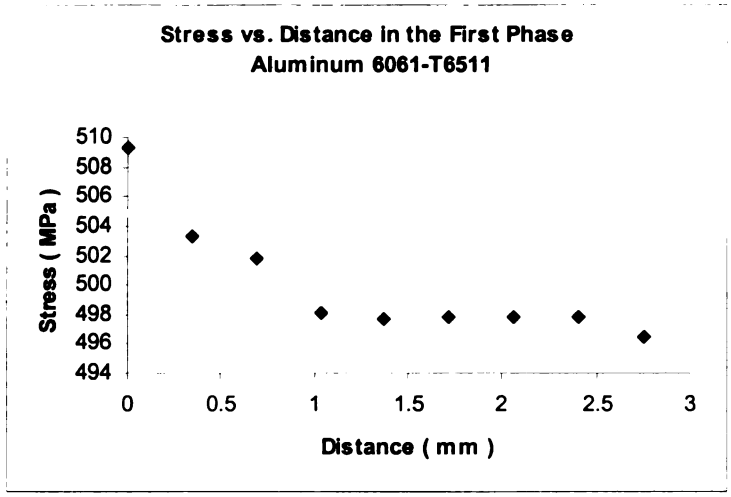

Figure 3.4.1.1.1 Stress vs. Distance in the First Phase (Aluminum)

In Figure 3.4.1.1, the experimental and computed results indicate that the radius of the projectile is convex. This result matches our theoretical analysis. In the first phase, the strain is approximately 0.148 except near to impact end. The stress is about 498 MPa. It indicates that the strain is a constant in the first phase. This result matches our theoretical investigation well.

In the second phase, according to Equation (3.33) and the above parameters of the projectile, we have

$$\begin{bmatrix} 0.275 & -1.5613 & 29.56 \\ 0 & -0.0093 & 1 \\ 3.7032 & -10.56 & 23.63 \end{bmatrix} \begin{bmatrix} C_1 \\ C_2 \\ C_3 \end{bmatrix} = \begin{bmatrix} 0.2565 \\ 0.0093 \\ 0.269 \end{bmatrix}$$

Solve the above matrix equation. Then

$$C_1 = 0.1321,\ C_2 = 0.0426\mu/\sec,\ C_3 = 0.0097cm/\mu\sec$$

Dynamic Yielding Stress σ:

$$\sigma = \frac{2700 \times 0.0426}{2} e^{\frac{2\times(0.1321)}{0.0426}} \times 10^4 = 283Mpa$$

From Equations (3.24), (3.25) and (3.35), we have:

a) Plastic Dynamic Stress σ:

$$\sigma = 14.91 \times (e^{\frac{2(\varepsilon - 0.1321)}{0.0426}}) \quad (Pa)$$

b) Plastic Wave Propagation Velocity C_p:

$$C_p = e^{\frac{\varepsilon + 0.1321}{0.0426}} \quad (cm/\mu\sec)$$

c) Displacement Function $u(x,t)$:

$$u(x,t) = 0.1321x + 0.0426x(\ln C_p - 1) + 0.0097t \quad (cm)$$

d) Plastic Strain ε:

$$\varepsilon = 0.1321 + 0.0426 \ln C_p$$

e) Particle Velocity v:

$$v = -0.0426C_p + 0.0097 \quad (cm/\mu\sec)$$

f) Diameter of Projectile:

$$D = 1.22936(1 + \frac{0.1321}{2} + \frac{0.0426}{2} \ln C_p) \quad (cm)$$

$$0.275cm \le x \le 3.7032cm$$

Table 3.4.1.2 gives the values of the strain ε, the stress σ, C_p and the diameter in the second phase from $0.764cm \le D \le 0.9626cm$. Figure 3.4.1.2, Figure 3.4.1.3, Figure 3.4.1.4 and Figure 3.4.1.5 show the relationship among variables.

Figure 3.4.1.2 indicates the relationship between the diameter and the stress. From this figure, the stress decreases gradually along the projectile. In the second phase,

Figure 3.4.1.3 indicates that the dynamic stress decays as the strain decreases. When the strain is very small, the stress can be expressed approximately by a straight line. Figure 3.4.1.4 indicates that in the second phase the shape of the projectile is like a mushroom after impact. The reason for the mushroom shape is due to the velocity of the plastic wave propagation. However, if the velocity of the plastic wave is higher (about above 4000 m/s), the shape of projectile can be approximately replaced by a straight line. This explains why Taylor could use a straight line to substitute the curve of the projectile and good agreement was obtained. Table 3.4.1.2 gives the value when the static stress is 283 MPa. It matches well the given static stress value of Aluminum 6061–T6511, 275 MPa. The Lagrangian Diagram of the plastic wave propagation is shown in Figure 3.4.1.5. The data for Lagrangian Diagram is shown in Table Lagrangian Diagram Data-1. This one describes the propagation of the plastic wave in the projectile after impact using the displacement and time as variables. From Table 3.4.1.1.1, the impact velocity and Equation (3.3), $c_1 = 0.0628 \times 10^{-6}$ cm/s.

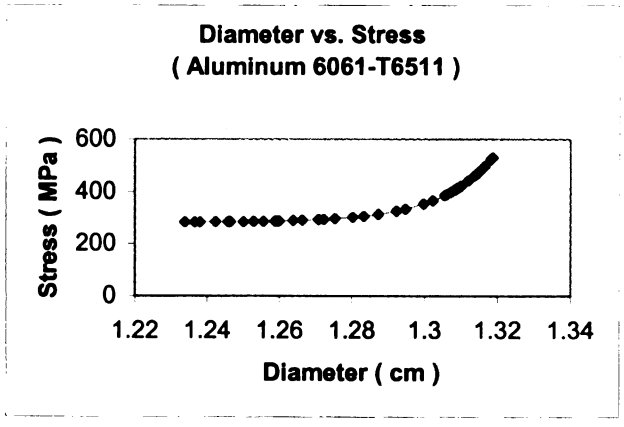

Figure 3.4.1.2 Diameter vs. Stress (Aluminum)

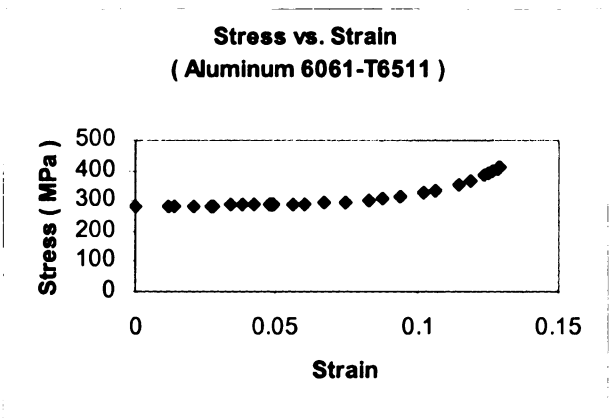

Figure 3.4.1.3 Stress vs. Strain (Aluminum)

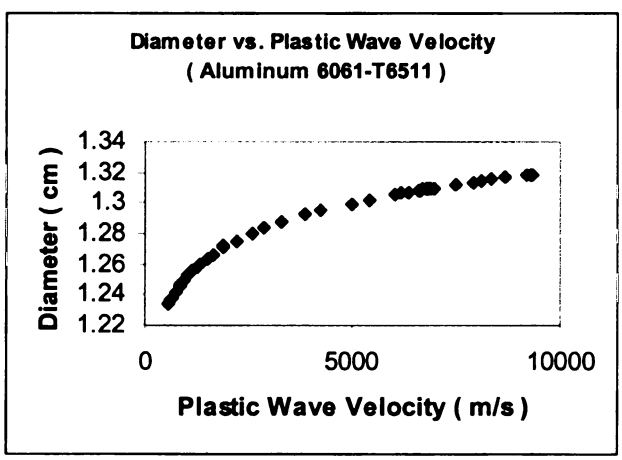

Figure 3.4.1.4 Diameter vs. Plastic Wave Velocity (Aluminum)

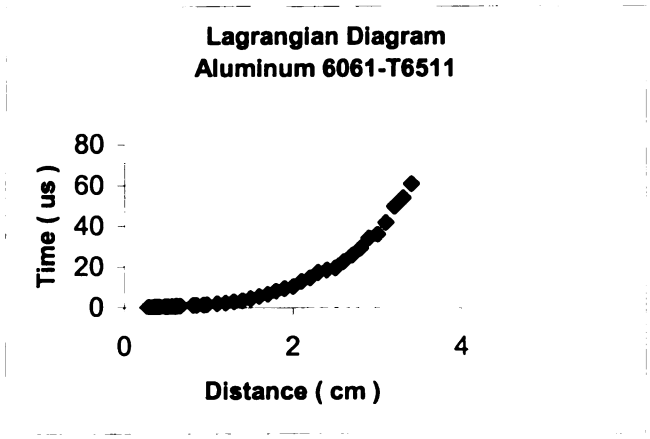

Figure 3.4.1.5 Lagrangian Diagram (Aluminum)

3.4.2 Material: Copper 145-Hard-H02

The physical and measured parameters, geometrical parameters and computed parameters of the projectile are as follows:

Density: $\rho = 8960 kg/m^3$
Static Yield Stress: $\sigma_s = 32\,MPa$
Young Modulus: $E = 110 \times 10^9\, N/m^2$
Elastic Wave Velocity: $C_e = 3504 m/s$
Impact Velocity: $V_0 = 49.56 m/s$
Original Length: $L = 9.525 cm$
Final Length: $L_0 = 9.4425 cm$
$L_p = 2.60 cm$
$L_e = 6.788 cm$
Projectile Diameter: $D_1 = 1.22936 cm$
Measured $h = 0.335 cm$; Computed $h = 0.363 cm$
$h_d = 0.320 cm$
$2R_h = 1.3025 cm$
$2R_0 = 1.3178 cm$
$\Delta L = (L - L_0) - (h - h_d) = 0.1105 cm$
$t_p = (L + L_e)/C_e = 46.56 \times 10^{-6} s$
$t_h = h/V_0 = 71.23 \times 10^{-6} s$

In the first phase, the diameter of projectile can be obtained using Equation (3.20):

$$D = 1.31775e^{\frac{0.005x}{h}}, \qquad 0 \le x \le 0.335\,cm$$

Table 3.4.2.1 shows the measured values of D and theoretically computed values of D. This table indicates the measured diameter matches the computed diameter very well. Figure 3.4.2.1 is drawn from Table 3.4.2.1. The series 2 represents the computed theoretical curve and the series 1 represents the measured curve. In Figure 3.4.2.1, the experimental and computed results indicate that the radius of the projectile is convex. This result matches our theoretical analysis. In this phase, the strain is approximately 0.12 except near the impact end. It indicates that the strain is a constant in the first phase. This result matches our theoretical investigation well.

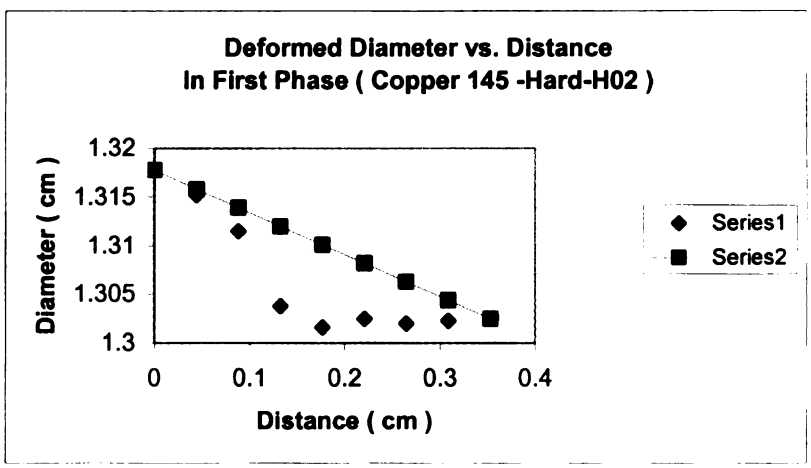

Figure 3.4.2.1 Deformed Diameter vs. Distance in First Phase (Copper)

In the second phase, according to Equation (3.33) and the above parameters, we have

$$\begin{bmatrix} 0.353 & -2.226 & 71.23 \\ 0 & -0.004956 & 1 \\ 2.737 & -10.49 & 46.56 \end{bmatrix} \begin{bmatrix} C_1 \\ C_2 \\ C_3 \end{bmatrix} = \begin{bmatrix} 0.325 \\ 0.004956 \\ 0.1105 \end{bmatrix}$$

Solve the above matrix, then

$$C_1 = 0.0420,\ C_2 = 0.0229\ (\mu\text{sec}/cm)\ \ C_3 = 0.0051\ (cm/\mu\text{sec});$$

Dynamic Yielding Stress:

$$\sigma = \frac{8960 \times 0.0229}{2} e^{\frac{2\times(0.0420)}{0.0229}} \times 10^4 = 33\ (MPa)$$

From Equations (3.24), (3.25) and (3.35), we have:

a) Plastic Dynamic Stress σ:

$$\sigma = 102.59 \times (e^{\frac{2(\varepsilon - 0.0420)}{0.0229}})\ (Pa)$$

b) Plastic Wave Propagation Velocity C_p:

$$C_p = e^{\frac{\varepsilon - 0.0420}{0.0229}}\ (cm/\mu\text{sec})$$

c) Displacement Function $u(x,t)$:

$$u(x,t) = 0.0420x + 0.0229x(\ln C_p - 1) + 0.0051t\ (\ cm/\mu\text{sec}\ )$$

d) Plastic Strain ε:

$$\varepsilon = 0.0420 + 0.0229 \ln C_p$$

e) Particle Velocity v:

$$v = -0.0229 C_p + 0.0051 (\ cm/\mu\text{sec}\ )$$

f) Diameter of Projectile: $D = 1.22936(1 + \frac{0.0420}{2} + \frac{0.0229}{2} \ln C_p)\ (cm)$

$$0.325 \le x \le 2.925\ cm$$

Table 3.4.2.2 gives the values of the strain ε the stress σ, C_p and the diameter in the second phase from $1.22936\ cm \le D \le 1.3025\ cm$.

In the second phase, from Figure 3.4.2.2, the maximum strain is 0.1194. In the first phase, the strain value is about 0.12, this indicates the strain is continuous from the first phase to the second phase. The relationship between the stress and the strain is shown in Figure 3.4.2.2. From this figure, the stress decreases gradually along the projectile. In the second phase, Figure 3.4.2.3 indicates that the dynamic stress decays as the plastic wave propagates, the shape of the projectile is like a mushroom after impact, too. In Figure 3.4.2.4, the dynamic stress, the dynamic strain decay sharply after the propagation of the plastic wave around the interface of the first phase and the second phase. The computed static stress of Copper 145-Hard-H02 is 33 MPa. It matches the given static yielding stress of the material very well. When the propagation of the plastic wave in the projectile stops, its velocity is 1597 m/s. As the propagation of the plastic wave, the decaying will gradually become slow. Figure 3.4.2.5 shows the Lagrangian Diagram of the plastic wave propagation. The data for Lagrangian Diagram are shown in Table Lagrangian Diagram Data-1. From Table 3.4.2.1.1, the impact velocity and Equation (3.3), $c_1 = 0.0413 \times 10^{-6}$ cm/s.

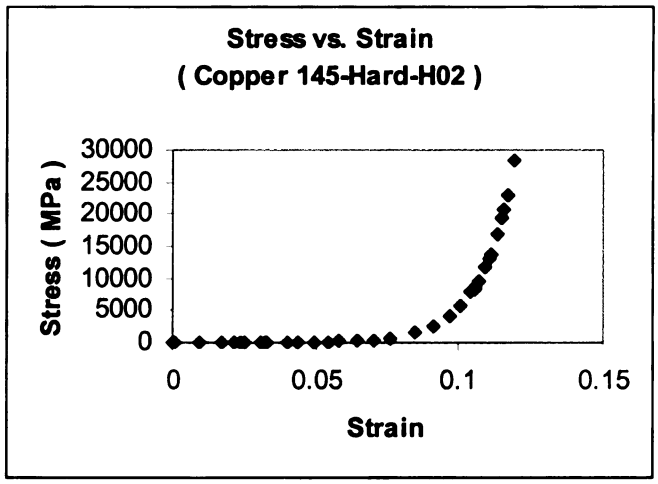

Figure 3.4.2.2 Stress vs. Strain (Copper)

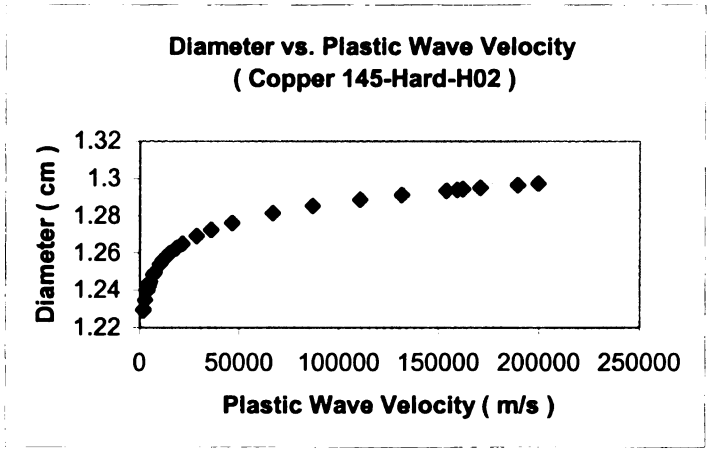

Figure 3.4.2.3 Diameter vs. Plastic Wave Velocity (Copper)

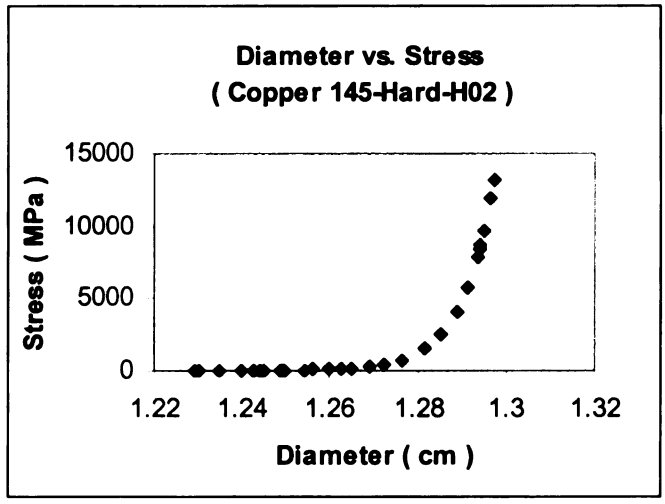

Figure 3.4.2.4 Diameter vs. Stress (Copper)

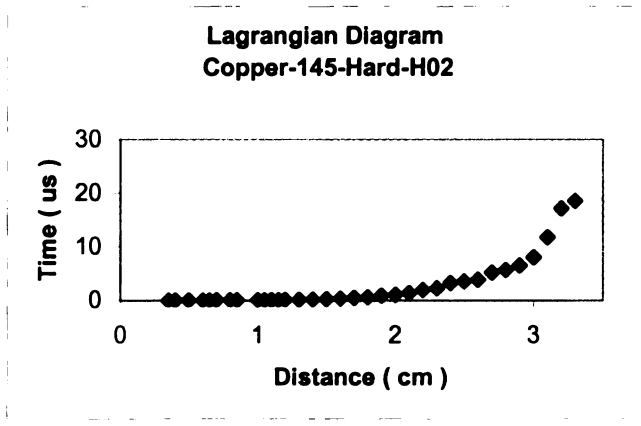

Figure 3.4.2.5 Lagrangian Diagram (Copper)

3.4.3 Material: Steel C1045

The physical and measured parameters, geometrical parameters and computed parameters of the projectile are as follows:

Density: $\rho = 7870 kg/m^3$
Static Yield Stress: $\sigma_s = 585 MPa$
Young Modulus: $E = 200 \times 10^9 N/m^2$
Elastic Wave Velocity: $C_e = 5041 m/s$
Impact Velocity: $V_0 = 57.85 m/s$
Original Length: $L = 7.8232 cm$
Final Length: $L_0 = 7.683 cm$
$L_p = 2.1532 cm$
$L_e = 5.44 cm$
Projectile Diameter: $D_1 = 1.22936 cm$
Measured $h = 0.240 cm$; Computed $h = 0.223 cm$
$h_d = 0.211 cm$
$2R_h = .125925 cm$
$2R_0 = 1.26925 cm$
$\Delta L = (L - L_0) - (h - h_d) = 0.1012 cm$
$t_p = (L + L_e)/C_e = 26.31 \times 10^{-6} s$
$t_h = h/V_0 = 39.76 \times 10^{-6} s$

In the first phase, the diameter of projectile is obtained using Equation (3.20):

$$D = 1.26925 e^{\frac{0.0079x}{h}}, \qquad 0 \le x \le 0.24\ cm$$

Table 3.4.3.1 shows the measured values of D and theoretically computed values of D. Figure 3.4.3.1 indicates the measured diameter matches the computed diameter very well. The series 2 represents the computed theoretical curve and the series 1 represents the measured curve. In Figure 3.4.3.1, the experimental and computed results indicate that the radius of the projectile is convex. In this phase, the strain is approximately 0.052 except near to impact end. It indicates that the strain is approximately a constant in the first phase.

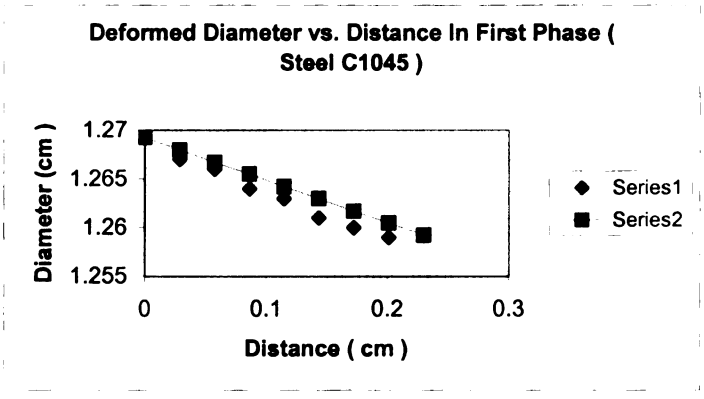

Figure 3.4.3.1 Deformed Diameter vs. Distance in the First Phase (Steel)

In the second phase, according to Equation (3.33) and the above parameters, we have

$$\begin{bmatrix} 0.23 & -1.415 & 39.76 \\ 0 & -0.005785 & 1 \\ 2.3832 & -8.1064 & 26.31 \end{bmatrix} \begin{bmatrix} C_1 \\ C_2 \\ C_3 \end{bmatrix} = \begin{bmatrix} 0.211 \\ 0.005785 \\ 0.1212 \end{bmatrix}$$

Solving the above matrix, then

$$C_1 = 0.1151; \quad C_2 = 0.0384 \mu\text{sec}/cm; \; C_3 = 0.0060\, cm/\mu\text{sec}.$$

Dynamic Yielding Stress:

$$\sigma = \frac{7870 \times 0.0384}{2} e^{\frac{2\times(0.1151)}{0384}} \times 10^4 = 613 \ (MPa)$$

From Equations (25), (24), (30), (43) and (26) in Section 2, we have:

a) Plastic Wave Propagation Velocity C_p:

$$C_p = e^{\frac{\varepsilon - 0.1151}{0.0384}} \ (cm/\mu\text{sec})$$

b) Plastic Dynamic Stress σ:

$$\sigma = 15.11 \times (e^{\frac{2(\varepsilon - 0.1151)}{0.0384}}) \ (Pa)$$

c) Displacement Function $u(x,t)$:

$$u(x,t) = 0.1151x + 0.0384x(\ln C_p - 1) + 0.006t \ (\ cm\ )$$

d) Plastic Strain ε:

$$\varepsilon = 0.1151 + 0.0384 \ln C_p$$

e) Particle Velocity v:

$$v = -0.1151 C_p + 0.006 \ (\ cm / \mu \sec\ )$$

f) Diameter of Projectile:

$$D = 1.22936(1 + \frac{0.1151}{2} + \frac{0.0384}{2} \ln C_p) \ (\ cm\ )$$

$$0.211 cm \le x \le 2.3642 cm$$

Table 3.4.3.2 gives the values of the strain ε the stress σ, C_p and the diameter in the second phase from $1.22936\ cm \le D \le 11.25925\ cm$. For this test, although the impact velocity is 59 m/s, its maximum strain is much less than the maximum one in Aluminum 6061-T6511. When the plastic wave stops propagating, its velocity is 499 m/s. The computed static yielding stress is 612 MPa and the given static yielding stress is 585 MPa. These data match very well. The Lagrangian Diagram of the plastic wave propagation is shown in Figure Lagrangian Diagram (Steel C1045). The data for Lagrangian Diagram are shown in Table Lagrangian Diagram Data-3. From Figure 3.4.3.1, Figure 3.4.3.2 and Figure 3.4.3.3 indicate the relationships of the diameter vs. the velocity of the plastic wave, the diameter vs. stress and the stress vs. strain. From Table 3.4.3.1.1, the impact velocity and Equation (3.3), $c_1 = 0.11125 \times 10^{-6}$ cm/s.

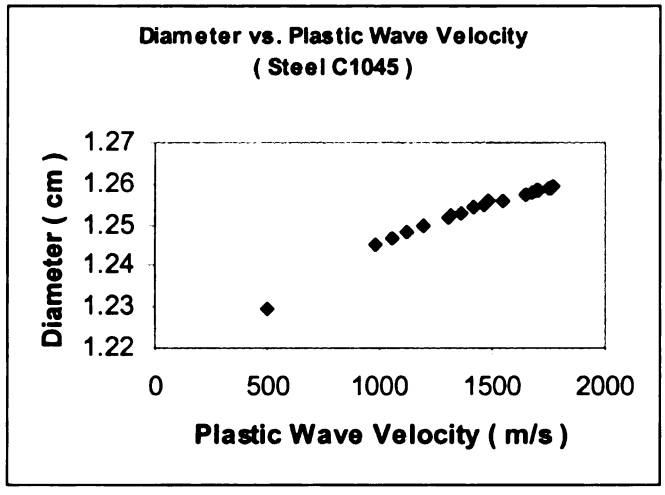

Figure 3.4.3.2 Diameter vs. Plastic Wave velocity (Steel)

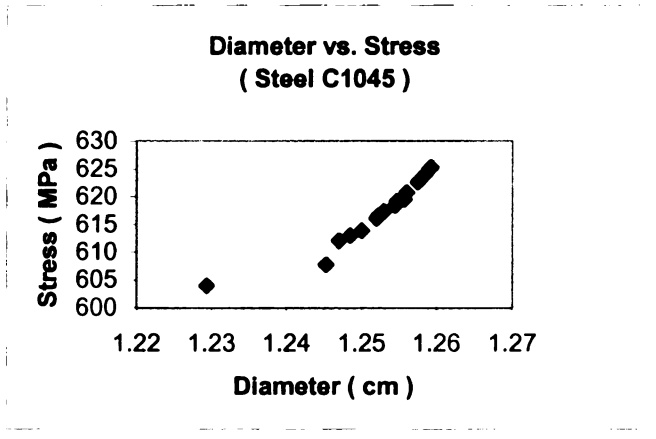

Figure 3.4.3.3 Diameter vs. Stress (Steel)

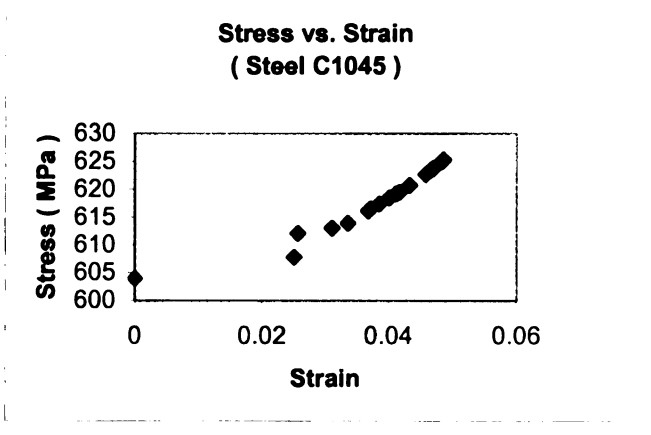

Figure 3.4.3.4 Stress vs. Strain (Steel)

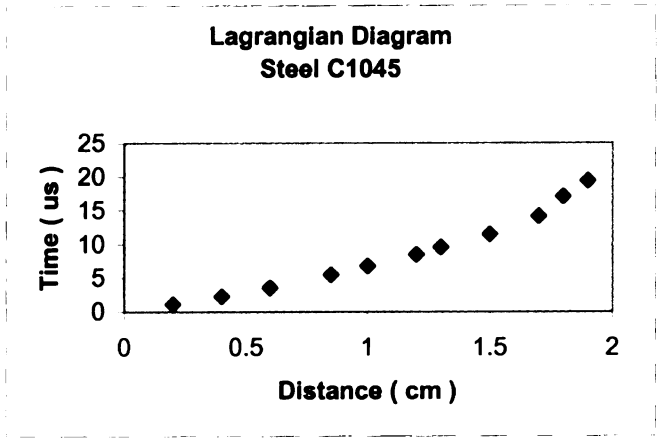

Figure 3.4.3.5 Lagrangian Diagram (Steel)

3.5 Results

1. Three test results indicate that the propagation of the plastic wave can be divided into two phases. The shape curve of the projectile in the first phase is concave, and the shape curve of the projectile in the second phase is convex. The strain is a constant in the first phase. This conclusion is approximate near the impact end.

2. When using our model to determine the dynamic stress of the projectiles, the results are as follows:

Material	Static Yield (MPa)	Computed Yield Stress (MPa)	Discrepancies
Aluminum 6061-T6511	275	283.92	3.24%
Copper 145-Hard-H02	32	33	3.125%
Steel C1045	585	612	4.6%

This table indicates that the model can be used to calculate the dynamic stress of the projectile.

3. Many models proposed by other people cannot predict that the shape curve of the projectile in the second phase is convex, as in Johnson-Cook model. These models can be used in the first phase.

4. Using the model proposed by the author, the dynamic stress, dynamic strain, the velocity of the propagation of the plastic wave and the velocity of the particle can be calculated.

5. In order to verify our theoretical investigation, three of the Taylor tests are carried out for Copper 145-Hard-H02, Aluminum 6061-T6511, and Steel C1045. The experimental results show good agreement between the shape curves of the projectiles predicted by the constitutive equation and experimental results.

6. It should be pointed out that the model proposed by the author does not consider the effect of the strain rate of the propagation of the plastic wave in the projectile. So, the model is not very accurate around the interface between the first phase and the second phase. This will be improved in the next chapters.

3.6 Tables

Table-Experimental Data-1-Aluminum 6061-T651

Distance x (mm)	Diameter (mm)
0	13.3525
0.2	1.3275
0.4	1.3275
0.6	13.27
0.8	13.2425
1	13.2075
1.2	13.2175
1.4	13.195
1.6	13.22
1.8	13.1975
2	13.22
2.2	13.23

2.4	13.2075
2.6	13.195
2.8	13.1875
3	13.1855
3.2	13.1845
3.4	13.1825
3.6	13.165
3.8	13.1475
4	13.1525
4.2	13.145
4.4	13.145
4.6	13.123
4.8	13.1375
5	13.13
5.2	13.12
5.4	13.12
5.6	13.1
5.8	13.1075
6	13.095
6.2	13.0975
6.4	13.0825
6.6	13.09
6.8	13.0975
7	13.095
7.2	13.08
7.4	13.0875
7.6	13.0925
7.8	13.0875
8.2	13.0875
8.4	13.06
8.6	13.0725
8.8	13.0675
9	13.07
9.2	13.0725
9.4	13.0625
9.6	13.0625
9.8	13.055
10	13.055
11	13.0225
12	12.9975
13	12.9475
14	12.9225
15	12.8725
16	12.8325

17	12.8025
18	12.7525
19	12.7225
20	12.7075
21	12.6625
22	12.6375
23	12.5975
24	12.6125
25	12.5875
26	12.555
27	12.5275
28	12.5
29	12.4625
30	12.4575
31	12.4225
32	12.38
33	12.365
34	12.3375
35	12.3325
36	12.3425
37	12.35
38	12.34
39	12.35
40	12.34
41	12.34
42	12.3425
43	12.3375

Table-Experimental Data-2-Copper 145-Hard-H02

Distance x (mm)	Diameter (mm)
0	13.1775
0.5	13.12
1	13.035
1.5	13.04
2	13.0075
2.5	13.025
3	13.0225
3.5	13.0275
4	13.0125
4.5	13.0225
5	13.005

5.5	12.9975
6	13
6.5	12.99
7	12.975
7.5	12.9825
8	12.9725
8.5	12.965
9	12.9725
9.5	12.96
10	12.96
10.5	12.9425
11	12.945
11.5	12.935
12	12.9125
12.5	12.905
13	12.8875
13.5	12.8725
14	12.8525
14.5	12.8225
15	12.815
15.5	12.7875
16	12.7625
16.5	12.74
17	12.725
17.5	12.7125
18	12.6925
19	12.65
20	12.6725
21	12.6
22	12.5625
23	12.5425
24	12.4975
25	12.505
26	12.485
27	12.4825
28	12.4475
29	12.44
30	12.425
31	12.415
32	12.3945
33	12.415
34	12.4025

Table-Experimental Data-3- Steel C1045

Distance x (mm)	Diameter (mm)
0	12.6925
0.5	12.6725
1	12.6
1.5	12.5975
2	12.5925
2.5	12.5925
3	12.58
3.5	12.5925
4	12.58
4.5	12.59
5	12.585
5.5	12.5925
6	12.5825
6.5	12.595
7	12.5925
7.5	12.59
8	12.585
8.5	12.595
9	12.585
9.5	12.565
10	12.5575
11	12.5475
12	12.545

Table 3.4.1.1 Measured Diameter vs. Computed Diameter (Aluminum)

Distance x cm	Measured Diameter cm	Computed Diameter cm
0.00	1.33525	1.33525
0.34	1.3275	1.333
0.69	1.3256	1.3314
1.03	1.321	1.3294
1.38	1.3206	1.3275
1.72	1.3208	1.3256
2.06	1.322	1.3236
2.14	1.32075	1.3217
2.75	1.3191	1.3191

Table 3.4.1.1.1 Stress vs. Strain (Aluminum)

x (mm)	ε_{p1}	σ_{p1} (MPa)
0.00	0.1723	509.33
0.34	0.1596	503.31
0.69	0.1565	501.79
1.03	0.1491	498.09
1.38	0.1484	497.74
1.72	0.1487	497.74
1.72	0.1487	497.88
2.06	0.1507	498.90
2.41	0.1486	497.84
2.75	0.1459	496.45

Table 3.4.1.2 Stress, Strain, Plastic Wave Velocity vs. Diameter (Aluminum)

$D(cm)$	$C_p(m/s)$	ε	$\sigma(MPa)$
1.31875	13644	0.1454	813
1.31855	13568	0.1451	806
1.31825	13410	0.1446	795
1.3165	12557	0.1418	731
1.31525	11953	0.1397	689
1.3145	11621	0.1385	667
1.31375	11298	0.1373	646
1.312	10554	0.1344	600
1.31	9790	0.1312	556
1.3095	9608	0.1304	546
1.30925	9519	0.13	541
1.309	9430	0.1296	536
1.30875	9341	0.1292	531
1.3085	9233	0.1287	525
1.30825	9147	0.1283	521
1.30725	8809	0.1267	504
1.30625	8485	0.1251	488
1.3055	8249	0.1239	477
1.30225	7284	0.1186	434
1.29975	6616	0.1145	408
1.29475	5470	0.1064	368
1.29225	4968	0.1023	357
1.28725	4108	0.0942	331
1.28325	3527	0.0877	319
1.28025	3143	0.0828	308
1.27525	2599	0.0747	303
1.27225	2184	0.0673	297
1.27075	1840	0.0673	297
1.26625	1671	0.06	293
1.26375	1435	0.0559	291
1.25975	1408	0.0494	289.76

1.25925	1382	0.0486	289.55
1.25875	1220	0.0478	289.34
1.2555	1100	0.0425	288
1.25275	1050	0.0381	290
1.25	990	0.0336	289.5
1.24625	858	0.0275	286.6
1.24575	842	0.0267	285.96
1.24225	736	0.021	285.46
1.238	626	0.0141	284.28
1.2365	590	0.0116	284.18
1.23375	450	0	283.92

Table Lagrangian Diagram Data-1
Aluminum 6011-T6511

Distance (cm)	Time (μs)
0.28	0.299305
0.3	0.322824
0.34	0.369525
0.36	0.414603
0.38	0.448642
0.4	0.480192
0.42	0.516859
0.48	0.605525
0.5	0.646663
0.52	0.67253
0.56	0.8
0.6	0.87146
0.62	0.907893
0.66	0.974601
0.82	1.231046
0.86	1.345642
0.94	1.520544
0.98	1.624938
1.1	2.031394
1.2	2.407222
1.3	3.077652
1.4	3.600823
1.5	4.553734
1.6	5.545927
1.7	6.508423
1.8	8.130081
1.9	9.481038
2	10.48768
2.1	12.7815
2.2	14.55027

2.3	17.3716
2.4	18.41903
2.5	19.516
2.6	22.6087
2.7	25.71429
2.8	29.19708
2.9	34.23849
3	36.01441
3.1	41.77898
3.2	49.68944
3.3	53.83361
3.4	60.71429

Table 3.4.2.1 Measure Diameter vs. Computed Diameter (Copper)

Distance x (cm)	Measured Diameter (cm)	Computed Diameter (cm)
0	1.31775	1.31775
0.044125	1.3152	1.3158
0.08825	1.3115	1.3139
0.13238	1.3038	1.3120
0.1765	1.3016	1.3101
0.22063	1.3025	1.3082
0.26475	1.3020	1.3063
0.30887	1.3023	1.3044
0.353	1.3025	1.3025

Table 3.4.2.1.1 Strain vs. Distance (Copper)

Distance x (cm)	Strain
0.00	0.1438
0.044125	0.1396
0.08825	0.1336
0.13238	0.1211
0.1765	0.1175
0.22063	0.11898
0.26475	0.118175
0.30887	0.11866
0.353	0.1189

Table 3.4.2.2 Stress, Strain, Plastic Wave Velocity vs. Diameter (Copper)

$D(cm)$	$C_p(m/s)$	ε	$\sigma(MPa)$
1.30275	293682	0.1194	34699
1.30125	264461	0.117	28144
1.3005	249866	0.1157	25094
1.3	241288	0.1149	23400
1.299	225005	0.1133	20349
1.2975	202617	0.1109	16534
1.2973	198241	0.1104	15796
1.2965	188121	0.1092	14257
1.295	169403	0.1068	11567
1.2943	160754	0.1056	10419
1.294	157971	0.1052	10063
1.2935	151822	0.1043	9505
1.29125	129788	0.1007	6803
1.28875	108512	0.0966	4766
1.2853	84601	0.0909	2809
1.2815	64817	0.0848	1722
1.27625	44719	0.0763	836
1.2725	34261	0.0702	504
1.26925	27182	0.0649	330
1.265	20111	0.058	195
1.26275	17116	0.0543	150
1.26	13875	0.0495	110
1.2563	10770	0.0437	79
1.2543	9365	0.0405	68
1.2498	6809	0.0332	51
1.249	6462	0.032	49
1.2485	6213	0.0311	48
1.2448	4759	0.025	42
1.244	4516	0.0238	41
1.2425	4067	0.0214	39
1.24	3400	0.0173	37
1.235	2387	0.0092	35
1.23	1668	0.001	34
1.2294	1597	0	33

Table-Lagrangian Diagram Data-2
Copper-145-Hard-02

Distance (cm)	Time (μs)
0.35	0.011966
0.4	0.015178
0.5	0.019989
0.6	0.024835
0.65	0.028841
0.7	0.034474
0.8	0.04009
0.85	0.044875
1	0.05859
1.05	0.06482
1.1	0.069098
1.15	0.074785
1.2	0.091289
1.3	0.117634
1.4	0.161584
1.5	0.224692
1.6	0.345252
1.7	0.476097
1.8	0.631889
1.9	0.896311
2	1.103205
2.1	1.402431
2.2	1.906908
2.3	2.290837
2.4	3.268864
2.5	3.587315
2.6	3.862725
2.7	5.205321
2.8	5.687589
2.9	6.538895
3	8.04721
3.1	11.77364
3.2	17.2043
3.3	18.54975

Table 3.4.3.1 Measured Diameter vs. Computed Diameter (Steel)

Distance x (cm)	Measured Diameter (cm)	Computed Diameter (cm)
0	1.26925	1.26925
0.02875	1.267	1.268
0.0575	1.266	1.2667
0.08625	1.264	1.2655
0.115	1.263	1.2642
0.14375	1.261	1.263
0.1725	1.26	1.2617
0.20125	1.259	1.2605
0.23	1.25925	1.25925

Table 3.4.3.1.1 Strain vs. Distance (Steel)

Distance x (cm)	Strain
0.00	0.06489
0.02875	0.0612
0.0575	0.0596
0.08625	0.0563
0.115	0.0547
0.14375	0.0515
0.1725	0.0498
0.20125	0.0482
0.23	0.0486

Table 3.4.3.2 Stress, Strain, Plastic Wave Velocity vs. Diameter (Steel)

$D(cm)$	$C_p(m/s)$	ε	$\sigma(MPa)$
1.25925	1010.3	0.0486	630.99
1.25908	1010	0.0484	630.79
1.25905	1009.9	0.0483	630.69
1.259	1008.8	0.0482	630.60
1.2583	1008.7	0.0471	630.06
12.5825	1008.6	0.047	629.56
1.2582	1008.5	0.0469	629.47
1.258	1008.2	0.0466	629.38
1.2575	1007.4	0.0458	628.42
1.256	1005	0.0433	626.41
1.2557	1003.3	0.0417	625.26
1.2547	1002.8	0.0412	624.92
1.2545	1001.7	0.0401	624.19
1.253	1000.1	0.0385	623.22
1.2522	999	0.0372	622.48
1.252	998	0.0368	622.27
1.25	995	0.0336	620.69
1.2485	993	0.0311	619.63
1.247	987	0.0257	617.76
1.24725	986	0.0251	617
1.22936	499	0	612

Table Lagrangian Diagram Data-3
Steel C1045

Distance (cm)	Time (μs)
0.2	1.1293
0.4	2.2779
0.6	3.5356
0.85	5.5087
1	6.7613
1.2	8.47457
1.3	9.5658
1.5	11.5119
1.7	14.20217
1.8	17.0778
1.9	19.40756

CHAPTER 4

ANALYSIS FOR PLASTIC DYNAMIC MODELS IN THE TAYLOR TEST

Today, the Taylor test has not often been used for its original purpose of obtaining dynamic, yield stress of materials. It has come into its own purpose in recent years for checking constitutive equations by comparing the shapes of projectiles with predictions. From the experimental results, there are three main characteristics in the Taylor test. The first one is that in the second zone of specimens the shapes appear to be like mushroom. The second one is that as the propagation of the plastic wave the strain and the velocity of the plastic wave will decrease. The third one is when the propagation of the plastic wave stops the strain is zero but the velocity of the plastic wave propagation is not zero, either. The constitutive equation proposed in this thesis has predicted the three characteristics. In this chapter, we will use models proposed by other persons to verify whether or not these models can predict the three characteristics in the specimens of the Taylor test.

4.1 Analysis for Power Law Plasticity Model

This is an isotropic plasticity model with rate effect, which uses a power law hardening rule. Elastoplastic behavior with isotropic hardening is provided by this model. The yield stress is a function of plastic strain and can be written as

$$\sigma = k(\varepsilon_e + \varepsilon)^n$$

where ε_e is the elastic strain to yield , ε is the effective plastic strain, k is strength

coefficient and $n < 1$ is hardening exponent.

When this model is used to describe the propagation of plastic wave in the second zone of the specimen, the procedures of solving the equation of plastic wave in Appendix -D is followed. Based on this model, it yields

$$T(\varepsilon) = \frac{d\sigma}{d\varepsilon} = nk(\varepsilon_e + \varepsilon)^{n-1}$$

Let $\varepsilon = f(C_p)$, where $C_p = \frac{x}{t}$ is the velocity of the plastic wave. Then

$$T[f(C_p)] = nk[\varepsilon_e + f(C_p)]^{n-1} \qquad (4.1)$$

Taking Equation (4.1) back into Equation (D-5), it yields

$$\rho C_p^2 = nk[\varepsilon_e + f(C_p)]^{n-1}$$

$$\Rightarrow \quad \varepsilon = f(C_p) = (\frac{\rho C_p}{nk})^{\frac{1}{n-1}} - \varepsilon_e \qquad (4.2)$$

According to von Karman's solution in Appendix - D, the following equations can be achieved:

The displacement function

$$u(x,t) = t \int_{C_{po}}^{C_p} [(\frac{\rho C_p^2}{nk})^{\frac{1}{n-1}} - \varepsilon_e] dC_p$$

$$= A_{11} C_p{}^{A12} t - x\varepsilon_e - t(A_{11} C_{p0}{}^{A12} - C_{p0}\varepsilon_e) \qquad (4.3)$$

where $A_{11} = \frac{n-1}{n+1}(\frac{\rho}{nk})^{\frac{1}{n-1}}$, $A_{12} = \frac{n+1}{n-1}$ and C_{p0} is an initial plastic wave propagation velocity.

If the procedures in Chapter 3 are followed, the radius of the specimen, r, in the second zone is

$$r = r_0\{1 + \frac{1}{2}[(\frac{\rho C_p^2}{nk})^{\frac{1}{n-1}} - \varepsilon_e]\}$$

The second derivative of r about x is

$$r'' = r_0[\frac{(3-n)}{(n-1)^2}(\frac{\rho}{nkt^2})^{\frac{1}{n-1}}(x)^{\frac{2-n}{n-1}}] \qquad (4.4)$$

where r_0 is the initial radius of a specimen.

Now we check three main characteristics in this model one by one:

A. It can be seen that after impact, the radius of the specimen will become a curve. But because r'' is greater then zero, the shape of the specimen does not appear to be mushroom. This does not match the first characteristic.

B. As the plastic wave propagates, if the strain decreases, the velocity of the plastic wave will increase. This one does not match the second characteristic.

C. When the strain is zero, the velocity of the plastic wave is not zero. This one matches the third characteristic.

Example: Suppose in the Taylor Test, a specimen is made from Aluminum 1100, with parameters as follows:

Aluminum 1100, $k = 0.598$, $n = 0.216$, $\rho = 2710 kg/m^3$

Then, from the foregoing formulas, the displacement function, strain and the radius and the second derivative of the specimen in the second zone can be obtained as follows:

$$\varepsilon = 1.682 \times 10^{-7} C_p^{-2.55}$$

$$u(x,t) = -4.789 \times 10^{-6} C_p^{-1.55} t + 1.4789 \times 10^{-6} C_p^{-1.55} t$$

$$r = r_0[(1 + 8.41 \times 10^{-8} (\frac{t}{x})^{2.55}]$$

$$r'' = r_0(76.13 \times 10^{-8} \frac{t^{2.55}}{x^{4.55}})$$

In this example, because $r'' > 0$ then the contour of the specimen is not like a mushroom.

Summarizing, this model only matches one characteristic of the plastic wave propagation in the Taylor test. The other two characteristics cannot be matched.

4.2 Analysis for Hartig Model

This model was proposed by Ernst K. Hartig in 1893. It was used to investigate the nonlinearity in small deformation and tangent modulus of metals, especially in cast iron, for both tension and compression. It can be written as

$$\sigma = \frac{E_o}{b}(1 - e^{-b\varepsilon})$$

where E_0 is zero stress modulus and $b > 0$ is a constant.

Similarly, if the same procedures are followed in Appendix - D, based on this model it yields

$$T(\varepsilon) = \frac{d\sigma}{d\varepsilon} = E_0 e^{-b\varepsilon} = E_0 e^{-bf(C_p)}$$

$$\Rightarrow \qquad T(\varepsilon) = E_0 e^{-bf(C_p)} \qquad (4.5)$$

Taking Equation (4.5) back into Equation (D-5) in Appendix - D, it yields

$$\rho C_p^2 = E_0 e^{-bf(C_p)}$$

$$\Rightarrow \qquad \varepsilon = f(C_p) = -\frac{\ln[\frac{\rho}{E_0} C_p^2]}{b}$$

According to von Karman's solution in Appendix - D, the following equations can be achieved:

The displacement function

$$u(x,t) = t \int_{C_{po}}^{C_p} -\frac{\ln[\frac{\rho}{E_0} C_p^2]}{b} dC_p$$

$$= -\{\frac{1}{b}\ln\frac{\rho}{E_0}(x - C_p t) + \frac{2}{b}[x(\ln C_p - 1) - C_{p0}(\ln C_{p0} - 1)t]\}$$

The radius of the specimen in the second zone is

$$r = r_0[1 - \frac{1}{2b}\ln(\frac{\rho C_p^2}{E_0})]$$

The second derivative of r about x is

$$r'' = \frac{r_0}{bx^2}$$

Now we check three main characteristics in this model:

A. It can be seen that after impact, the radius of the specimen will become a curve. But r'' is greater then zero ($b > 0$), the shape of the specimen does not appear to be mushroom. This does not match the first characteristic.

B. Under the condition of the strain absolute values being taken, if the strain decreases, the velocity of the plastic wave will decrease. This one matches the second

characteristic. When the strain is zero, the velocity of the plastic wave is not zero. This one does not match the third characteristic.

So it can be concluded that because r'' is greater then zero, the shape of the specimen does not appear to be mushroom. This is a characteristic not matching the experimental results.

4.3 Analysis for Rate Sensitive Power Law Plasticity

This one models strain rate sensitive material with power law hardening. This model follows a constitutive relationship of the form:

$$\sigma = k\varepsilon^m \dot{\varepsilon}^n$$

where k, m, n are material constants and $m < 1$ and $n < 1$.

When this model is used to describe the propagation of plastic wave in the second zone of the specimen, the strain rate must be set to a constant. The procedures of solving the equation of plastic wave in Appendix - D are followed. Based on this model, it yields

$$T(\varepsilon) = \frac{d\sigma}{d\varepsilon} = mk\dot{\varepsilon}^n \varepsilon^{m-1}$$

Define $\varepsilon = f(C_p)$, it yields

$$\rho C_p^2 = mk\dot{\varepsilon}^n \varepsilon^{m-1} \qquad (4.6)$$

Taking Equation (4.6) back into Equation (D-5) in Appendix - D, it yields

$$\varepsilon = f(C_p) = \left(\frac{\rho C_p^{\,2}}{mk\dot{\varepsilon}^n}\right)^{\frac{1}{m-1}}$$

According to von Karman's solution in Appendix - D, the following equations can be achieved:

The displacement function: $u(x,t) = A_{11}t(C_p^{A12} - C_{p0}^{A12})$

where $A_{11} = \frac{m-1}{m+1}(\frac{\rho}{mk\dot{\varepsilon}^n})^{\frac{1}{m-1}}$, $A_{12} = \frac{m+1}{m-1}$

The radius of the specimen in the second zone is

$$r = r_0\{1 + \frac{1}{2}(\frac{\rho C_p^2}{mk\dot{\varepsilon}^n})^{\frac{1}{m-1}}\}$$

The second derivative of r about x is

$$r'' = r_0[\frac{(3-m)}{(m-1)^2}(\frac{\rho}{mk\dot{\varepsilon}^n t^2})^{\frac{1}{m-1}}(x)^{\frac{4-2m}{m-1}}]$$

where r_0 is the radius of a specimen. Because r'' is greater than zero, the shape of the specimen does not appear to be a mushroom.

Example: Take A356 Aluminum as an example with the material parameters being $m = 0.7, k = 0.002Mpa$ and $n = 0.32$. At the same time suppose $\dot{\varepsilon} = 10^6\ 1/s$, then from the foregoing formulas, the displacement function, strain and the radius and the second derivative of the specimen in the second zone can be obtained as follows:

$$\varepsilon = 131C_p^{-6.67},$$

$$u(x,t) = -30.17t(C_p^{-5.67} - C_{p0}^{-5.67}),$$

$$r = r_0(1 + 65.67C_p^{-6.67}),$$

$$r'' = r_0(3359 \times t^{\frac{2}{0.3}} x^{-8.67})$$

In this example, because $r'' > 0$ then the contour of the specimen is not like a mushroom, it does not match the first characteristic. As the plastic wave propagates, if the strain decreases, the velocity of the plastic wave will increase. This one does not match the second characteristic. When the strain is zero, the velocity of the plastic wave is infinite. This one does not match the third characteristic. So, there are not characteristics to match the ones of the propagation of the plastic wave in the Taylor test.

4.4 Analysis for Johnson-Cook Model

The Johnson-Cook model is mainly used for problems where the strain rates vary over a large range and adiabatic temperature increases due to plastic heating cause material softening in most metals. Typical applications include explosive metal forming, ballistic penetration and impact. Without considering thermal effect, this model can be expressed

$$\sigma = (A + B\varepsilon^n)(1 + C\ln\dot{\varepsilon})$$

where A, B, C are material constants and $n < 1$.

When this model is used to calculate the propagation of the plastic wave in the Taylor Test, the procedures in Appendix - D are followed and the strain rate is supposed to be a constant. From this model, it yields

$$T(\varepsilon) = \frac{d\sigma}{d\varepsilon} = Bn(1 + C\ln\dot{\varepsilon})\varepsilon^{n-1}$$

Let $\varepsilon = f(C_p)$, thus

$$\rho C_p^2 = \frac{d\sigma}{d\varepsilon} = Bn(1 + C\ln\dot{\varepsilon})\varepsilon^{n-1}$$

$$\Rightarrow \quad \varepsilon = f(C_p) = [\frac{\rho C_p^2}{Bn(1 + C\ln\dot{\varepsilon})}]^{\frac{1}{n-1}} \qquad (4.7)$$

According to von Karman's solution in Appendix - D, the following equations can be achieved:

The displacement function $u(x,t) = A_{11}t(C_p^{A12} - C_{p0}^{A12})$

where $A_{11} = \frac{n-1}{n+1}[\frac{\rho}{nB(1 + C\ln\dot{\varepsilon})}]^{\frac{1}{n-1}}$, $A_{12} = \frac{n+1}{n-1}$

The radius of the specimen in the second zone

$$r = r_0\{1 + \frac{1}{2}[\frac{\rho C_p^2}{Bn(1 + C\ln\dot{\varepsilon})}]^{\frac{1}{n-1}}\}$$

The second derivative of r about x is

$$r'' = r_0\{\frac{(3-n)}{(n-1)^2}[\frac{\rho}{Bn(1 + C\ln\dot{\varepsilon})t^2}]^{\frac{1}{n-1}}(x)^{\frac{4-2n}{n-1}}\}$$

where r_0 is the radius of a specimen. Because r'' is greater then zero, the shape of the specimen does not appear to be a mushroom.

In the next four examples, four materials are specimens in the Taylor tests and the Johnson-Cook model is used to compute the plastic wave propagation, where set $\dot{\varepsilon} = 10^6$ 1/s.

Example 1

Amco Iron, $A = 175\,MPa$, $B = 380\,MPa$, $C = 0.06$, $n = 0.32$

$\rho = 7890 kg / m^3$

Computed results as follows:

$$\varepsilon = 121576 C_p^{-2.94},$$

$$u(x,t) = -62630 t (C_p^{-1.94} - C_{p0}^{-1.94}),$$

$$r = r_0 (1 + 60788 C_p^{-2.94}),$$

$$r'' = r_0 (704147 \times x^{-4.94} t^{2.941}).$$

Example 2

OFHC Copper, $A = 89\,MPa$, $B = 292\,MPa$, $C = 0.025$, $n = 0.31$

$\rho = 8330 kg / m^3$

Computed results as follows:

$$\varepsilon = 81658 C_p^{-2.89},$$

$$u(x,t) = -43010 t (C_p^{-1.898} - C_{p0}^{-1.898}),$$

$$r = r_0 (1 + 40828 C_p^{-2.89}),$$

$$r'' = r_0 (458992 \times x^{-4.89} t^{2.898}).$$

Example 3

4340 Steel, $A = 792\,MPa$, $B = 510\,MPa$, $C = 0.014$, $n = 0.26$

$$\rho = 7830kg / m^3$$

Computed results as follows:

$$\varepsilon = 29695C_p^{-2.7},$$

$$u(x,t) = -17440t(C_p^{-1.7} - C_{p0}^{-1.7}),$$

$$r = r_0(1 + 14847C_p^{-2.7}),$$

$$r'' = r_0(148326.53 \times x^{-4.7}t^{2.7}).$$

Example 4

7039 Aluminum, $A = 336MPa$, $B = 343MPa$, $C = 0.01$, $n = 0.41$

$$\rho = 2720kg / m^3$$

Computed results as follows:

$$\varepsilon = 2429621C_p^{-3.38},$$

$$u(x,t) = -1016650t(C_p^{-2.39} - C_{p0}^{-2.39}),$$

$$r = r_0(1 + 1214811C_p^{-3.38}),$$

$$r'' = r_0(17984548 \times x^{-5.38}t^{3.389}).$$

The foregoing formulas and the common characteristics of the above four examples show that:

A. Although the material is different, the radius of the specimen will become a curve in the second zone. But because r'' s are greater then zero, the shapes of the

specimens do not appear to be mushroom. This does not match the first characteristic.

B. As the plastic wave propagates, if the strain decreases, the velocity of the plastic wave will increase. This one does not match the second characteristic.

C. When the strain is zero, the velocity of the plastic wave is infinite. This one does not match the third characteristic.

In his paper, Maudlin also proves that the Johnson-Cook model cannot describe the propagation of the plastic wave in the Taylor Test. This conclusion matches our one.

4.5 Analysis for Malvern Model

One of the earliest models used to describe rate-dependent material behavior is due to Malvern in 1951. The model can be written as

$$\sigma = \sigma_1(\varepsilon) + a\ln(1 + b\dot{\varepsilon})$$

where $\sigma_1(\varepsilon)$ is the static stress and a and b are constants which describe the rate sensitivity. The linear form of the Malvern model is

$$\sigma = \sigma_1(\varepsilon) + k\dot{\varepsilon}$$

where k is a material constant. For Harden Aluminum, the linear form of Malvern is that

$$\sigma = (20000 - \frac{10}{\varepsilon}) + 1000000\dot{\varepsilon}$$

Suppose a specimen in the Taylor Test is made from Harden Aluminum. The linear Malvern model is used to describe the propagation of the plastic wave in the second zone, then it yields

$$T(\varepsilon) = \frac{d\sigma}{d\varepsilon} = \frac{10}{\varepsilon^2}$$

Let $\varepsilon = f(C_p)$, then

$$\rho C_p^2 = \frac{d\sigma}{d\varepsilon} = \frac{10}{\varepsilon^2}$$

Taking the above equation back into Equation (D-5) in Appendix - D, it yields

$$\varepsilon = f(C_p) = \sqrt{\frac{10}{\rho}} \frac{1}{C_p} \qquad (4.8)$$

From this formula, if the velocity of the plastic wave propagation gradually decreases, the strain ε will increase. Apparently, this one does not mach the experimental results, that is, the second characteristic. When the strain is zero, the velocity of the plastic wave propagation is not a constant. This one does not match the third characteristic of the Taylor test.

According to von Karman's solution in Appendix, the following equations can be achieved:

The displacement function $u(x,t) = t\sqrt{\frac{10}{\rho}} \ln \frac{C_p}{C_{p0}}$

The radius of the specimen in the second zone is

$$r = r_0(1 + \frac{1}{2}\sqrt{\frac{10}{\rho}} \frac{1}{C_p})$$

The second derivative of r is

$$r'' = r_0(1 + \frac{1}{2}\sqrt{\frac{10}{\rho}} t x^{-3})$$

where r_0 is the radius of a specimen. Because r'' is greater then zero, the shape of the specimen does not appear to be a mushroom. This one does not match the first characteristic of the Taylor test.

4.6 Analysis for Strain Rate Dependent Plasticity

In this model, the yield stress is defined as

$$\sigma = \sigma_1(\dot{\varepsilon}) + E_p \varepsilon$$

where E_p is plastic tangent modulus and is given in terms of Young's modulus and the tangent modulus. $\sigma_1(\dot{\varepsilon})$ is the stress caused by the strain rate.

$$T(\varepsilon) = \frac{d\sigma}{d\varepsilon} = E_p$$

If this model is used in the Taylor test, then first define $\varepsilon = f(C_p)$ and it yields

$$\rho C_p^2 = \frac{d\sigma}{d\varepsilon} = E_p \qquad (4.9)$$

Because E_p is a constant, the plastic wave velocity will be a constant and the strain is a constant. According to this model, the shape of the specimen will be a straight line. For example, for 4140 Steel, $\rho = 7850 kg/m^3$ and $E_p = 22 \times 10^5 Pa$. If the procedures in Appendix- D are followed, then one can calculate that the strain is $\varepsilon = 0.19\sigma$ and $r = r_0(1 + 0.0935\sigma)$. The shape of the specimen is a straight line. These conclusions totally do not match the experimental results.

4.7 Analysis for Power Law

The Power Law can be written as

$$\sigma = \sigma_1(\varepsilon)\dot{\varepsilon}^n$$

where $n < 1$ is a material constant and $\sigma_1(\varepsilon)$ is quasi-static stress.

Set $\dot{\varepsilon}$ be a constant. Based on this model, it yields

$$T(\varepsilon) = \frac{d\sigma}{d\varepsilon} = \frac{\partial\sigma_1}{\partial\varepsilon}\dot{\varepsilon}^n$$

Let $\varepsilon = f(C_p)$, it yields

$$T[f(C_p)] = \frac{\partial\sigma_1}{\partial\varepsilon}\dot{\varepsilon}^n \qquad (4.10)$$

Taking the above equation back into Equation (D-5) in Appendix -D, it yields

$$\rho C_p^2 = \frac{\partial\sigma_1}{\partial\varepsilon}\dot{\varepsilon}^n$$

Define $T_{inv}(\frac{\rho C_p^2}{\dot{\varepsilon}^n})$ is an inverse function of $\frac{\partial\sigma_1}{\partial\varepsilon}(\varepsilon)$, then

$$\varepsilon = f(C_p) = T_{inv}(\frac{\rho C_p^2}{\dot{\varepsilon}^n}) \qquad (4.11)$$

According to von Karman's solution in Appendix - D, the following equations can be achieved:

$$u(x,t) = t\int_{C_{po}}^{C_p} T_{inv}(\frac{\rho C_p^2}{\dot{\varepsilon}^n})dC_p$$

So it can be seen that the expressions of strain and displacement depend on the expressions of the material model. Only the model is given for a material; the Power

Law can be used in the Taylor Test.

4.8 Analysis for Logarithmic Law

Logarithmic law can be expressed in the form

$$\sigma = \sigma_1(\varepsilon) + k \ln \dot{\varepsilon}$$

where k is a material constant and $\sigma_1(\varepsilon)$ is quasi-static stress. Set $\dot{\varepsilon}$ be a constant. Based on this model $T(\varepsilon) = \frac{d\sigma}{d\varepsilon} = \frac{\partial \sigma_1}{\partial \varepsilon}$, let $\varepsilon = f(C_p)$, it yields:

$$T[f(C_p)] = \frac{\partial \sigma_1}{\partial \varepsilon}$$

Define $T_{inv}(\rho C_p^2)$ is an inverse function of $\frac{\partial \sigma_1}{\partial \varepsilon}(\varepsilon)$, then

$$\varepsilon = f(C_p) = T_{inv}(\rho C_p^2) \qquad (4.12)$$

Taking Equation (1) back into Equation (D-5) in Appendix, it yields

$$u(x,t) = t \int_{C_{po}}^{C_p} T_{inv}(\frac{\rho C_p^2}{\dot{\varepsilon}^n}) dC_p$$

So it can be seen that the expressions of strain and displacement depend on the expressions of the material model. Only the model is given for a material; the Power Law can be used in the Taylor Test.

CHAPTER 5

THE NUMERICAL ANALYSIS FOR PLASTIC WAVE PROPAGATION OF RD THEORY

In Chapter 3, RI theory is used to investigate the plastic wave propagation in the Taylor test. That is, the effect of strain rate is not considered. If the strain rate is considered, RD theory is applied to investigate the plastic wave propagation in the Taylor test. It is very difficult to get the analytical solution of the plastic wave equation of RD theory, so numerical methods are used. When numerical methods are used, the numerical computation is along the characteristic curve of the plastic wave. The plateau of RD theory, the characteristic equation, characteristic curves and Eulerian method and Hartree methods are discussed. The Eulerian method is an explicit numerical method and the Hartree method is an implicit numerical method.

5.1 Plastic Wave Equation Of RD Theory And Its Plateau

Shown in Figure 2.1, assume a rod with length L is subjected to impact loading with a constant velocity V_0. The relationship among stress, strain and strain rate is $\sigma = \sigma(\varepsilon, \dot{\varepsilon})$, where σ is stress, ε is strain and $\dot{\varepsilon}$ is strain rate. The transverse effect is neglected. $\sigma = \sigma(\varepsilon, \dot{\varepsilon})$ holds for plastic deformation of the material. The boundary conditions are $u(0,t) = V_0 t$ and $u(L,t_p) = 0$, where t_p is the time of the plastic wave reaching the other end of the rod. From Newton's Second Law, the plastic wave equation with the boundary conditions is given as follows:

$$\rho \frac{\partial^2 u}{\partial t^2} = \frac{\partial \sigma}{\partial \varepsilon} \frac{\partial^2 u}{\partial x^2} + \frac{\partial \sigma}{\partial \dot{\varepsilon}} \frac{\partial^3 u}{\partial x^2 \partial t} \qquad (5.1)$$

B.C: $u(0,t) = V_0 t$ and $u(L,t_p) = 0$

where ρ is the mass density, t is time, $u = u(x,t)$ is displacement function; $\varepsilon = \frac{\partial u}{\partial x}$ and $\dot{\varepsilon} = \frac{\partial \varepsilon}{\partial t} = \frac{\partial^2 u}{\partial x \partial t}$.

According to experimental results, the plastic wave propagation in the Taylor test can be divided into two phases. In the first phase, the strain is a constant. Physically, it is called plateau. It can be seen that there is a linear solution with the following form:

$$u(x,t) = V_0 (t + \frac{x}{k_0}) \qquad (5.2)$$

with a constant, k_0, satisfying Equation (5.1). And the first boundary condition is satisfied at $x = 0$. From this solution, the strain ε and the velocity of the particle v are obtained as follows:

$$\varepsilon = \frac{\partial u}{\partial x} = \frac{V_0}{k_0} \qquad (5.2.1)$$

$$v = \frac{\partial u}{\partial t} = V_0 \qquad (5.2.2)$$

Equation (5.2.2) is the first solution to Equation (5.1). For this solution, the strain is a constant and the velocity of the particle is equal to the impact velocity V_0. Physically, the constant strain is the plateau. That velocity of the particle being equal to V_0 means the plateau is near the impact end. So it can be concluded that there exists a plateau and this plateau is near to the impact end. Because the first solution to Equation (5.2) is a

linear solution, and it always satisfies the plastic wave propagation equation, this linear solution is independent of the constitutive equation of the material, $\sigma = \sigma(\varepsilon, \dot{\varepsilon})$ or $\frac{\partial \sigma}{\partial \varepsilon}$ and $\frac{\partial \sigma}{\partial \dot{\varepsilon}}$. This means that no matter what kinds of models have been proposed, the plateau always exists. That is, RD theory can predict the existence of the plateau and the plateau is near the impact end. Basedon this conclusion, RD theory and RI theory are the same in the first phase. Because the linear solution or the plateau is near the impact end, it gives boundary conditions for the second phase as follows:

$$u(x_0, t_0) = V_0(t_0 + \frac{x_0}{k_0}) \qquad (5.3)$$

$$\varepsilon(x_0, t_0) = \frac{V_0}{k_0} \qquad (5.3.1)$$

$$v(x_0, t_0) = V_0 \qquad (5.3.2)$$

where x_0 is the coordinate of the plateau and t_0 is the time of the plateau ending.

5.2 The Characteristic Equation

In order to investigate the propagation of the plastic wave in the second phase, the characteristic equation of the plastic wave equation should be gotten first and the numerical method applied to the characteristic curves.

Recall that the equation of motion

$$\rho \frac{\partial v}{\partial t} = \frac{\partial \sigma}{\partial x} \qquad (5.4)$$

During the propagation of plastic wave, v and σ are function of x and t, then the increments of v and σ can be written as

$$dv = \frac{\partial v}{\partial x}dx + \frac{\partial v}{\partial t}dt \qquad (5.5)$$

$$d\sigma = \frac{\partial \sigma}{\partial x}dx + \frac{\partial \sigma}{\partial t}dt \qquad (5.6)$$

The following strain-velocity relation should be satisfied:

$$\frac{\partial v}{\partial x} = \frac{\partial \varepsilon}{\partial t} \qquad (5.7)$$

In the RD theory, $\sigma = \sigma(\varepsilon, \dot{\varepsilon})$. Taking the derivative of the stress σ with respect to t, it yields

$$\frac{\partial \sigma}{\partial t} = \frac{\partial \sigma}{\partial \varepsilon}\frac{\partial \varepsilon}{\partial t} + \frac{\partial \sigma}{\partial \dot{\varepsilon}}\frac{\partial \dot{\varepsilon}}{\partial t}$$

Define $T = \frac{\partial \sigma}{\partial \varepsilon}$ and $T_1 = \frac{\partial \sigma}{\partial \dot{\varepsilon}}$, the above becomes

$$\frac{\partial \sigma}{\partial t} = \frac{\partial \sigma}{\partial \varepsilon}\frac{\partial \varepsilon}{\partial t} + \frac{\partial \sigma}{\partial \dot{\varepsilon}}\frac{\partial \dot{\varepsilon}}{\partial t} = T\frac{\partial \varepsilon}{\partial t} + T_1\frac{\partial \dot{\varepsilon}}{\partial t}$$

or

$$\frac{\partial \varepsilon}{\partial t} = \frac{1}{T}\frac{\partial \sigma}{\partial t} + \frac{T_1}{T}\frac{\partial \dot{\varepsilon}}{\partial t} \qquad (5.8)$$

Substituting Equation (5.8) into Equation (5.7), it yields

$$\frac{\partial v}{\partial x} = \frac{1}{T}\frac{\partial \sigma}{\partial t} - \frac{T_1}{T}\frac{\partial \dot{\varepsilon}}{\partial t}$$

$$\Rightarrow \qquad \frac{\partial v}{\partial x} - \frac{1}{T}\frac{\partial \sigma}{\partial t} = -\frac{T_1}{T}\frac{\partial \dot{\varepsilon}}{\partial t} \qquad (5.9)$$

Gather Equations (5.4), (5.5), (5.6) and (5.9) together

$$\begin{cases} \dfrac{\partial v}{\partial t} - \dfrac{1}{\rho}\dfrac{\partial \sigma}{\partial x} = 0 \\ dx\dfrac{\partial v}{\partial x} + dt\dfrac{\partial v}{\partial t} = dv \\ dx\dfrac{\partial \sigma}{\partial x} + dt\dfrac{\partial \sigma}{\partial t} = d\sigma \\ \dfrac{\partial v}{\partial x} - \dfrac{1}{T}\dfrac{\partial \sigma}{\partial t} = -\dfrac{T_1}{T}\dfrac{\partial \dot{\varepsilon}}{\partial t} \end{cases}$$

and write the above equation in the form of matrix

$$\Rightarrow \begin{bmatrix} 0 & 1 & -\dfrac{1}{\rho} & 0 \\ dx & dt & 0 & 0 \\ 0 & 0 & dx & dt \\ 1 & 0 & 0 & -\dfrac{1}{T} \end{bmatrix} \begin{bmatrix} \dfrac{\partial v}{\partial x} \\ \dfrac{\partial v}{\partial t} \\ \dfrac{\partial \sigma}{\partial x} \\ \dfrac{\partial \sigma}{\partial t} \end{bmatrix} = \begin{bmatrix} 0 \\ dv \\ d\sigma \\ -\dfrac{T_1}{T}\dfrac{\partial \dot{\varepsilon}}{\partial t} \end{bmatrix} \qquad (5.10)$$

The characteristic equation of the plastic wave equation can be obtained by letting determinant of the coefficient matrix of Equation(5.10) be equal to zero. From the above matrix, we obtain the characteristic equation

$$\frac{dx}{dt} = \pm\sqrt{\frac{1}{\rho}\frac{\partial \sigma}{\partial \varepsilon}} \qquad (5.11)$$

As we known, when $\vec{A}\vec{x} = \vec{b}$ and $\det(\vec{A}) = 0$, where $\vec{A}$ is a matrix, $\vec{x}$ is a column vector and $\vec{b}$ is a vector, then a necessary condition for the existence of finite solution for $\vec{x}$ is when $\vec{b}$ is substituted for any column of $\vec{A}$ the resulting determinant must also

vanish [Ames,36]. Taking the right column in Equation (5.10) into 1st column of the matrix, it gives the stress increment along the characteristic curves

$$d\sigma = \rho C_p dv + T_1 \frac{\partial \dot{\varepsilon}}{\partial t} dt, \quad \text{If } C_p > 0; \tag{5.12}$$

$$d\sigma = -\rho C_p dv + T_1 \frac{\partial \dot{\varepsilon}}{\partial t} dt, \quad \text{If } C_p < 0. \tag{5.13}$$

where $C_p = \frac{dx}{dt}$.

If one considers the equation $\frac{\partial v}{\partial x} = \frac{\partial \varepsilon}{\partial t}$, then

$$dv = \frac{dx}{dt} d\varepsilon = C_p d\varepsilon$$

Take it into Equation (5.12) and (5.13), then it yields

$$d\sigma = \rho C_p^2 d\varepsilon + T_1 \frac{\partial \dot{\varepsilon}}{\partial t} dt \tag{5.14}$$

$$d\sigma = -\rho C_p^2 d\varepsilon + T_1 \frac{\partial \dot{\varepsilon}}{\partial t} dt \tag{5.15}$$

Equations (5.14) and (5.15) describe differential relationships for a variety of variables of the plastic wave propagation and provide the theoretical bases to use numerical methods to compute the variables of the plastic wave propagation along the characteristic curves.

5.3 Numerical Analysis Methods

There are many numerical methods which can be used to compute variables in plastic wave propagation. Here only two methods are discussed. The first method is an

explicit numerical method, it called Eulerian method. The second method is an implicit numerical method, it is called Hartree method.

5.3.1 Eulerian Method

From Equation (5.14), the increment of the stress along the characteristic curve, if $C_p > 0$, can be written as

$$d\sigma = \rho C_p^2 d\varepsilon + T_1 \frac{\partial \dot{\varepsilon}}{\partial t} dt$$

In order to use numerical method along the characteristic curve, we use

$$d\sigma \approx \Delta\sigma = \sigma(i+1) - \sigma(i)$$

for point $(i+1)$ and point i, where $i = 0,1,2,3\cdots$, and notice that

$$\frac{\partial \dot{\varepsilon}}{\partial t} dt \approx [\frac{\Delta \dot{\varepsilon}}{\Delta t}(i)]\Delta t = \Delta\dot{\varepsilon}(i) = [\dot{\varepsilon}(i+1) - \dot{\varepsilon}(i)] = \frac{\varepsilon(i+1) - \varepsilon(i)}{\Delta t} - \frac{\varepsilon(i) - \varepsilon(i-1)}{\Delta t}$$

$$= \frac{\varepsilon(i+1) + \varepsilon(i-1)}{\Delta t}$$

then it gives Eulerian method as follows:

$$x(i+1) = x(i) + C_p(i)\Delta t \qquad (5.16)$$

$$\sigma(i+1) = \sigma(i) + \rho C_p^2(i)[\varepsilon(i+1) - \varepsilon(i)] + T_1(i)[\frac{\varepsilon(i+1) + \varepsilon(i-1)}{\Delta t}] \qquad (5.17)$$

$$C_p(i+1) = \{\frac{\sigma(i+1) - \sigma(i)}{\rho[\varepsilon(i+1) - \varepsilon(i)]}\}^{\frac{1}{2}} \qquad (5.18)$$

This method is very simple. If the initial values are given, then the computation

can go step by step along the characteristic curve. However, it asks that before computing variables at point $(i+1)$, the values at point i must be known. Especially, the strain at point $(i+1)$ must be given. But the convenience of this method is not very good.

5.3.2 Hartree Method

Hartree method is an implicit method along the characteristic curve. This method can be introduced as follows.

Suppose that a fixed rectangle grid is imposed on the integration with distance interval Δx and time interval Δt, as shown in Figure 5.1. The relations along the characteristics arethat

$$d\sigma + \rho C_p^2 d\varepsilon + T_1 \frac{\partial \dot{\varepsilon}}{\partial t} dt = 0$$

and

$$d\sigma - \rho C_p^2 d\varepsilon + T_1 \frac{\partial \dot{\varepsilon}}{\partial t} dt = 0$$

Define $G_\alpha = \rho C_p^2$, $H_\alpha = T_1 \frac{\partial \dot{\varepsilon}}{\partial t}$, $G_\beta = -\rho C_p^2$ and $H_\beta = T_1 \frac{\partial \dot{\varepsilon}}{\partial t}$, then one has

$$d\sigma + G_\alpha d\varepsilon + H_\alpha dt = 0 \qquad (5.19)$$

$$d\sigma + G_\beta d\varepsilon + H_\beta dt = 0 \qquad (5.20)$$

Suppose that solution is known at the mesh points and R, S, ... are equally spaced along the next line, $t = (j+1)\Delta t$. Draw the α and β characteristics from Equation (5.19) and (5.20) through R, back to their intersection with first line $t = j\Delta t$. These two points

of intersection are unknown. We wish to calculate σ_R, ε_R, x_p and x_Q.

The Hartree's computational form is as follows:

$$x_R - x_P = \frac{1}{2}[C_p(R) + C_p(P)]\Delta t \qquad (5.21)$$

$$x_R - x_Q = \frac{1}{2}[-C_p(R) - C_p(Q)]\Delta t \qquad (5.22)$$

$$(\sigma_R - \sigma_P) + \frac{1}{2}[\rho C_p^2(R) + \rho C_p^2(P)](\varepsilon_R - \varepsilon_P) + \\ + \frac{1}{2}[T_1(R)\frac{\Delta\dot{\varepsilon}}{\Delta t}(R) + T_1(P)\frac{\Delta\dot{\varepsilon}}{\Delta t}(P)]\Delta t = 0 \qquad (5.23)$$

$$(\sigma_R - \sigma_Q) + \frac{1}{2}[-\rho C_p^2(R) - \rho C_p^2(Q)](\varepsilon_R - \varepsilon_Q) + \\ + \frac{1}{2}[T_1(R)\frac{\Delta\dot{\varepsilon}}{\Delta t}(R) + T_1(Q)\frac{\Delta\dot{\varepsilon}}{\Delta t}(Q)]\Delta t = 0 \qquad (5.24)$$

The four equations can be used to solve four unknowns. In general, the variables at point R are to be solved and variables at point P and point Q are known. Notice that the interpolation for the values of σ, ε at P and Q are necessary at each step. And also, this system must be solved by iteration by using interpolated values at P and Q. However, this method does not suit every constitutive equation of a material. It only works for some constitutive equations, like the Malvern model. At the same time, the computation of this method is very complicated and the accumulation of errors is larger.

Comparing the Eulerian method with the Hartree method, the first method is an explicit method. It does not require iteration and the computation is simple, but the convenience is not good. The second method is an implicit method. The iteration must be used, which requires interpolated values at P and Q to solve the system. The convenience of the method is better than Eulerian method, but the computation is more

complicated than the former. The above two numerical characteristic methods are suited to any constitutive equation of materials.

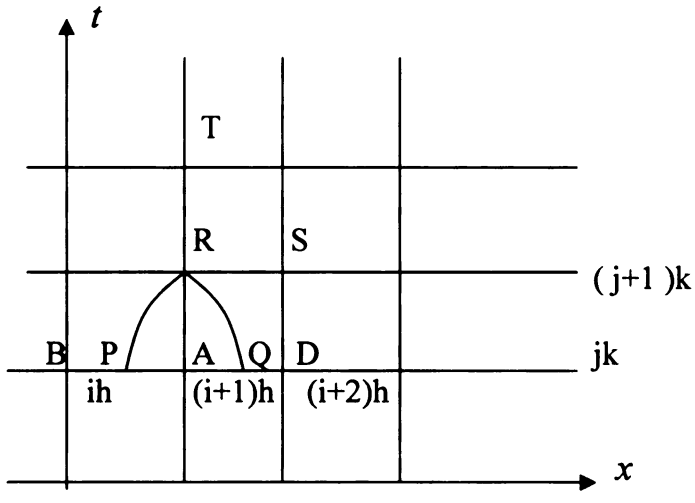

Figure 5.1 Hartree Method Diagram

CHAPTER 6

THE DYNAMIC STRESS COMPUTATION OF PROJECTILE ALUMINUM 6061-T6511 IN TAYLOR TEST

According to our discussion in Chapter 5, the plastic wave propagation in the projectile in the Taylor test can be divided into two phases. In this chapter, the dynamic stresses in the first phase and second phase will be computed in different constitutive equations of RD theory. The sample is Aluminum 6061-T6511, the first Taylor test in Chapter 3. The parameters of the sample are given as follows.

Density: ρ=2700 kg/m^3
Static Yield Stress: $\sigma_s = 275MPa$
Young Modulus: $E = 69 \times 10^9 N/m^2$
Elastic Wave Velocity: $C_e = 5055m/s$
Impact Velocity: $V_0 = 93m/s$
Original Length: $L = 7.8232cm$
Final Length: $L_0 = 7.512cm$
$L_p = 3.4282cm$
$L_e = 4.12cm$
Projectile Diameter: $D_1 = 1.22936cm$
Measured $h = 0.275cm$, Computed $h = 0.299cm$
$h_d = 0.2565cm$
$2R_h = .13195cm$
$2R_0 = .1335cm$
$\Delta L = (L - L_0) - (h - h_d) = 0.927cm$
$t_p = (L + L_e)/C_e = 23.63 \times 10^{-6} s$
$t_h = h/V_0 = 29.55 \times 10^{-6} s$

6.1 The Computation of Dynamic Stress In the First Phase by Johnson-Cook Model

In Chapter 3, Johnson-Cook model has been used to calculate the stress in the first

phase. According to analysis in the first phase, the Johnson-Cook model can be written as

$$\sigma = (A + B\varepsilon^n)$$

where $A = 275$ MPa, $B = 426$ MPa and $n = 0.34$. From the measured strain in Chapter 3 and the above model, the dynamic stress in the first phase of Aluminum 6061-T6511 can be computed as shown in Table 6.1. The relationship of stress σ_{p1} and x is shown in Figure 6.1.

Table 6.1 Stress, Strain vs. Distance in the First Phase Aluminum 6061-T6511

x (mm)	ε_{p1}	σ_{p1} (MPa)
0	0.1723	509.33
0.34	0.1596	503.31
0.69	0.1565	501.79
1.03	0.1491	498.09
1.38	0.1484	497.74
1.72	0.1487	497.74
1.72	0.1487	497.88
2.06	0.1507	498.90
2.41	0.1486	497.84
2.75	0.1459	496.45

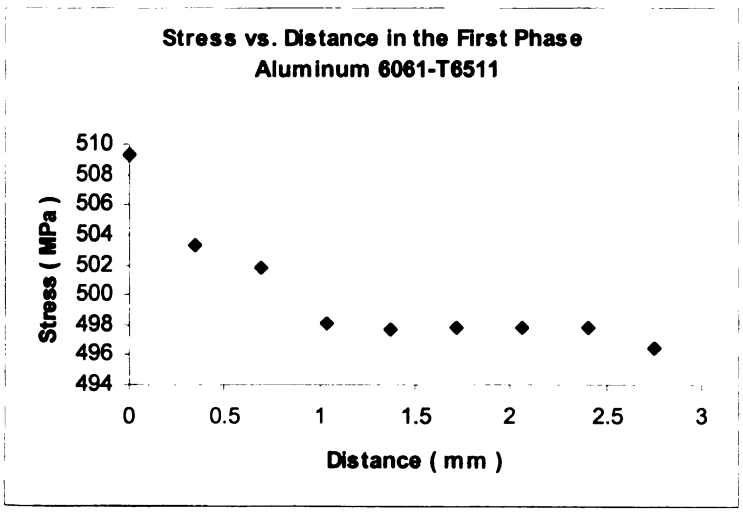

Figure 6.1 Stress vs. Distance in the First Phase Aluminum 6061-T6511

6.2 THE COMPUTATION OF DYNAMIC STRESS IN THE SECOND PHASE

In order to compute the dynamic stress in the second phase, the constitutive equation of the material should be chosen first. In this section, a modified Malvern model will be proposed and used to calculate the dynamic stress in the second phase.

6.2.1 Modified Malvern Model

As one of the pioneers who proposed the RD theory in plastic wave propagation, Malvern developed his model for aluminum, the Malvern Model. This model is simple and effective, especially when it is used to compute the dynamic stress along the characteristic curves in numerical computation. Today, this model gets more and more applications, for example, in powder metallurgy and the automotive industry.

The Malvern model can be expressed as

$$\sigma = \sigma_s(\varepsilon) + k\dot{\varepsilon} \qquad (6.1)$$

where σ_s is static stress, k is a constant of material, and $\dot{\varepsilon}$ is strain rate.

It can be seen that the Malvern model uses the static stress of the material to calculate the dynamic stress during the plastic wave propagation. This is because the value of the static stress is easy to get by tests. In order use the Malvern model, a new model based on the Malvern model is proposed. In this new model, the static stress is replaced by the dynamic stress from RI theory, Equation (2.15), . This model can be written

$$\sigma = \sigma_{RI}(\varepsilon) + k\dot{\varepsilon}$$

$$= \frac{\rho C_2}{2}(e^{\frac{2(\varepsilon - C_1)}{C_2}}) + k\dot{\varepsilon} \qquad (6.2)$$

This model is called the Modified Malvern model. It can be used to calculate the

stresses in the second phase of the projectile along the characteristic curves of the plastic wave propagation by the Eulerian method and the Hartree method numerically. And it is not difficult to verify that this model predicts that the shape of the projectile in the second phase is like a mushroom.

6.2.2 Eulerian Method

The Euleran method, the increment of the stress along the characteristic curve (for $C_p > 0$), can be written as

$$\sigma(i+1) = \sigma(i) + \rho C_p^2(i)\Delta\varepsilon(i) + T_1(i)\frac{\Delta\dot{\varepsilon}}{\Delta t}(i)$$

As from the Modified Malvern model, $T_1 = k$, then the above equation becomes

$$\sigma(i+1) = \sigma_{RI}(i) + \rho C_p^2(i)\Delta\varepsilon(i) + k\frac{\Delta\dot{\varepsilon}}{\Delta t}(i) \qquad (6.3)$$

Take Equation (6.2) into Equation (6.3), it gives

$$\sigma(i+1) = \frac{\rho C_2}{2}\{e^{\frac{2[\varepsilon(i)-C_1)]}{C_2}}\} + k\dot{\varepsilon}(i) + \rho C_p^2(i)\Delta\varepsilon(i) + k\frac{\Delta\dot{\varepsilon}}{\Delta t}(i) \qquad (6.4)$$

From Malvern experimental results, the physical parameter k is given $k = 1\times 10^6\ Pa\sec$. Suppose average strain rate during the plastic wave propagation is a constant, $\dot{\varepsilon} = 100\ \ 1/\sec$. Equation (6.4) becomes

$$\sigma(i+1) = \frac{\rho C_2}{2}\{e^{\frac{2[\varepsilon(i)-C_1)]}{C_2}}\} + k\dot{\varepsilon}(i) + \rho C_p^2(i)[\varepsilon(i+1) - \varepsilon(i)] \qquad (6.5)$$

From test data in Chapter 3 and the above equation, the computed results are shown in Figure 6.2 and Table 6.2.

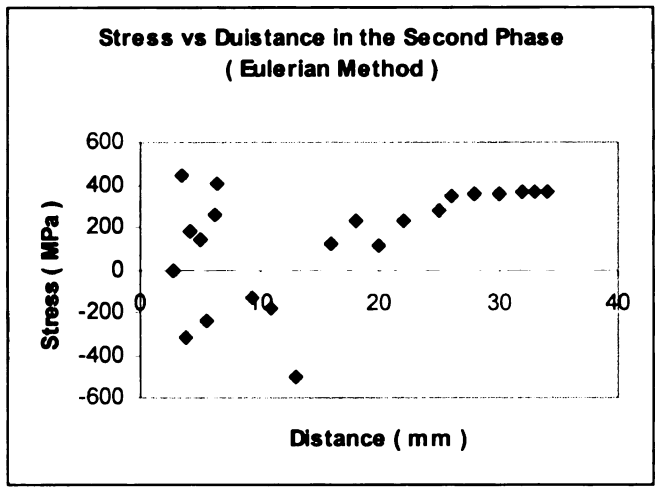

Figure 6.2 Stress vs. Distance in the Second Phase (Eulerian Method)

Table 6.2 Eulerian Method

Distance (mm)	σ (MPa)
2.8	0
3.4	441.71
3.9	-314.45
4.2	182.58
5	142.01
5.6	-238.64
6.3	257.8
6.4	401.15
9.4	-129.57
11	-179.7
13	-499.85
16	120.35
18	233.3
20	114.47
22	230.61
25	281.39
26	341.94
28	359.87
30	355.01
32	368.51
33	361.39
34	368.13

It can been seen that results from the Eulerian method are not accurate. The convergence is not good from $x = 0$ to $x = 18\,\text{mm}$. After that distance, convergence

tends to be better. From $x = 0$ to $x = 18\,\text{mm}$, the stresses computed from the Modified Malvern model are less than the stresses computed from the RI theory. Gradually, the stresses computed from the RD theory are greater than the stresses computed from the RI theory. It indicates if the plastic wave propagates very fast, this method cannot describe the propagation of the plastic wave well. Only when the strain is very small, the propagation of the plastic wave can be described by this method.

6.2.3 Hartree Method

When the Modified Malvern model is used to the Hartree method, the Hartree method from Chapter 5 can written as

$$
\begin{aligned}
&x_R - x_P = \frac{1}{2}[C_p(R) + C_p(P)]\Delta t \\
&x_R - x_Q = \frac{1}{2}[-C_p(R) - C_p(Q)]\Delta t \\
&(\sigma_R - \sigma_P) + \frac{1}{2}[\rho C_p^2(R) + \rho C_p^2(P)](\varepsilon_R - \varepsilon_P) + \\
&\qquad + \frac{k}{2}[\frac{\Delta\dot{\varepsilon}(R)}{\Delta t} + \frac{\Delta\dot{\varepsilon}(P)}{\Delta t}]\Delta t = 0 \\
&(\sigma_R - \sigma_Q) + \frac{1}{2}[-\rho C_p^2(R) - \rho C_p^2(Q)](\varepsilon_R - \varepsilon_Q) + \\
&\qquad + \frac{k}{2}[\frac{\Delta\dot{\varepsilon}(R)}{\Delta t} + \frac{\Delta\dot{\varepsilon}(Q)}{\Delta t}]\Delta t = 0
\end{aligned}
\qquad (6.5)
$$

Notice that

$$
\frac{k}{2}[\frac{\Delta\dot{\varepsilon}(R)}{\Delta t} + \frac{\Delta\dot{\varepsilon}(P)}{\Delta t}]\Delta t \approx \frac{k}{2}[(\dot{\varepsilon}_R - \dot{\varepsilon}_A) + (\dot{\varepsilon}_A - \dot{\varepsilon}_P)] = \frac{k}{2}[(\dot{\varepsilon}_R - \dot{\varepsilon}_P)]
$$

$$
= \frac{k}{2}[\frac{\varepsilon_R - \varepsilon_P}{\Delta t} - \frac{\varepsilon_P - \varepsilon_R}{\Delta t}] = \frac{k}{\Delta t}[\varepsilon_R - \varepsilon_P]
$$

Similarly, $$\frac{k}{2}[\frac{\Delta\dot{\varepsilon}}{\Delta t}(R)+\frac{\Delta\dot{\varepsilon}}{\Delta t}(Q)]\Delta t=\frac{k}{\Delta t}[\varepsilon_R-\varepsilon_P]$$

Then the Hartree method can be written as

$$x_R-x_P=\frac{1}{2}[C_p(R)+C_p(P)]\Delta t$$

$$x_R-x_Q=\frac{1}{2}[-C_p(R)-C_p(Q)]\Delta t$$

$$(\sigma_R-\sigma_P)+\frac{1}{2}[\rho C_p^2(R)+\rho C_p^2(P)](\varepsilon_R-\varepsilon_P)+\frac{k}{\Delta t}[\varepsilon_R-\varepsilon_P]=0$$

$$(\sigma_R-\sigma_Q)+\frac{1}{2}[-\rho C_p^2(R)-\rho C_p^2(Q)](\varepsilon_R-\varepsilon_Q)+\frac{k}{\Delta t}[\varepsilon_R-\varepsilon_Q]=0 \qquad (6.6)$$

Because Equation (6.6) is a non-linear system of equations, when applying Equation (6.6) to calculate the dynamic stresses, the initial values of x_P, x_Q, $C_P(R)$, $C_p(P)$, $C_P(Q)$, ε_P, ε_Q, σ_P and σ_Q are very important. There are two methods to apply Equation (6.6) to calculate the dynamic stresses in the second phase. The first method is to use arbitrary mesh points to calculate the dynamic stresses. Since the length of the projectile is not very long, there is not enough space to get many test data. In order to get other data, the interpolation method must be used. However, the errors from the interpolation functions affect the accuracy of thecomputation. The second method is to use the particular mesh points to calculate the dynamic stresses. That is, the points calculated from RI theory's values are used as mesh points to compute the dynamic stresses. Next, Equation (6.6) is used to compute the stresses and strains of Aluminum 6061-T6511 in the second phase of the Taylor Test step by step.

6.2.3.1 Using Arbitrary Mesh Point to Calculate Dynamic Stresses

For the next computation, $\Delta t = \frac{t_p}{20} = 1.1815\ \mu s$

1. Get the values of RI theory at different mesh points, 5 points, shown in Table 6.3.

Table 6.3 Initial Values for Hartree Method

$x_R\ (mm)$	$\sigma_{RI}\ (Mpa)$	ε	$C_p\ (m/s)$
0	530.79	0.1454	9355
8.6	398.66	0.1269	6391
17	302.36	0.0828	2612
25.5	287.68	0.0478	1281
34.28	283.92	0	560

2. Using different values of x to get the interpolation functions of σ_{RI}, ε and C_p about x. Here Lagrangian interpolation method is used.

$$\sigma_{RI}(x) = 0.00415(x-8.6)(x-17)(x-25.5)(x-34.3) - 0.00127x(x-25.5)(x-34.3) - 0.0144x(x-8.6)(x-17)(x-34.3) - 0.0087x(x-8.6)(x-17)(x-34.3) - 0.0021x(x-8.6)(x-17)(x-25.5) \quad (6.7)$$

$$\varepsilon(x) = 1.147\times10^{-6}(x-8.6)(x-17)(x-25.5)(x-34.3) - 4.038\times10^{-6}x)(x-17)(x-25.5)(x-34.3) + 3.94\times10^{-6}x(x-8.6)(x-17)(x-34.3) - - 1.48\times10^{-6}x(x-8.6)(x-17)(x-34.3) \quad (6.8)$$

$$C_p(x) = 0.073(x-8.6)(x-17)(x-25.5)(x-34.3) - 0.2x(x-17)(x-25.5)(x-34.3) + 0.124x(x-8.6)(x-25.5)(x-34.3) - 0.039x(x-8.6)(x-17)(x-34.3) + 0.043x(x-8.6)(x-17)(x-25.5) \quad (6.9)$$

3. Using the below equation to get initial values

$$x_P = x_R - C_p(A)\Delta t$$

$$x_Q = x_R + C_p(A)\Delta t \tag{6.10}$$

4. Using x_P and x_Q computed from Equation (6.10) to compute interpolation values σ_P, σ_Q, ε_P, ε_Q, C_P and C_Q of Equations (6.8), (6.9) and (6.10). The computed results are shown in Table 6.4.

Table 6.4 Computed Results From Hartree Method (1)

x_P mm	x_Q mm	x_R mm	$C_p(P)$ m/s	$C_p(Q)$ m/s	$C_p(R)$ m/s	ε_P	ε_Q	ε_R	σ_P MPa	σ_Q MPa	σ_R MPa
7.55	9.65	8.6	6799	3743	6391	0.1388	0.1130	0.1452	414.65	383.00	-6.173
13.91	20.09	17.00	3743	1824	2612	0.1130	0.0550	0.0442	329.00	286.00	9.727
23.98	27.00	25.5	1335	1216	1281	0.000	0.000	0.000	279.00	282.00	279.00

From the above values for three points, if not enough mesh points are obtained, themethod is not very accuracte. During the plastic wave propagation, the plastic wave propagates initially very fast and then decreases gradually. So the interval of time must be taken very small for the initial plastic wave propagation. However, the increase of the number of the interval of time causes the accumulation of computation error. On the other hand, when the Hartree method is used, the initial values must be local values near the true values of x_P, x_Q, $C_P(R)$, $C_p(P)$, $C_P(Q)$, ε_P, ε_Q, σ_P and σ_Q. That is to say, the interpolation should be avoided. Otherwise, the computed values cannot converge to the true values. In order to use the Hartree method well, the initial values

should be given or obtained by simple computation as much as possible.

6.2.3.2 Using Specific Mesh Point to Calculate Dynamic Stresses

From the above computation, the Hartree method is very sensitive to the errors from computing x_P, x_Q, $C_P(R)$, $C_p(P)$, $C_P(Q)$, ε_P, ε_Q, σ_P and σ_Q. To improve the accuracy of computed results, the mesh points are placed the measured values x_P, x_Q. The values of $C_p(P)$, $C_P(Q)$, σ_P and σ_Q are from computed RI theory's values. The interval of time is taken differently for every mesh point. The following flow chart tells us how to compute necessary data for the Hartree Method. The computed results are shown in Table 6.5

The following calculation begins in the second phase.
The following values should be known: $x_P, x_Q, \varepsilon_P, \varepsilon_Q, \sigma_P, \sigma_Q, C_p(P), C_p(Q), \Delta t, k$.
The following values are from the measurements of a projectile: x_P, x_Q The following values are from the calculation: $\varepsilon_r(x_p) = \frac{D_P - D_0}{D_0}$ $\varepsilon_r(x_Q) = \frac{D_Q - D_0}{D_0}$ Using the rule of plastic incompressibility to calculate ε_P, ε_Q: $\varepsilon_P = -2\varepsilon_r(x_P)$ $\varepsilon_Q = -2\varepsilon_r(x_Q)$

The values of are from the computation of RI theory: $\sigma_P, \sigma_Q,\ C_p(P), C_p(Q)$
The computation of x_R: $x_R = \frac{(x_P + x_Q)}{2}$
The computation of velocity of plastic wave at point R: $C_p(R) = \frac{C_p(P) + C_p(Q)}{2}$
The computation of time interval: $\Delta t = \frac{2(x_P - x_Q)}{C_p(P) + C_p(R)}$
Material constant k from Malvern experimental result.
Using Hartree method finds the following values: $\varepsilon_R,\ \sigma_R$
Strain rate can be calculated as follows: $\dot{\varepsilon}_R = \frac{\varepsilon_P - \varepsilon_R}{\Delta t}$ or $\dot{\varepsilon}_R = \frac{\varepsilon_R - \varepsilon_Q}{\Delta t}$
Repeat the above steps for next point.

The relationship of the stress σ_R and x is shown in Figure 6.3. The distribution of the dynamic stress in the projectile is shown in Figure 6.4. Now we discuss the propagation of the plastic wave from the first phase to the second phase with the help of Figure 6.4.

Table 6.5 Computed Results From Hartree Method (2)

x_P mm	x_Q mm	x_R mm	$C_p(P)$ m/s	$C_p(Q)$ m/s	$C_p(R)$ m/s	ε_P	ε_Q	ε_R	σ_P MPa	σ_Q MPa	σ_R MPa	Δt $\times 10^{-2}$ μsec
2.80	3.40	3.10	9355	8470	8912	0.1454	0.1405	0.1430	813	704	1171	6.372
3.40	5.00	4.20	8470	7732	8100	0.1405	0.1361	0.1384	704	625	975	9.875
5.00	6.30	5.65	7732	6716	7224	0.1361	0.1292	0.1329	625	531	940	17.99
6.30	9.40	7.85	6716	6182	8912	0.1292	0.1251	0.1272	531	487	740	48.00
9.40	14.00	11.70	6182	4224	5203	0.1251	0.1064	0.1151	487	368	491	88.40
14.00	16.00	15.00	4224	2885	3554	0.1064	0.0877	0.099	368	318	433	56.30
16.00	24.50	18.25	2885	1907	2396	0.0877	0.0673	0.0842	318	296	472.3	166.9
20.00	24.50	22.25	1907	1303	1605	0.0673	0.0486	0.0592	296	288	460	280.4
24.50	28.00	26.25	1303	959	1131	0.0486	0.0336	0.0416	288	285	415.8	309.5
28.00	32.00	30.00	959	644	801	0.0336	0.0141	0.0254	285	284	386.5	499.1
32.00	34.00	33.50	1335	1216	602	0.0141	0.0000	0.014	284	283	384	332.2

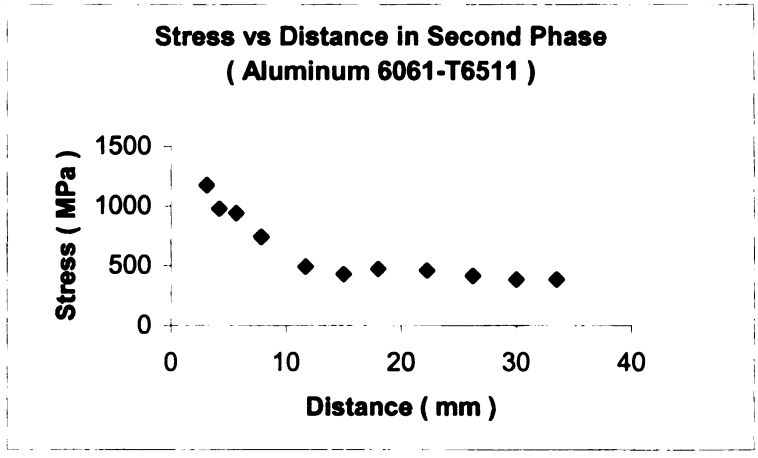

Figure 6.3 Stress vs. Distance in Second Phase (Aluminum 6061-T6511)

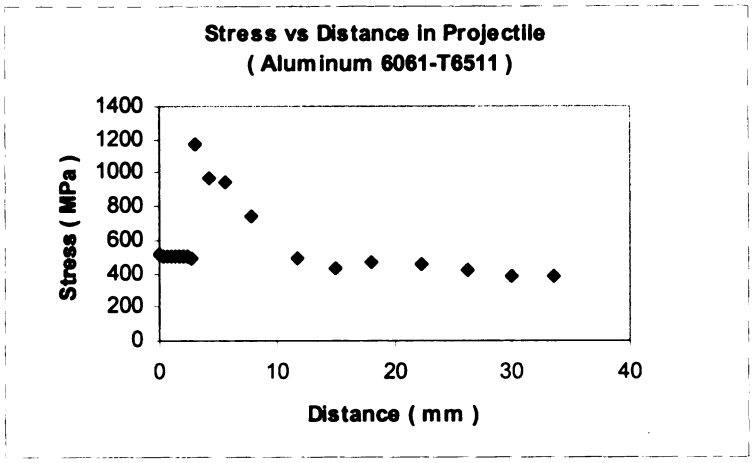

Figure 6.4 Stress vs. Distance in Projectile (Aluminum 6061-T6511)

1. When the projectile heats the rigid wall around the impact end of the projectile, $x \leq 0.69$ mm, the stress changes a little. But after $x > 0.69$ mm, the strain and the stress do not change. Basically, they are constants. For strain, ε is about 0.15 or so. For stress, $\sigma = 498$ MPa. They indicate that when using the first solutions of the plastic wave equations (RD theory or RI theory) to solve the dynamic stresses in the first phase, the theory can explain experimental results well. At the same time, it indicates that the theory can be applied a distance from the impact end. If we check other Taylor tests in Chapter 3, then it can be discovered that above conclusions are true.

2. When the plastic wave propagates from the first phase entering the second phase, the dynamic stress increases suddenly. This one takes place at the interface between the first phase and the second phase. The interface is about at $x = 2.75$ mm. The dynamic stress value is about the twice of the value of the dynamic stress in the first phase. This tells us that the maximum dynamic stress value takes place at the interface between the first phase and the second phase.

3. As the plastic wave propagates from the first phase to the second phase, the

values of the dynamic stresses gradually decay, that is, the effect of the strain rate plays an import role in this region. After a distance from the interface, $x = 12$ mm, the change of the stress gradually is steady. The effect of the strain rate plays a less important role. This means that RD theory can be replaced by RI theory. This conclusion matches one of Bell's tests. The distribution of the strain rate along the projectile is shown in Figure 6.5 and the third column in Table 6.6.

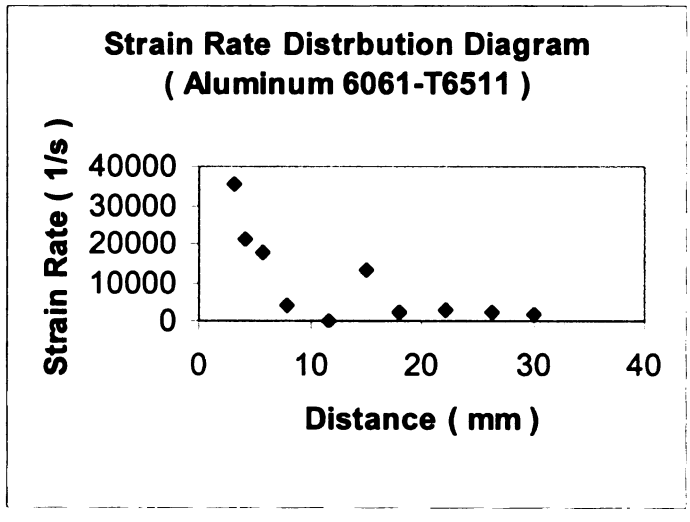

Figure 6.5 Strain Rate Distribution Diagram

Table 6.6 Computed Results From Modified Malvern Model vs. Johnson-Cook Model

Distance (mm)	Strain	Strain Rate (1/s)	Stress (MPa) New RD Model	Stress (MPa) Johnson-Cook Model
0	0.1723	0	509.33	509.33
0.343	0.1596	0	503.31	503.31
0.6875	0.1565	0	501.79	501.79
1.03125	0.1491	0	498.09	498.09
1.375	0.1484	0	497.74	497.74
1.71875	0.1487	0	497.88	497.88
2.0625	0.1486	0	497.84	497.84
2.40625	0.1486	0	497.84	497.84
2.75	0.1459	0	496.45	496.45
3.10	0.1430	35650	1171	572.71
4.20	0.1384	21265	975	564.21
5.65	0.1329	17780	940	560.77
7.85	0.1272	4166	740	547.1
11.70	0.1151	0	491	485.12
15.00	0.099	13140	43 0	535.77
18.25	0.0842	2097	472	510.54
22.25	0.0592	2889	460	489.23
26.25	0.04163	2252	415	468.12
30.00	0.0254	1642	386	441.3
33.50	0.014	4214	384	421.71

4. When both the Johnson-Cook model and the Modified Malvern model are used to compute the dynamic stress's distribution along the projectile, the computed results are shown in Table 6.6 and Figure 6.6. From the Figure 6.6, the ways of the stress decay are different for two models. The Johnson-Cook model is not sensitive to the change of the stress. The maximum stress computed from the Modified Malvern model is about twice of the value computed from the Johnson-Cook model.

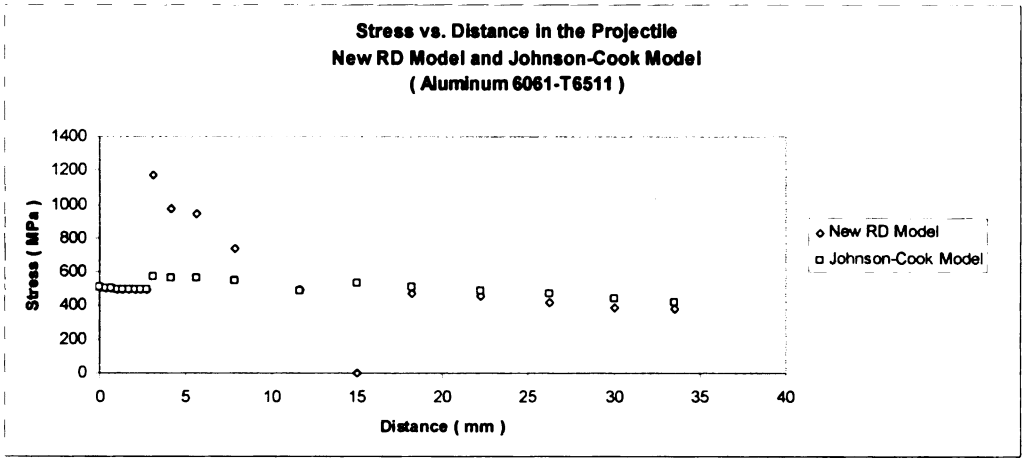

Figure 6.6 Stres vs. Distance in the Projectile From Modified Malvern Model and Johnson-Cook Model

CHAPTER 7

CONCLUSIONS AND FUTURE WORKS

7.1 Conclusion

In this thesis, the propagation of the plastic wave and its applications in the Taylor Impact Test are discussed. The shape curves and the dynamic yielding stress of the projectile are used to verify our theoretical investigation. A complete method to calculate the dynamic yielding stress, strain, and the velocity of the plastic wave in the projectile is developed.

Our investigation indicates that according to the shape curve, the projectile can be divided into three phases. After impact, the shape curve of the first phase is concave, the one of the second phase is convex and the third one is a straight line.

When the plastic wave propagates in the projectile, the first phase can be described by a linear solution of the plastic wave equation (RI theory). It is an adiabatic process. The strain and wave velocity are constants.

The second phase can be described by a nonlinear solution of the plastic wave equation. In this phase, the velocity of the plastic wave, the strain and the strain rate are not constants. In order to get the nonlinear solution of the equation of the plastic wave, a constitutive equation (RI) is proposed. Based on this constitutive equation, the shape curve of the projectile is convex can be predicted, and the dynamic yielding stress of the projectile can be calculated. Other models cannot predict that the shape curve of the projectile in the second phase is convex.

In order to consider the effect of the strain rate in the propagation of the plastic wave, the Modified Malvern model is proposed. This model, the characteristic method and the numerical method are used to analyze the propagation of the plastic wave.

Our investigation indicates that with the propagation of the plastic wave the effect of the strain rate gradually decreases. So, at a distance from the impacted end, the RD theory can be replaced by the RI theory. This conclusion matches the Bell's test result. The von Karman solution is a characteristic equation of the plastic wave equation. The RD theory can predict the existence of the plateau around the impacted end. The existence of the plateau is independent of the model of the materials.

As an application of the theory, the Taylor Impact Tests with three different materials and impact velocities are carried out. Using the constitutive equation proposed in this investigation to compute the dynamic stress in the projectiles gets good results. The experimental results indicate that the shape curves of projectiles after impact match the conclusions from our theoretical results very well. The theoretical analyses in the three materials indicate that there exists the maximum dynamic stress around the interface between the first phase and the second phase.

7.2 Taylor Formula and New Formula

When deriving his formula, Taylor did not use the theory of plastic wave propagation. So he thought that his formula could be used to calculate the dynamic yielding strength of a material roughly. In this thesis, the theory of plastic wave propagation is used to calculate the dynamic yielding strength of a material. The result is better than the one from Taylor's formula. But more parameters are needed. Comparison between two formulas are shown as follows:

Taylor's Formula

1. Objective: find $\sigma_{dy}(\varepsilon)$

2. Test: $V_0, L, L_0, L_e, H, \rho$

3. Analysis:

$$\sigma_{dy} = \frac{\rho V_0 (L - H)}{2(L - L_0)\ln\frac{L}{H}}$$

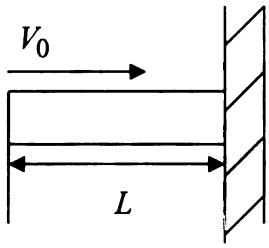

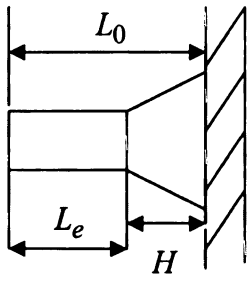

New Formula

1. Objective: find $\sigma_{dy}(\varepsilon, \dot{\varepsilon})$ $\sigma_d(x)$ and $\dot{\varepsilon}(x)$

2. Test: $V_0, L, L_0, L_e, \rho, h, h_d, R_d, R_h, k, C_1, C_2$
where k is a material constant from Malvern model, C_1 and C_2 are integration constants.

3. Analysis:

1) $\sigma_{dy}(RI) = \frac{\rho C_2}{2} e^{\frac{2C_1}{C_2}}$

2) $\sigma_{dy}(RD) = \sigma_{dy}(RI) + k\dot{\varepsilon}$

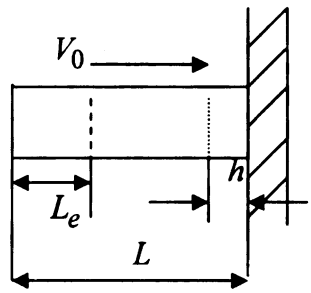

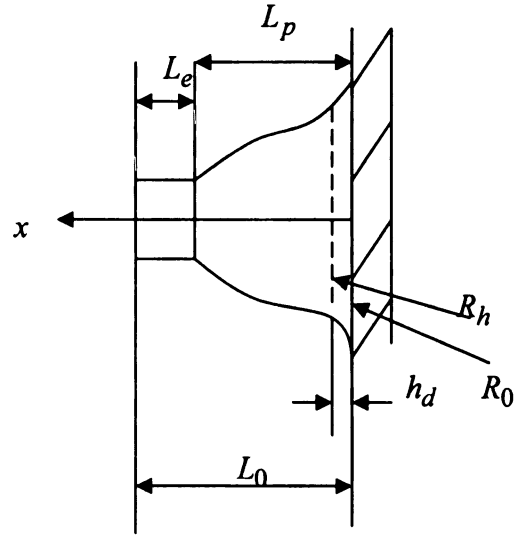

Using the rule of plastic incompressibility, h can be calculated from h_d and the

measured data

$$h = \frac{2\ln\frac{R_h}{R0}}{\ln(1+\frac{2r_0^2}{R_0^2\ln\frac{R_h}{R_0}})} h_d$$

The computed results and measured results are as follows

Table 7.1 Values of h From Computed Results and Measured Results

Material	Computed Results (cm)	Measured Results (cm)	Discrepancies
Aluminum 6061-T6511	0.299	0.275	8.7%
Copper 145-Hard-H02	0.363	0.353	2.8%
Steel C1045	0.223	0.211	2.9%

The computation of dynamic stress in the first phase is by the Johnson-Cook model. From the measured strain and the model, the dynamic stress in the first phase of Aluminum 6061-T6511 can be computed. In order to compute the dynamic stress in the second phase, the modified Malvern model is proposed and used to calculate the dynamic stress in the second phase. This model can be written

$$\sigma = \sigma_{RI}(\varepsilon) + k\dot{\varepsilon} = \frac{\rho C_2}{2}[e^{\frac{2(\varepsilon - C_1)}{C_2}}] + k\dot{\varepsilon}$$

When the Modified Malvern model is used to the Hartree method, the Hartree method can be written as

$$x_R - x_P = \frac{1}{2}[C_p(R) + C_p(P)]\Delta t$$

$$x_R - x_Q = \frac{1}{2}[-C_p(R) - C_p(Q)]\Delta t$$

$$(\sigma_R - \sigma_P) + \frac{1}{2}[\rho C_p^2(R) + \rho C_p^2(P)](\varepsilon_R - \varepsilon_P) + \frac{k}{\Delta t}[\varepsilon_R - \varepsilon_P] = 0$$

$$(\sigma_R - \sigma_Q) + \frac{1}{2}[-\rho C_p^2(R) - \rho C_p^2(Q)](\varepsilon_R - \varepsilon_Q) + \frac{k}{\Delta t}[\varepsilon_R - \varepsilon_Q] = 0$$

Because the above equation is a non-linear system of equations, when applying this equation to calculate the dynamic stresses, the initial values of x_P, x_Q, $C_P(R)$, $C_p(P)$, $C_P(Q)$, ε_P, ε_Q, σ_P and σ_Q are very important. The values of $C_p(P)$, $C_P(Q)$, σ_P and σ_Q are from computed RI theory's values. The interval of time is taken differently for every mesh point. The flow chart tells us how to compute necessary data for the Hartree Method step by step.

When both the Johnson-Cook model and the Modified Malvern model are used to compute the dynamic stress's distribution along the projectile, the computed results are shown in Figure 6.6. From the Figure 6.6, the ways of the stress decay are different for the two models. The Johnson-Cook model is not sensitive to the change of the stress. The maximum stress computed from the Modified Malvern model is about twice of the value computed from the Johnson-Cook model.

7.3 Future Works

The future investigation will mainly focus on tests. This work will include measuring the length of the first phase. From the point of view of theory, this length should be different for different materials and impact loading. These data are very important, as this is the first step to compute the dynamic stress and the strain under the

impact loading.

In this investigation, a constitutive equation is proposed. This constitutive equation only considers the effect of the strain, not the strain rate. At the same time, from the present models of the RD theory, these models can not describe accurately the propagation of the plastic wave. So, a new kind of constitutive equation of the RD theory needs to be studied.

During the plastic wave propagation, the effect of the strain rate decreases. After a distance and time, the effect of the strain rate can be neglected. So, this distance should be carefully investigated. We need to find which factors influence this distance.

At the interface of the first phase and the second phase, the theoretical study and tests (Bell) indicate that there exists shock wave for aluminum and copper even for lower impact velocities. So, we should investigate the relationships between the physical characteristics of materials and impact velocities.

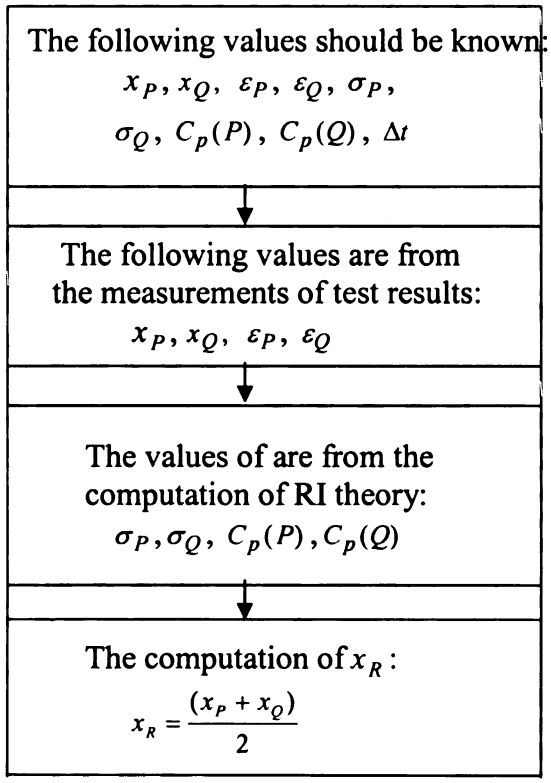

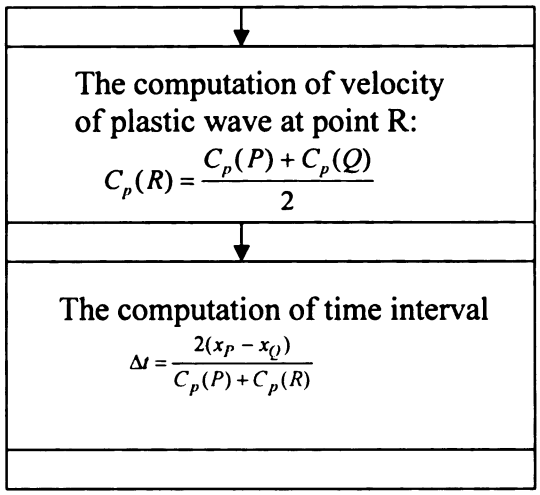

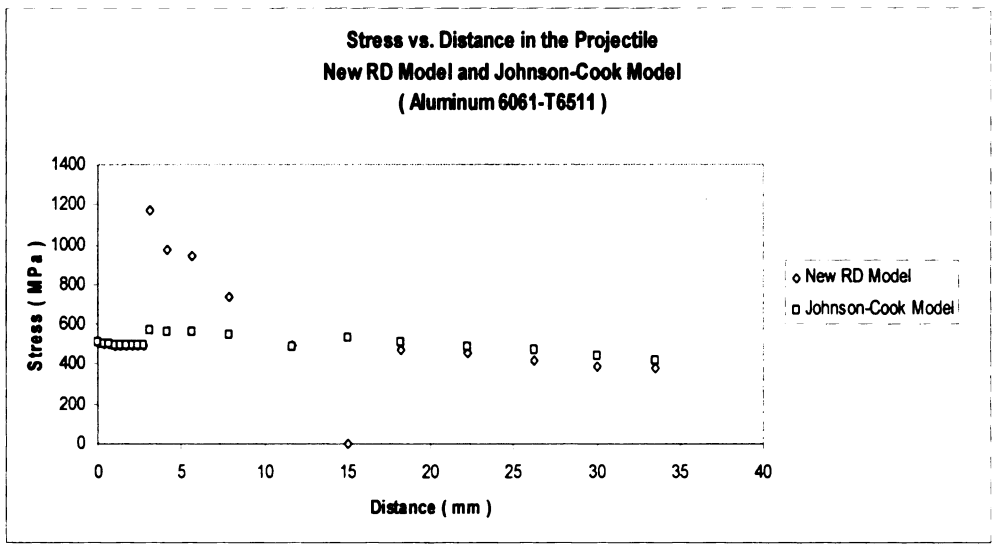

Figure 6.6 Stres vs. Distance in the Projectile From Modified Malvern Model and Johnson-Cook Model

Appendix A

Consider the following plastic wave equation

$$\rho \frac{\partial v}{\partial t} = \frac{\partial \sigma}{\partial x} \qquad \text{(A-1)}$$

During the propagation of plastic wave, v and σ are functions of x and t. Then the increments of v and σ can be written as

$$dv = \frac{\partial v}{\partial x} dx + \frac{\partial v}{\partial t} dt \qquad \text{(A-2)}$$

$$d\sigma = \frac{\partial \sigma}{\partial x} dx + \frac{\partial \sigma}{\partial t} dt \qquad \text{(A-3)}$$

Also, the following equation is satisfied

$$\frac{\partial v}{\partial x} = \frac{\partial \varepsilon}{\partial t} \qquad \text{(A-4)}$$

With RI theory, $\sigma = \sigma(\varepsilon)$. Take the derivative with respect to t, then

$$\frac{\partial \sigma}{\partial t} = \frac{\partial \sigma}{\partial \varepsilon} \frac{\partial \varepsilon}{\partial t}$$

$$\Rightarrow \qquad \frac{\partial \varepsilon}{\partial t} = \frac{1}{\dfrac{\partial \sigma}{\partial \varepsilon}} \frac{\partial \sigma}{\partial t} \qquad \text{(A-5)}$$

Take Equation (A-5) into Equation (A-4), then it yields

$$\frac{\partial v}{\partial x} = \frac{1}{\dfrac{\partial \sigma}{\partial \varepsilon}} \frac{\partial \sigma}{\partial t} \qquad \text{(A-6)}$$

Putting Equations (A-1), (A-2), (A-3) and (A-6) together, then we have

$$\begin{cases} \rho\dfrac{\partial v}{\partial t}=\dfrac{\partial \sigma}{\partial x} \\ dv=\dfrac{\partial v}{\partial x}dx+\dfrac{\partial v}{\partial t}dt \\ d\sigma=\dfrac{\partial \sigma}{\partial x}dx+\dfrac{\partial \sigma}{\partial t}dt \\ \dfrac{\partial v}{\partial x}=\dfrac{1}{\dfrac{\partial \sigma}{\partial \varepsilon}}\dfrac{\partial \sigma}{\partial t} \end{cases}$$

Rewrite the above equation as follows

$$\begin{cases} \dfrac{\partial v}{\partial t}-\dfrac{1}{\rho}\dfrac{\partial \sigma}{\partial x}=0 \\ dx\dfrac{\partial v}{\partial x}+dt\dfrac{\partial v}{\partial t}=dv \\ dx\dfrac{\partial \sigma}{\partial x}+dt\dfrac{\partial \sigma}{\partial t}=d\sigma \\ \dfrac{\partial v}{\partial x}-\dfrac{1}{\dfrac{\partial \sigma}{\partial \varepsilon}}\dfrac{\partial \sigma}{\partial t}=0 \end{cases}$$

$$\Rightarrow \begin{bmatrix} 0 & 1 & -\frac{1}{\rho} & 0 \\ dx & dt & 0 & 0 \\ 0 & 0 & dx & dt \\ 1 & 0 & 0 & -\frac{1}{\frac{\partial\sigma}{\partial\varepsilon}} \end{bmatrix} \begin{bmatrix} \frac{\partial v}{\partial x} \\ \frac{\partial v}{\partial t} \\ \frac{\partial\sigma}{\partial x} \\ \frac{\partial\sigma}{\partial x} \end{bmatrix} = \begin{bmatrix} 0 \\ dv \\ d\sigma \\ 0 \end{bmatrix} \qquad \text{(A-7)}$$

The characteristic equation of the plastic wave equation can be obtained by letting determinant of the coefficient matrix of Equation (A-7) be equal to zero,

$$\begin{vmatrix} 0 & 1 & -\frac{1}{\rho} & 0 \\ dx & dt & 0 & 0 \\ 0 & 0 & dx & dt \\ 1 & 0 & 0 & -\frac{1}{\frac{\partial\sigma}{\partial\varepsilon}} \end{vmatrix} = 0$$

$$\Rightarrow \qquad \frac{1}{\rho}(dt)^2 - (dx)^2 \frac{1}{\frac{\partial\sigma}{\partial\varepsilon}} = 0$$

$$\Rightarrow \qquad (\frac{dx}{dt})^2 = \frac{1}{\rho}\frac{\partial\sigma}{\partial\varepsilon}$$

$$\Rightarrow \qquad \frac{dx}{dt} = \pm\sqrt{\frac{1}{\rho}\frac{\partial\sigma}{\partial\varepsilon}} \qquad \text{(A-8)}$$

Equation (A-8) tells us that the velocity of the plastic wave propagation is $\sqrt{\frac{1}{\rho}\frac{\partial\sigma}{\partial\varepsilon}}$.

Notice that under the condition of the plastic wave being caused by a sudden constant load, all values of velocity of any element from $v = 0$ from $v =$ constant (and

consequently all values of ε from $\varepsilon = 0$ to $\varepsilon =$ constant) may be regarded as starting instantaneously at $t = 0$ from $x = 0$ and each is propagating with velocity $\sqrt{\frac{1}{\rho}\frac{\partial\sigma}{\partial\varepsilon}}$.

So, $\sqrt{\frac{1}{\rho}\frac{\partial\sigma}{\partial\varepsilon}}$ is independent of time t [Taylor, 3]. Take the integration for the both sides of Equation (A-8). Then

$$x = \pm\sqrt{\frac{1}{\rho}\frac{\partial\sigma}{\partial\varepsilon}}t + C_0$$

where C_0 is an integration constant.

Assume when $t = 0$, $x = 0$. Then $C_0 = 0$. So, it yields

$$\frac{x}{t} = \pm\sqrt{\frac{1}{\rho}\frac{\partial\sigma}{\partial\varepsilon}} \qquad \text{(A-11)}$$

Since for RI theory, $\sigma = \sigma(\varepsilon)$, we have

$$\frac{d\sigma}{d\varepsilon} = \frac{\partial\sigma}{\partial\varepsilon}$$

then Equation (A-9) becomes

$$\frac{x}{t} = \pm\sqrt{\frac{1}{\rho}\frac{d\sigma}{d\varepsilon}} \qquad \text{(A-10)}$$

That is, Equation (A-10) is the characteristic equation of the plastic wave equation for RI theory. During the propagation of plastic wave, Equation (A-10) is an identity. Define C_p as the velocity of the plastic wave propagation. Then we have

$$C_p = \sqrt{\frac{1}{\rho}\frac{d\sigma}{d\varepsilon}} \qquad \text{(A-11)}$$

Appendix B Derivation of Inequality

From mathematics textbooks, we have that Cauchy inequality:

$$\left|\int_a^b f(x)g(x)dx\right| \le \left[\int_a^b f^2(x)dx\right]^2\left[\int_a^b g^2(x)dx\right]^2$$

According to von Karman's derivation in his paper [2], the critical velocity for impact is defined as

$$v_c = \int_0^{\varepsilon_m}\sqrt{\frac{1}{\rho}\frac{d\sigma}{d\varepsilon}}d\varepsilon$$

Applying the Cauchy inequality into the above one, we have

$$v_c = \int_0^{\varepsilon_m}\sqrt{\frac{1}{\rho}\frac{d\sigma}{d\varepsilon}}d\varepsilon$$

$$= \int_0^{\varepsilon_m}[\frac{1}{\rho}]^{\frac{1}{2}}[\frac{d\sigma}{d\varepsilon}]^{\frac{1}{2}}d\varepsilon$$

$$= [\frac{1}{\rho}]^{\frac{1}{2}}\int_0^{\varepsilon_m}[\frac{d\sigma}{d\varepsilon}]^{\frac{1}{2}}d\varepsilon$$

$$= [\frac{1}{\rho}]^{\frac{1}{2}}\int_0^{\varepsilon_m}[\frac{d\sigma}{d\varepsilon}]^{\frac{1}{2}}\times 1 d\varepsilon$$

$$\le [\frac{1}{\rho}]^{\frac{1}{2}}\left[\int_0^{\varepsilon_m}1^2 d\varepsilon\right]^{\frac{1}{2}}\left[\int_0^{\varepsilon_m}[(\frac{d\sigma}{d\varepsilon})^{\frac{1}{2}}]^2 d\varepsilon\right]^{\frac{1}{2}}$$

$$= [\frac{1}{\rho}]^{\frac{1}{2}}[\varepsilon_m]^{\frac{1}{2}}\left[\int_0^{\varepsilon_m}\frac{d\sigma}{d\varepsilon}d\varepsilon\right]^{\frac{1}{2}}$$

$$= [\frac{1}{\rho}]^{\frac{1}{2}}\varepsilon_m^{\frac{1}{2}}[\sigma(\varepsilon_m)]^{\frac{1}{2}}$$

$$= \left[\frac{\varepsilon_m \sigma_m}{\rho} \right]^{\frac{1}{2}}$$

where $\sigma_m = \sigma(\varepsilon_m)$

That is: $$v_c \leq \left(\frac{\varepsilon_m \sigma_m}{\rho} \right)^{\frac{1}{2}}$$

Appendix C Dynamic Models of Materials

1. J.O.Thompson Model (Cubic Stress- Strain Model, 1891)

$$\varepsilon = a\sigma + b\sigma^2 + c\sigma^3$$

where a, b and c are constants; ε is the strain and σ is the stress.

2. E.K.Hartig Model (1893)

$$\sigma = \frac{E_0}{b}(1 - e^{-b\varepsilon})$$

where E_0 is the zero stress modulus; b is a constant; ε is the strain and σ is the stress.

3. L. Malvern Model (Liner Model , 1961)

$$\sigma = \sigma_0 + \frac{1}{k}\dot{\varepsilon}$$

where σ is the stress; $\dot{\varepsilon}$ is the nominal strain rate; σ_0 represented the static stress-strain relation; k is a constant.

4. Power Law Of Plasticity

$$\sigma_y = k(\varepsilon_{yp} + \bar{\varepsilon}_p)^n$$

where σ_y is the yield stress; ε_{yp} is the elastic strain to yield; $\bar{\varepsilon}_p$ is the effective plastic strain; k is the strength coefficient and n is the hardening exponent.

5. Strain Rate Dependent Plasticity Model

$$\sigma_y = \sigma_0 \dot{\bar{\varepsilon}}_p + E_p \bar{\varepsilon}_p$$

$$E_p = \frac{EE_t}{E - E_t}$$

where σ_y is the yield stress; σ_0 is the yield strength; $\bar{\varepsilon}_p$ is the effective plastic strain; $\dot{\bar{\varepsilon}}_p$ is the effective plastic strain rate; E is Young's modulus; E_t is the tangent modulus.

6. Rate Sensitive Power Law Of Plasticity

$$\sigma = k\varepsilon^m \dot{\varepsilon}^n$$

where σ is the yield stress; $\dot{\varepsilon}$ is the normalized effective plastic strain rate; ε is the effective plastic strain; k, n and m are constants.

7. Johnson-Cook Strain Rate and Temperature Model (1985)

$$\sigma = \left(A + B\varepsilon^n\right)\left(1 + C\ln\dot{\varepsilon}^*\right)(1 - T^{*m})$$

where σ is the flow stress; ε is the equivalent plastic strain; $\dot{\varepsilon}^* = \frac{\dot{\varepsilon}}{\dot{\varepsilon}_0}$ is the dimensionless plastic strain rate for $\dot{\varepsilon}_0 = 1.0\ s^{-1}$; T^m is homologous temperature; A, B, C, n and m are material constants.

8. Anisotropic Viscoplastic Model

$$\sigma(\varepsilon_{eff}^p, \varepsilon_{eff}^p) = \sigma_0 + Q_{r1}(1 - \exp(-C_{r1}\varepsilon_{eff}^p)) + Q_{r2}(1 - \exp(-C_{r2}\varepsilon_{eff}^p)) +$$
$$+ Q_{x1}(1 - \exp(-C_{x1}\varepsilon_{eff}^p)) + Q_{x2}(1 - \exp(-C_{x2}\varepsilon_{eff}^p)) + V_k \dot{\varepsilon}_{eff}^{pVm}$$

where $\sigma(\varepsilon_{eff}^{p}, \dot{\varepsilon}_{eff}^{p})$ is the yield stress; σ_0 is the initial stress value; ε_{eff}^{p} is the effective plastic strain; $\dot{\varepsilon}_{eff}^{p}$ is the plastic strain rate; Q_{r1}, Q_{r2}, C_{r1} and C_{r2} are the isotropic hardening parameters; Q_{x1}, Q_{x2}, C_{x1} and C_{x2} are the kinematics hardening parameters; V_k and V_m are the viscous material parameters.

Appendix D: von Karman's Solution

Shown in Figure D-1 is a homogeneous rod extending from $x = -\infty$ to $x = 0$. Assume that the endpoint at $x = 0$ is suddenly put in motion with a constant velocity V_0. Let the stress-strain relation of the material be

$$\sigma = \sigma(\varepsilon) \qquad (D.1)$$

where σ is stress and ε strain. Stresses that depend on the time-rate of strain are neglected, so are the stresses due to high-velocity waves, such as shock wave. The relation $\sigma = \sigma(\varepsilon)$ holds only for plastic deformation as the elastic deformation is negligible when compared with the plastic deformation. The lateral contraction of the material is also neglected in the following formulation.

With the above assumptions, the equation of motion for an element of the rod with length dx as shown in Figure D-1 can be written as:

$$\rho \frac{\partial^2 u}{\partial t^2} = \frac{\partial \sigma}{\partial x} \qquad (D.2)$$

where $u = u(x,t)$ is the displacement of the element in the longitudinal direction, ρ is the density of the rod and t is time. Since $\varepsilon = \dfrac{\partial u}{\partial x}$, then Equation (D.2) can be written in the form

$$\rho \frac{\partial^2 u}{\partial t^2} = \frac{d\sigma}{d\varepsilon} \frac{\partial^2 u}{\partial x^2}$$

Let

$$\rho \frac{\partial^2 u}{\partial t^2} = T \frac{\partial^2 u}{\partial x^2} \qquad (D.3)$$

where $T = \dfrac{d\sigma}{d\varepsilon}$ is a given function between plastic stress and plastic strain.

The boundary conditions for Equation (D.3) are $u = V_0 t$ at $x = 0$. Since the motion V_0 is constant during the time period of t_0, it is also noted that $u = 0$ for $x = -\infty$. A solution to Equation (D.3) in the following form was suggested by von Karman

$$u = V_0[t + \frac{x}{c_1}] \qquad (D.4)$$

where c_1 is an arbitrary propagating velocity. From this solution, it can be found that the strain ε is a constant and is equal to $\dfrac{V_0}{c_1}$.

A second solution was also mentioned by von Karman with the following expression:

$$\frac{T}{\rho} = \frac{x^2}{t^2} \qquad (D.5)$$

Since $T = \dfrac{d\sigma}{d\varepsilon}$ is a given function of ε, based on Equation (D.5), it can be rewritten as

$$\frac{d\sigma}{d\varepsilon} = \rho\xi^2 \qquad (D.6)$$

if $\xi = \dfrac{x}{t}$ is used.

From Equation (D.6), ε can be considered as a function of the variable ξ. Assume $\varepsilon = f(\xi)$, then the displacement u can be expressed as follows

$$u = \int_{-\infty}^{x} \frac{\partial u}{\partial x} dx = \int_{-\infty}^{x} \varepsilon dx = \int_{-\infty}^{x} f(\xi) dx = t \int_{-\infty}^{\xi} f(\xi) d\xi \qquad (D.7)$$

where $dx = td\xi$ is used.

With differentiation of Equation (D.7), the following equations can be obtained

$$\frac{\partial^2 u}{\partial t^2} = \frac{\xi^2}{t} f'(\xi)$$
$$\frac{\partial^2 u}{\partial x^2} = \frac{1}{t} f'(\xi) \qquad (D.8)$$

With substitution of Equations (D.8) into Equation (D.3), the following two equations can be identified

$$\rho \xi^2 = T \qquad (D.9)$$

$$f'(\xi) = 0 \qquad (D.10)$$

That is, one of them must hold. Equation (D.10) matches with the solution given by Equation (D.4), whereas Equation (D.9) matches with the expression given by Equation (D.5).

The complete solution presented by von Karman can be summarized as follows:

(a) For $|x| < c_1 t$, where c_1 is an arbitrary propagating velocity, the strain ε is constant and equal to $\frac{V_0}{c_1}$.

(b) For $c_1 t < |x| < c_0 t$, where c_0 is the propagating velocity of elastic wave,

$$T(\varepsilon) = \rho \frac{x^2}{t^2}$$

(c) For $|x| > c_0 t$, $\varepsilon = 0$

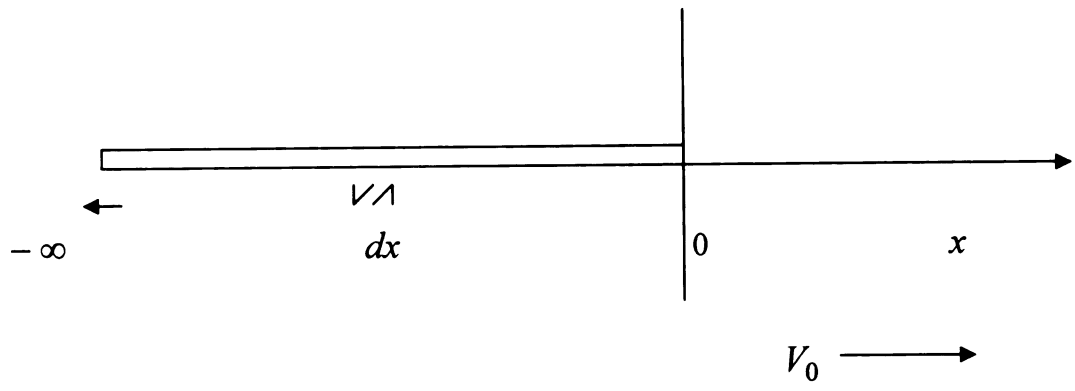

Figure D-1

Appendix E: Taylor's Test

A technique determining the dynamic yield stress of materials was developed by Taylor. The method involves impacting a right circular cylinder onto a rigid target at a constant velocity V_0, as shown in Figure E-1, and measuring the post-impact deformation of the cylinder. The cylinder has a length $L_0 + H$ and is assumed to be rigid strain-hardening, i.e. elastic strains are neglected. One-dimensional plastic wave propagation analysis was developed to identify the yield stress.

In Taylor dynamic study, the material was assumed to be rate independent, i.e. $\sigma = \sigma(\varepsilon)$. Figure E-2 shows the cylinder at some point of impact. The deformed surface is propagating away from the rigid target at a plastic wave velocity C_p. The deformed portion has an instantaneous length L, cross sectional area A, density ρ and stress σ. The particle velocity behind the plastic wave is assumed to be at rest, i.e. $v = 0$. The undeformed portion travels with an instantaneous velocity v_0, which is less than V_0. It has an instantaneous length h, cross-sectional area A_0 and density ρ_0. The stress in the undeformed portion is assumed to be at yielding point σ_y.

Based on the law of conservation of mass, the flows of mass into the interface I from both portions are equal to each other, i.e.

$$\rho(C_p - v)A = \rho_0(C_p - v_0)A_0$$

$$\rho C_p A = \rho_0(C_p - v_0)A_0$$

Assume $\rho = \rho_0$, it yields

$$C_p A = (C_p - v_0) A_0 \qquad (E.1)$$

The decreasing velocity of the underformed portion is

$$\frac{dh}{dt} = -(C_p - v_0) \qquad (E.2)$$

Based on material incompressibility, the strain directly behind the plastic wave front can be calculated, i.e.

$$\varepsilon = \frac{L - L_0}{L_0} = \frac{\frac{V_{vol}}{A} - \frac{V_{vol}}{A_o}}{\frac{V_{vol}}{A_0}} = \frac{A_0 - A}{A} = \frac{A_0}{A} - 1 \qquad (E.3)$$

where V_{vol} is the volume of the material and L is the length of the deformed portion. Combining Equation (E.3) and Equation (E.1), the following relation can be established

$$\varepsilon = \frac{v_0}{C_p - v_0} \qquad (E.4)$$

Consider an element with length dx and unit cross-sectional area 1 ahead of the plastic wave front, as shown in Figure E-2. Assume the velocity of the initial state of the element is v_{00}; the velocity of the final state of the element is v_{01}. It takes time dt for the element to deform from the initial state to the final state. From Newton's law

$$Fdt = mdv$$

$$Fdt = \rho_0 dx \cdot 1 \cdot (v_{01} - v_{00})$$

Assuming the initial state of the element is $v_{00} = v_0$ and the final state of the element is at rest, $v_{01} = 0$, the above equation can be rewritten as

$$(\sigma - \sigma_y)dt = \rho_0 dx(-v_{00})$$

$$(\sigma - \sigma_y) = -\rho_0 v_0 \frac{dx}{dt} \qquad (E.5)$$

In analogy to Equation (E.2), the following equation an be established for the element

$$\frac{dx}{dt} = -(C_p - v_0) \qquad (E.6)$$

Taking Equation (E.6) into Equation (E.5), it yields

$$\sigma - \sigma_y = \rho_0 (C_p - v_0) v_0 \qquad (E.7)$$

The equation of motion of the undeformed portion is

$$\rho_0 A_0 h \frac{dv_0}{dt} = \sigma_y A_0$$

$$\rho_0 h \frac{dv_0}{dt} = \sigma_y \qquad (E.8)$$

Recall Equation (E.2),

$$dt = -\frac{dh}{C_p - v_0} \qquad (E.9)$$

With substitution of Equation (E.9) into Equation (E.8), it yields

$$\rho_0 h dv_0 = -\sigma_y \left(\frac{dh}{C_p - v_0}\right)$$

$$-(C_p - v_0)dv_0 = \frac{\sigma_y}{\rho_0}\frac{dh}{h} \qquad (E.10)$$

Assuming C_p is a constant, and taking integration from V_0 to 0 and from L_0 to H, where L_0 is the original length, then we have

$$-\frac{1}{2}(C_p - v_0)^2\Big|_{-V_0}^{0} = \frac{\sigma_y}{\rho_0}\ln h\Big|_{L_0}^{H}$$

$$\frac{V_0^2}{2} + V_0 C_p = \frac{\sigma_y}{\rho_0}\ln\frac{H}{L_0} \qquad (E.11)$$

where specific $-V_0$ is used because the velocity is negative in x direction.

It was further assumed by Taylor that the undeformed portion of the specimen decelerates at a uniform rate. Then it can be seen that the plastic wave propagates a distance $(L_1 - H)$, where L_1 is the final length of the cylinder and H is the final length of the undeformed portion, as shown in Figure E-3. The plastic wave propagating time is

$$t = \frac{L_1 - H}{C_p} \qquad (E.12)$$

If it is assumed that the time of deceleration is uniform, it is approximately equal to

$$t = \frac{2(L_0 - L_1)}{V_0} \qquad (E.13)$$

From Equation (E.12) and Equation (E.13), it gives

$$C_p = \frac{V_0}{2}\frac{(L_1 - H)}{(L_0 - L_1)} \qquad (E.14)$$

Taking Equation (E.14) into Equation (E.13), the yield stress obtained from Taylor's study because

$$\frac{\sigma_y}{\rho_0 V_0^2} = \frac{(L_0 - H)}{2(L_0 - L_1)}\frac{1}{\ln(\frac{L_0}{H})} \qquad (E.15)$$

The yield stress in the above equation only involves measurements of the undeformed portion of the cylinder and the impact velocity.

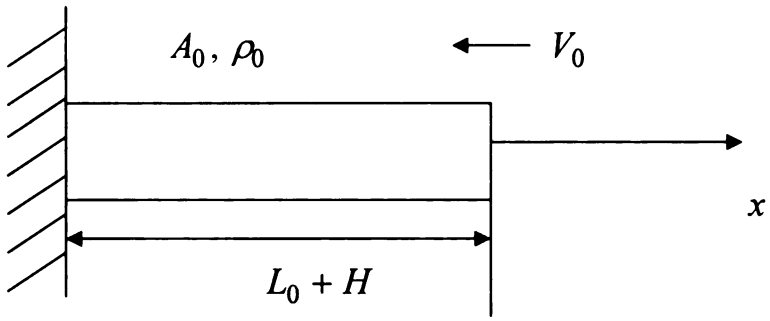

Figure E-1 Schematic of the rod before impact test.

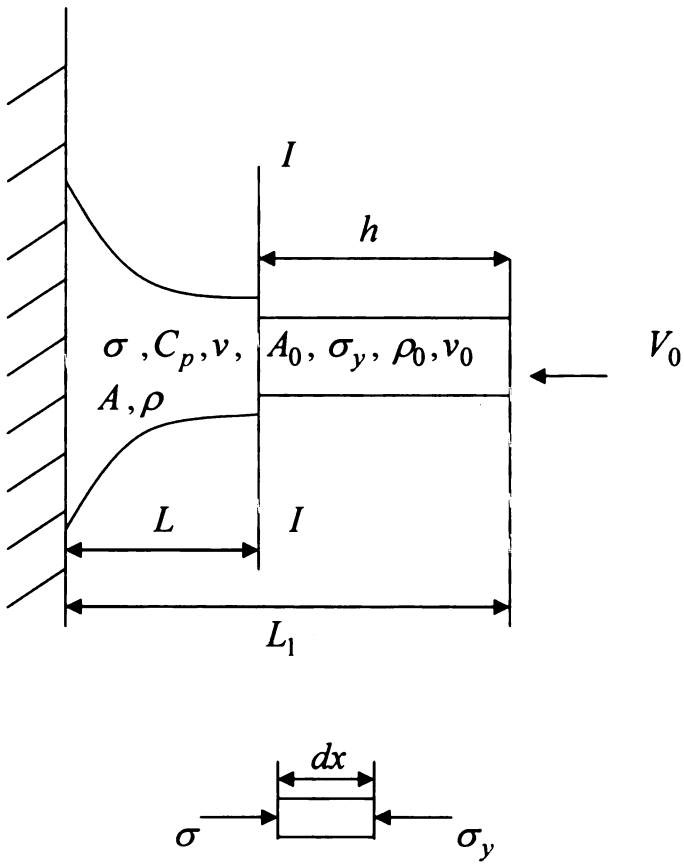

Figure E-2 Schematic of the rod during impact test.

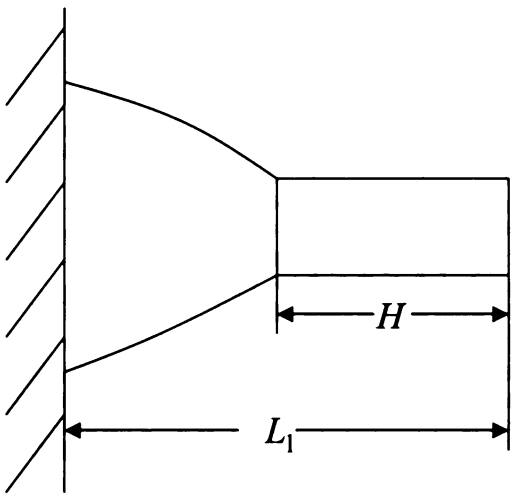

Figure E-3- Schematic of the rod at the end of impact test.

Appendix F: Formulation of Plastic Wave Propagation

The investigation of a plastic wave propagating in continuum media can be based on interfacial conditions. It based on the laws of the conservation of mass, conservation of momentum and conservation of energy. In the analysis, the stress, strain, density, particle velocity, plastic wave velocity and internal energy are taken as state variables. The laws of conservation of mass, momentum and energy are combined with equation of state and constitutive equation to constitute a complete set of equations.

As shown in Figure F-1, there is an interface I to which a plastic wave propagates from the right end of the media. Assume that behind the plastic wave front, the cross sectional area is A, the density is ρ, the stress is σ, the particle velocity is v, the velocity of the plastic wave is C_p and the specific energy density is I_E. Ahead of the plastic wave front, the cross sectional area is A_0, the density is ρ_0, the stress is σ_0(yield stress), the particle velocity is v_0 and the specific energy density is I_{E0}. The velocities are referred to an Eulerian coordinate system fixed in space.

1. Conservation of Mass

At the interface I, the conservation of mass requires that the rate of mass flowing into the plastic wave front equals the rate of mass exiting the plastic wave front. Hence

$$\rho A(C_p - v) = \rho_0 A_0 (C_p - v_0) \qquad (F.1)$$

If the particles entering the plastic wave front are rest immediately after the plastic deformation, i.e. $v = 0$, Equation (F-1) can be rewritten as

$$\rho A C_p = \rho_0 A_0 (C_p - v_0) \qquad \text{(Taylor-1)}$$

However, if $v_0 = 0$ is imported, Equation (F-1) will become

$$\rho A (C_p - v) = \rho_0 A_0 C_p \qquad \text{(MFJ-1)}$$

2. Conservation of Momentum

The law of conservation of momentum requires that the change of a mass entering the plastic wave front in an increment of time Δt equals the impulse imparted to the mass over the same time Δt, i.e. $F\Delta t = m\Delta v$. Consider a free element ahead of the plastic wave front. The mass of the element is $\Delta m_0 = \rho_0 A_0 (C_p - v_0)\Delta t$. Before entering the plastic wave front, the particle velocity of the element is v_0. After entering the plastic wave front, the particle velocity of the element is v. The force acting on the element is $(\sigma A + \sigma_0 A_0)$. Thus, from Newton's law

$$F\Delta t = \Delta m_0 (v - v_0)$$

$$\Rightarrow \quad (\sigma A + \sigma_0 A_0)\Delta t = \rho_0 A_0 (C_p - v_0)\Delta t (v - v_0)$$

$$\Rightarrow \quad (\sigma A + \sigma_0 A_0) = \rho_0 A_0 (C_p - v_0)(v - v_0) \qquad \text{(F-2)}$$

In MFJ's analysis, let $v_0 = 0$ and consider the sign of σ_0 is negative, then Equation (F-2) becomes

$$\sigma A - \sigma_0 A_0 = \rho_0 A_0 C_p v \qquad \text{(MFJ-2)}$$

In the Taylor's formulation, since $v = 0$ and $A = A_0 = 1$, and then consider

the sign of v_0 is negative, Equation (F-2) becomes

$$\sigma - \sigma_0 = \rho_0 (C_p - v_0) v_0 \qquad \text{(Taylor-2)}$$

3. Conservation of Energy

The law of conservation of energy requires that the energy before entering the interface I and the work done by the acting forces is equal to the energy after exiting the interface. For an element with a mass of $\Delta m_0 = \rho_0 A_0 (C_p - v_0)\Delta t$, it yields

$$\begin{aligned}
&[\rho_0 (C_p - v_0) A_0 \Delta t] I_{E0} + \frac{1}{2}\rho_0 (C_p - v_0) A_0 \Delta t (C_p - v_0)^2 \\
&+ (\sigma A v \Delta t + \sigma_0 A_0 v \Delta t) = \\
&= [\rho_0 (C_p - v_0) A_0 \Delta t] I_E + \frac{1}{2}\rho_0 (C_p - v_0) A_0 \Delta t (C_p - v)^2 \\
&\rho_0 (C_p - v_0) A_0 I_{E0} + \frac{1}{2}\rho_0 (C_p - v_0) A_0 (C_p - v_0)^2 + (\sigma A + \sigma_0 A_0) v = \\
&= \rho_0 (C_p - v_0) A_0 I_E + \frac{1}{2}\rho_0 (C_p - v_0) A_0 (C_p - v)^2
\end{aligned}$$

$$I_E - I_{E0} = (\sigma \frac{A}{A_0} + \sigma_0) \frac{v}{\rho_0 (C_p - v_0)} + \frac{(C_p - v_0)^2}{2} - \frac{(C_p - v)^2}{2}$$

(F-3)

Eliminating v by using combing Equation (F-1), Equation (F-2) with Equation (F-3), it gives

$$I_E - I_{E0} = \frac{1}{2}(\sigma + \sigma_0)(\frac{1}{\rho_0} - \frac{1}{\rho}) \qquad \text{(F-4)}$$

In MFJ analysis, let $v_0 = 0$ and $A = A_0$. Combing Equation (F-3) with Equation (MFJ-1) and Equation (MFJ-2) and consider the sign of σ_0 is negative, then

$$I_E - I_{E0} = \frac{1}{2}[C_p^2 - (C_p - v)^2] + (\frac{\sigma}{\rho} - \frac{\sigma_0}{\rho_0}) \qquad \text{(MFJ-3)}$$

In Taylor's formulation, the conservation of energy is not considered.

Collect Equations (F-1), (F-2) and (F-4), a complete set of equations for formulation plastic wave propagation is

$$\rho A(C_p - v) = \rho_0 A_0 (C_p - v_0) \qquad (*)$$

$$(\sigma A + \sigma_0 A_0) = \rho_0 A_0 (C_p - v_0)(v - v_0) \qquad (**)$$

$$I_E - I_{E0} = \frac{1}{2}(\sigma + \sigma_0)(\frac{1}{\rho_0} - \frac{1}{\rho}) \qquad (***)$$

In the above equations, there are 10 variables. However, A, A_0, ρ_0, v_0 and I_{E0} are usually a given and measurable. If so, there are 5 variables in the equations, two more equations are needed. In general, an equation of state and a constitutive equation are combined with 5 original equations to solve 5 variables.

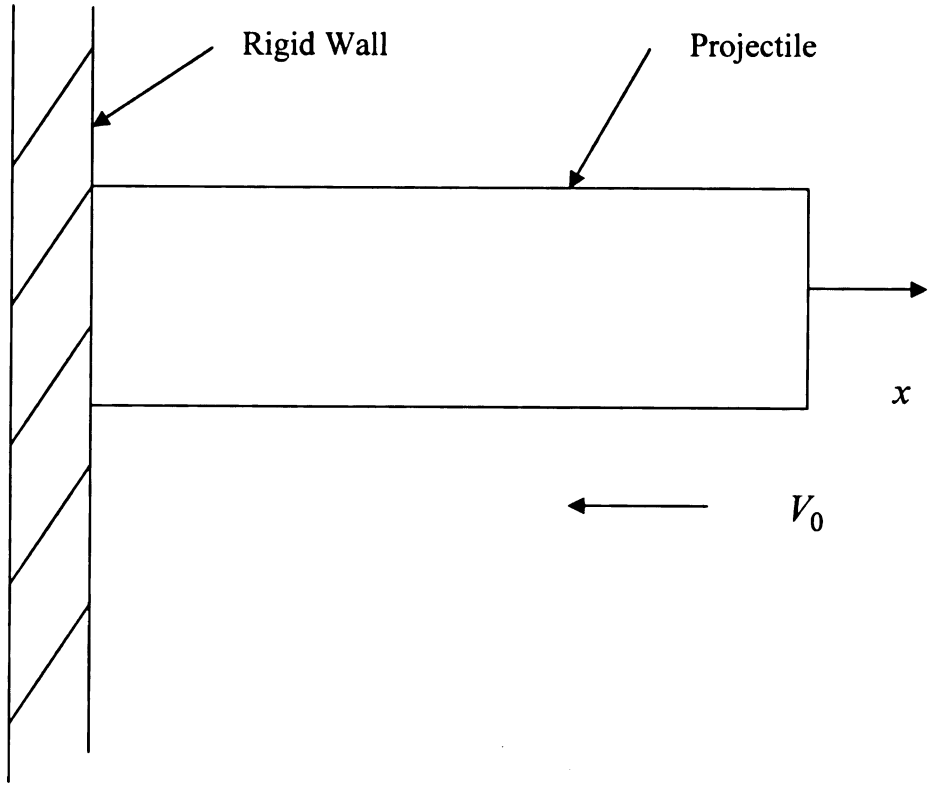
Rigid Wall
Projectile
x
V_0

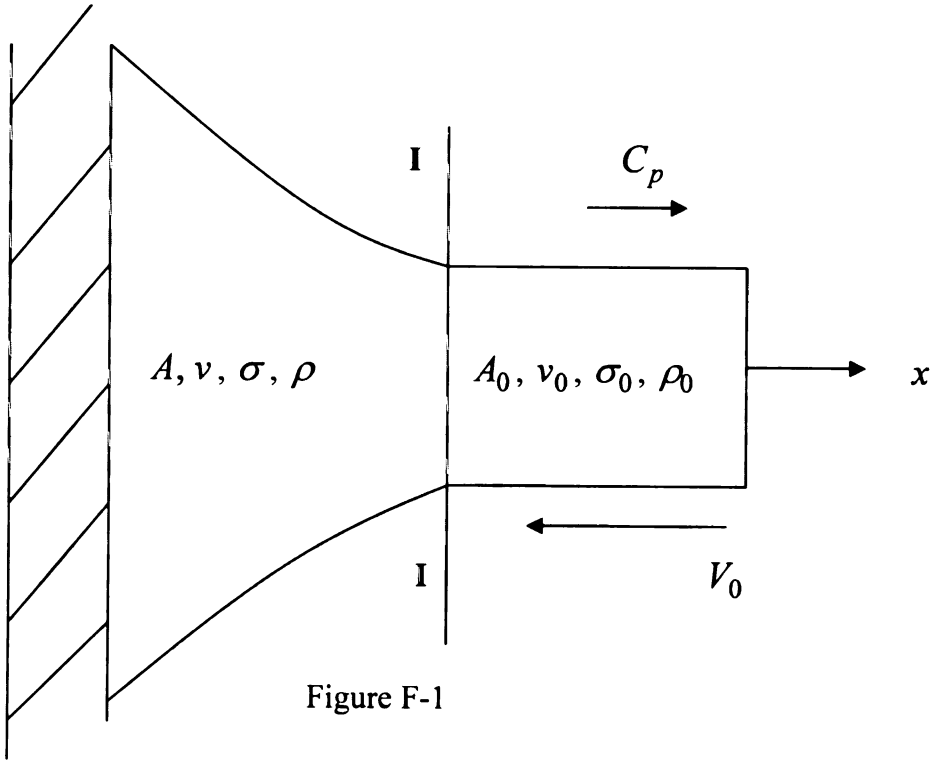
I
C_p
A, v, σ, ρ
$A_0, v_0, \sigma_0, \rho_0$
x
I
V_0

Figure F-1

Appendix G Maudlin-Foster-Jones Model

In Maudlin-Foster-Jones (MFJ)model, the conservation relationships (jump conditions) in conjunction with postulated material constitutive behavior are applied to study steady plastic wave propagation. Strength constitutive behavior and an equation of state (EOS) are combined with the jump equations. For example, the von Mises yield surface, Johnson-Cook (JC) or MTS (Mechanical Threshold Stress) flow stress models, and Mie-Grunisen EOS are used as constitutive equations in the paper by Maudlin-Foster-Jones. Obviously, the choice of constitutive equation is not unique, but the main technical points were illustrated in their paper. The following one is a summary from the Maudlin-Foster-Jones paper. The details can be referred to the article.

1. Preliminaries

Consider an axi-symmetric cylinder with radius of r_0, as shown in Figure G-1. An area strain is defined as

$$\varepsilon_A = \frac{A_0 - A}{A} \qquad (G.1)$$

where A_0 is the initial undeformed area, while A is current deformed area.

Taking differentiation of Equation (G.1), it gives

$$d\varepsilon_A = -\frac{A_0}{A^2} dA \qquad (G.2)$$

A volumetric strain increment referenced to the initial configuration can be defined as

$$d\varepsilon_v = \frac{dV_{vol}}{V_v} \qquad (G.3)$$

where V_{vol} is the current volume, V_v is the initial volume. ε_v is the volume strain.

An increment of small Lagrangian strain is defined as

$$dE_{ij} = \frac{1}{2}[L_{im}F_{mj} + L_{jm}F_{mi}]dt \qquad (G.4)$$

where F_{ij} is the deformation gradient, i.e.

$$F_{ij} = \frac{\partial x_i}{\partial X_j}$$

2. Conservation Relationships (Jump Conditions)

As shown in Figure G-2, assume that behind the plastic wave the cross-sectional area is A, the density is ρ, the specific internal energy density is I_E, the stress is σ and the velocity of the particle is v. Ahead of the plastic wave, the cross-sectional area is A_0, the density is ρ_0, the specific internal energy density is I_{E0}, the stress is σ_0 and the velocity of the particle is v_0. The velocity of plastic wave is C_p.

From the law of conservation of mass, we have

$$\rho_0 A_0 C_p = \rho A(C_p - v) \qquad (G.5)$$

From the law of conservation of momentum, we have

$$\sigma A - \sigma_0 A_0 = -\rho_0 A_0 C_p v \qquad (G.6)$$

From the law of the conservation of energy

$$I_E - I_{E0} = \frac{1}{2}[C_p^2 - (C_p - v)^2] + \frac{\sigma}{\rho} - \frac{\sigma_0}{\rho_0} \qquad (G.7)$$

Equation (G.5) can be rearranged to yield

$$(\frac{\rho_0 A_0}{\rho A} - 1)C_p = -v \qquad (G.8)$$

The expression within parenthesis can be rewritten as

$$\frac{\rho_0 A_0}{\rho A} - 1 = \frac{A_0}{A}(\frac{\rho_0}{\rho} - 1) + (\frac{A_0}{A} - 1) \qquad (G.9)$$

With use of $\rho = \frac{1}{V_{vol}}$ and $\rho_0 = \frac{1}{V_v}$, it yields

$$\frac{\rho_0}{\rho} - 1 = \frac{\frac{1}{V_v} - \frac{1}{V_{vol}}}{\frac{1}{V_v}} = \frac{V_{vol} - V_v}{V_v} = \frac{\Delta V_{vol}}{V_v} = \varepsilon_v \qquad (G.10)$$

In the limit of incompressible flow, $A_0 L_0 = AL$. Hence

$$\frac{A_0}{A} = \frac{L}{L_0} = \frac{L_0 + \Delta L}{L_0} = 1 + \varepsilon \qquad (G.11)$$

where ε is one dimensional engineering strain, L is the deformed length of cylinder and ΔL is the increment of L_0. Equation (G.9) becomes

$$\frac{\rho_0 A_0}{\rho A} - 1 = \varepsilon + \varepsilon\varepsilon_v + \varepsilon_v \qquad (G.12)$$

and the conservation of mass equation, i.e. Equation (G.5), becomes

$$C_p = -\frac{v}{\varepsilon(\varepsilon_v + 1) + \varepsilon_v} \qquad (G.13)$$

Similar algebraic manipulations will yield conservation of momentum in the

following form

$$\frac{\sigma}{1+\varepsilon} - \sigma_0 = -\rho_0 C_p v \qquad (G.14)$$

The conservation of mass equation can then be used to eliminate the particle velocity v in Equation (G.14), it gives

$$\frac{\sigma_0 - \dfrac{\sigma}{1+\varepsilon}}{[\varepsilon_v(1+\varepsilon)+\varepsilon]} = -\rho_0 C_p^2 \qquad (G.15)$$

The wave velocity C_p can then be eliminated from Equation (G.14) and the following can be achieved

$$[\sigma_0 - \frac{\sigma}{1+\varepsilon}][\varepsilon_v(1+\varepsilon)+\varepsilon] = -\rho_0 v^2 \qquad (G.16)$$

It is the equation for the constant particle velocity in terms of stress and strain across the wave front.

Finally, the conservation of mass and conservation of momentum equations can be used to rewrite the conservation of energy equation,

$$\rho_0(I_E - I_{E0}) = \frac{1}{2}[\varepsilon_v(\varepsilon+1)+\varepsilon][\sigma_0 + \frac{\sigma_1}{1+\varepsilon}] \qquad (G.17)$$

in terms of stress and strain. It is a form of the Hugoniot equation. Equations (G.15), (G.16) and (G.17) in general require an equation of state and a constitutive equation to completely specify the curves in stress and strain space. This problem will be solved in the next section.

3. Constitutive Relationships

Specification of a yield surface provides an equation relating the deviatoric stress

s_{ij} to a yield stress or flow stress σ_f. MFJ model uses von Mises surface and a flow stress model that is functionally dependent on equivalent plastic strain ε_p, strain rate $\dot{\varepsilon}_p$, and temperature T:

$$\frac{3}{2}s_{ij}s_{ji} = \sigma_f^2(\varepsilon_p, \dot{\varepsilon}_p, T) \qquad (G.18)$$

In Maudlin-Foster-Jones' paper, two flow stress models are investigated; the Johnson-Cook model and the MTS model. Here only the Johnson-Cook model is illustrated.

The Johnson-Cook model has the following form:

$$\sigma_f = [\sigma_y + B\varepsilon_p^n][1 + C\ln\dot{\varepsilon}_p][1 - (\frac{T - T_t}{T_m - T_t})^m] \qquad (G.19)$$

The first factor in Equation (G.19) represents strain hardening with σ_y interpreted as the initial yield stress, B is a strain-hardening coefficient, and n is a strain-hardening exponent. The second factor accounts for strain-rate hardening effects with C being a strain-rate hardening coefficient. The last factor represents thermal softening relative to room temperature T_t, decreasing to zero as the melting point T_m is realized. The quantity m is a softening exponent.

If follow von Karman and Duwez and Kolsky by relating the plastic wave velocity to the partial derivative of the stress with respect to strain suggested by a method of characteristics solution of the equation motion for the uniaxial stress problem, then it gives

$$C_p^2 = \frac{1}{\rho_0}\frac{\partial\sigma_{xx}}{\partial E_{xx}} \qquad (G.20)$$

where ρ_0 is the initial density and E_{xx} is the small Lagrangian strain given by Equation

(G.4).

For the Johnson-Cook model, the plastic wave velocity can be calculated as follows:

$$\frac{\partial \sigma_{JC}}{\partial \varepsilon_p} = Bn\phi_p^{n-1}[1 + C\ln\varepsilon_p][1 - (\frac{T - T_t}{T_m - T_t})^m]$$

When we use the energy jump equation to combine with a Mie-Grunisen EOS and a von Mises yield function, then we obtain an analogous Hugoniot result:

$$\sigma_x = -\frac{\frac{1}{2}(\varepsilon_A + \varepsilon_v + \varepsilon_A\varepsilon_v)\sigma_y + I_{E0}\rho_0 + \frac{1}{\Gamma(1+\mu)}[\frac{2}{3}\sigma_f + (k_1\mu + k_2\mu^2 + k_3\mu^3)(1 - \frac{\Gamma}{2}\mu)]}{\frac{1}{2}(\varepsilon_A + \varepsilon_v + \varepsilon_A\varepsilon_v)\frac{1}{(1+\varepsilon_A)} + \frac{1}{\Gamma(1+\mu)}} \qquad (G.21)$$

If the volumetric strain now assumed to be small, then we have that:

$$\sigma_x = -\frac{\frac{1}{2}\varepsilon_A\sigma_y + I_{E0}\rho_0 + \frac{1}{\Gamma}(\frac{2}{3}\sigma_f - \varepsilon_v k_1)}{\frac{1}{2}\frac{\varepsilon_A}{(1+\varepsilon_A)} + \frac{1}{\Gamma}} \qquad (G.22)$$

where k_1 is a linear coefficient, k_2 is a quadratic coefficient, k_3 is a cubic coefficient, Γ is Grunisen coefficient, $\mu_0 = \frac{\rho}{\rho_0} - 1$.

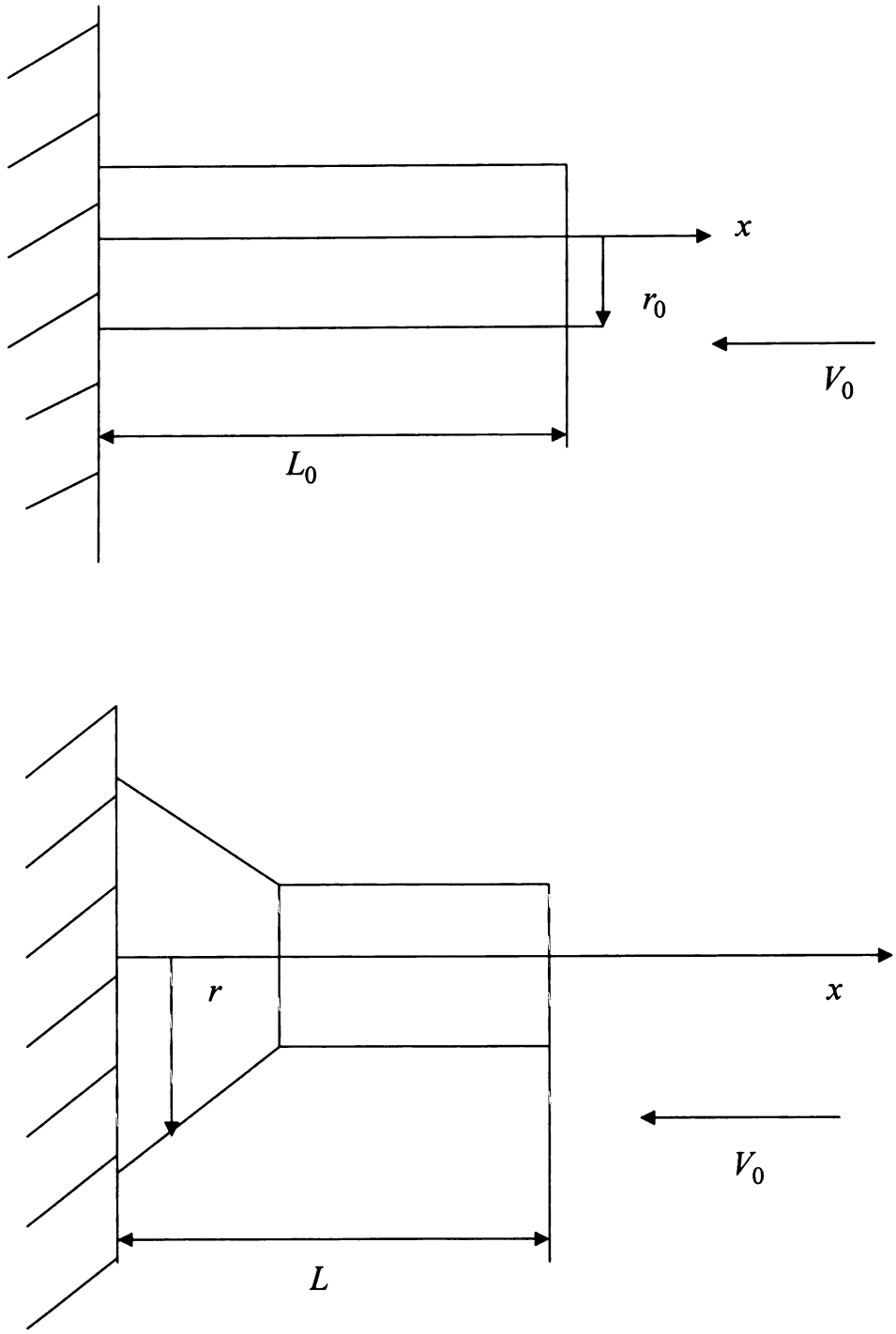

Figure G-1

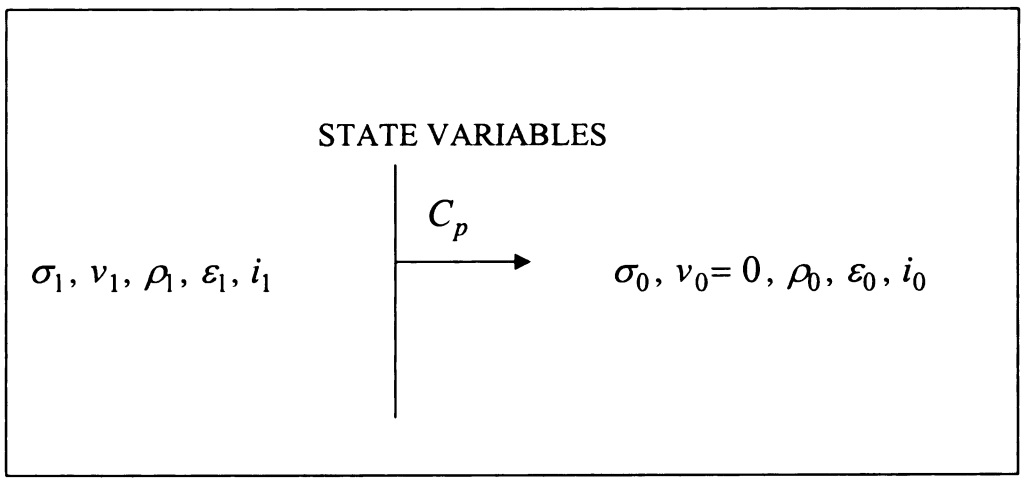

Figure G-2

Variables relative to the plastic wave front. Variables with subscript 0 are up stream of the plastic wave and subscripts 1 are downstream.

Appendix-H

Name	Model	$\frac{\partial\sigma}{\partial\varepsilon}$	$\frac{\partial\sigma}{\partial\dot{\varepsilon}}$	Material	Contents
Hartig	$\sigma = \frac{E}{b}(1-e^{-b\varepsilon})$	$Ee^{-b\varepsilon}$	0	X	$b > 0$
Logarithmic Law	$\sigma = \sigma_1(\varepsilon) + k\ln\dot{\varepsilon}$	$\frac{\partial\sigma_1}{\partial\varepsilon}$	$\frac{k}{\dot{\varepsilon}}$	X	X
Power Law	$\sigma = \sigma_1(\varepsilon)\dot{\varepsilon}^n$	$\dot{\varepsilon}^n \frac{\partial\sigma_1}{\partial\varepsilon}$	$n\sigma_1\dot{\varepsilon}^{n-1}$	X	X
Malvern Model $k = 10^6 1/s$	$\sigma = (20000 - \frac{10}{\varepsilon}) + 1000000\dot{\varepsilon}$	$\frac{\partial\sigma_1}{\partial\varepsilon}$	k	Aluminum	
Power Law Plasticity	$\sigma = k(\varepsilon_e + \varepsilon)^n$	$nk(\varepsilon_e + \varepsilon)^{n-1}$	0	Aluminum 1100	$k = 0.598$, $n = 0.216$
Strain Rate Dependent Plasticity	$\sigma = E_p\varepsilon + \sigma_0(\dot{\varepsilon})$	$\frac{\partial E_p}{\partial\varepsilon}$	$\frac{\partial\sigma_0}{\partial\dot{\varepsilon}}$	4140 Steel	X
Johnson-Cook Model	$\sigma = (A + B\varepsilon^n)^* (1 + C\ln\dot{\varepsilon})$	$B\varepsilon^{n-1}(1 + C\ln\dot{\varepsilon})$	$\frac{A + B\varepsilon^n}{\dot{\varepsilon}}$	X	X
Rate Sensitive Power Law Plasticity	$\sigma = k\varepsilon^m\dot{\varepsilon}^n$	$mk\dot{\varepsilon}^n\varepsilon^{m-1}$	$nk\varepsilon^m\dot{\varepsilon}^{n-1}$	A356 Aluminum	$k = 0.002$, $m = 0.7$, $n = 0.32$

Johnson-Cook Model

Material	A(MPa)	B(MPa)	C	n
OFHC	89	292	0.0025	031
Catridge Brass	117	505	0.009	0.42
Nickle 200	163	648	0.006	0.33
Armco Iron	175	380	0.06	0.32
Carpenter Elertrc Iron	290	336	0.055	0.4
1006 Steel	350	275	0.022	0.36
2024-T351 Aluminum	265	426	0.015	0.34
7038 Aluminum	336	343	0.01	0.41
4340 Steel	792	510	0.014	0.26
S-7 Tool Steel	154	476	0.012	0.18
Tungsten	1056	176	0.016	0.12
Depleted Uranium	1079	1119	0.007	0.25
Tantalum	140	300	X	0.3

Appendix I Elastic Wave in The Taylor Test

In the Taylor test [2], a compressive elastic wave and a compressive plastic wave occur in rod when it strikes onto a rigid wall. The elastic wave moves into the rod faster than the plastic wave and reflects from the free end of the rod as a tensile wave. The reflected elastic wave collides with the ongoing plastic wave somewhere in the rod. When they meet, the tensile elastic wave reflects from the plastic wave front again as a compressive wave and moves toward the free end of the rod. This back and forth process continues until the propagation of the elastic wave stops as the effect of interior material friction force.

In the absence of body forces, the elastic wave propagation can be expressed by the following wave equation, which is based on Newton second law and Hooke's law

$$E\frac{\partial^2 u_e}{\partial x^2} = \rho_e \frac{\partial^2 u_e}{\partial t^2}, \qquad 0 \le x \le L,\ t \ge 0; \qquad \text{(I-1)}$$

where x is the coordinate, t is time, $u_e(x,t)$ is elastic displacement, L is the length of the rod. E is Young's modulus and ρ_e is density.

There are three kinds of boundary condition in the elastic wave propagation of the Taylor test. The first kind is associated with the impacted end between the rod and the rigid wall, the second kind is the free boundary at the free end of the rod and the third kind is located right at the plastic wave front.

1. Impact Boundary

If the impact velocity of the rod onto the rigid wall is V_0 strikes the rigid wall, the boundary condition and the initial conditions can be expressed as follows:

$$u_e(0,t) = 0,$$

$$u_e(x,0) = 0,$$

$$\frac{\partial u_e(x,0)}{\partial t} = V_0$$

2. Free Boundary

At the free end of the rod, there is no strain. The boundary condition can be given by

$$\frac{\partial u_e(L,t)}{\partial x} = 0$$

When a compressive elastic wave propagates into the free end of the rod, it comes out as a tensile wave. Kuscher [35] used a laser velocity interferometer, the so-called VISAR, to measure the wave propagation in Taylor's test for a 9S20K steel rod. The propagation of the plastic wave front can be calculated based on the experimental technique. He also presented a Lagrangian diagram, i.e. $x - t$ plot, to express the one-dimensional wave propagation phenomenon. Kuscher found that the velovity of the plastic wave decreases exponentially along the rod which had an aspect ratio L/D=10 and an impact velocity $V_0 = 314m/s$.

3. Elasto-plastic Boundary

When the tensile elastic wave meets with the compressive plastic wave, an elasto-plastic boundary is created. The boundary essentially divides the rod into two regions, an elastic region and a plastic region. The investigation of the elasto-plastic boundary before the plastic wave can be based on the laws of the conservation of mass and conservation of momentum.

As shown in Figure I-1, there is an elasto-plastic boundary I. Assume that

behind the plastic wave front, the cross sectional area is A_p, the density is ρ_p, the stress is σ, the particle velocity is v_p, the velocity of the plastic wave is C_p while they are A_e, ρ_e, σ_e and v_e ahead of the plastic wave front, respectively.

At the elasto-plastic boundary, the conservation of mass requires that the rate of mass flowing into the plastic wave front equals the rate of mass exiting the plastic wave front. Hence

$$\rho_p A_p (C_p - v_p) = \rho_e A_e (C_p - v_e) \qquad (I\text{-}2)$$

The law of conservation of momentum requires that the change of a mass entering the plastic wave front in an increment of time Δt equals the impulse imparted to the mass over the same time Δt, i.e.

$$F\Delta t = m\Delta v$$

Consider a free element ahead of the plastic wave front. The mass of the element is

$$\Delta m_e = \rho_e A_e (C_p - v_e)\Delta t$$

Before entering the plastic wave front, the particle velocity of the element is v_e. After entering the plastic wave front, the particle velocity of the element is v_p. The force acting on the element is $(\sigma A_p - \sigma_e A_e)$. Thus, the forgoing equation becomes

$$(\sigma A_p - \sigma_e A_e)\Delta t = \rho_e A_e (C_p - v_e)\Delta t (v_p - v_e)$$

$$\Rightarrow \quad (\sigma A_p - \sigma_e A_e) = \rho_e A_e (C_p - v_e)(v_p - v_e) \qquad (I\text{-}3)$$

Rewrite Equations (I-2), (I-3) and set $A_p = A_e$, then become

$$v_e = C_p - \frac{\rho_p}{\rho_e}(C_p - v_p) \qquad (I\text{-}4)$$

$$\sigma_e = \sigma - \rho_e(C_p - v_e)(v_p - v_e) \qquad \text{(I-5)}$$

Equation (I-5) is a formula of the stress. According to Hooke's law, the strain at the elasto-plastic boundary should be

$$\varepsilon_e = \frac{\sigma - \rho_e(C_p - v_e)(v_p - v_e)}{E} \qquad \text{(I-5-1)}$$

At the elasto-plastic boundary, before the elastic wave meets the plastic wave, the elastic displacement should be zero. Then, it gives

$$u_{er}(L - l, t = 0) = 0$$

where u_{er} is the displacement function of the reflective elastic wave, l is the distance from the free end to the elasto-plastic boundary and t is the time of the propagation of the reflective elastic wave from the elasto-plastic boundary to the free end. Hence, when the elastic wave is reflected at the elasto-plastic boundary, the following conditions can be obtained as follows:

$$u_{er}(L - l, t = 0) = 0,$$

$$\frac{\partial u_{er}(x, t = 0)}{\partial t} = C_p - \frac{\rho_p}{\rho_e}(C_p - v_p),$$

$$\frac{\partial u_{er}(x, t = 0)}{\partial x} = \frac{\sigma - \rho_e(C_p - v_e)(v_p - v_e)}{E},$$

where $L - l \le x \le L$.

4. The Propagation of the Elastic Wave in the Rod

The equation of the elastic wave propagation with boundary conditions and initial conditions from the impacted end toward the free end in the rod can be written as

$$E\frac{\partial^2 u_e}{\partial x^2} = \rho_e \frac{\partial^2 u_e}{\partial t^2}, \qquad 0 \le x \le L,\ t \ge 0; \qquad \text{(I-6)}$$

B.C: $$u_e(0,t) = 0,\ \frac{\partial u_e(L,t)}{\partial x} = 0$$

I.C: $$u_e(x,0) = 0,\ \frac{\partial u_e(x,0)}{\partial t} = V_0$$

Now using the method of separation of variables to solve Equation (I-6).

Set $u_e(x,t) = X(x)T(t)$ and take it back the equation of the elastic wave, it yields

$$\frac{X''(x)}{X(x)} = \frac{T''(t)}{a^2 T(t)} \quad \text{, where } a = \sqrt{\frac{\rho_e}{E}}$$

The right side and the left side is equal each other, if and only if the above equation is equal to a constant $-\lambda$. Then

$$\frac{X''(x)}{X(x)} = \frac{T''(t)}{a^2 T(t)} = -\lambda$$

From the above equation, it yields

$$X''(x) + \lambda X(x) = 0 \qquad \text{(I-7)}$$

$$T''(x) + \lambda a^2 T(t) = 0 \qquad \text{(I-8)}$$

From the boundary conditions in Equation (I-6), it gives

$$u_e(0,t) = X(0)T(t) = 0$$

and $$\frac{\partial u_e(L,t)}{\partial x} = X'(x)T(t) = 0$$

So, it yields

$$\begin{cases} X(0) = 0 \\ X'(L) = 0 \end{cases} \qquad \text{(I-9)}$$

Combine Equation (I-7) and Equation (I-9), it gives

$$\begin{cases} X''(x) + \lambda X(x) = 0 \\ X(0) = 0 \\ X'(L) = 0 \end{cases} \qquad \text{(I-10)}$$

Assume the solution of Equation (I-10) is

$$X(x) = A\cos\beta x + B\sin\beta x, \qquad \text{where } \beta^2 = \lambda$$

Using the boundary conditions, it gives

$$A = 0,$$

and $$B\beta\cos\beta L = 0$$

So, $$\beta = \frac{n\pi}{2L}, \qquad n = 1,2,3\cdots$$

or $$\lambda = (\frac{n\pi}{2L})^2, \quad n = 1,2,3\cdots \qquad \text{(I-11)}$$

In this way, we obtain a series of eigenvalues, λ_n, and the responding function, X_n

$$\lambda_n = (\frac{n\pi}{2L})^2 \ , n = 1,2,3\cdots$$

$$X_n(x) = B_n \sin\frac{n\pi}{2L}x, \quad n = 1,2,3\cdots \qquad \text{(I–12)}$$

Combine Equation (I-7) and Equation (I-11), another equation about the time-dependent part can be obtained

$$T_n''(t) + \frac{a^2n^2\pi^2}{4L^2}T_n(t) = 0$$

Apparently, the solution of the above equation is

$$T_n(t) = C_n' \cos\frac{n\pi at}{2L} + D_n' \sin\frac{n\pi at}{2L} \qquad (\text{I-13})$$

From $u_e(x,t) = X(x)T(t)$, Equation (I-2) and (I-13), a solution can be obtained

$$u_n(x,t) = (C_n \cos\frac{n\pi at}{2L} + D_n \sin\frac{n\pi at}{2L})\sin\frac{n\pi}{2L}x$$

According to the principle of superposition, the solution of Equation (I-6) is given

$$u_e(x,t) = \sum_{n=1}^{\infty} (C_n \cos\frac{n\pi at}{2L} + D_n \sin\frac{n\pi at}{2L})\sin\frac{n\pi}{2L}x$$

Using the initial condition, $u_e(x,0) = 0$, then

$$u_e(x,0) = \sum_{n=1}^{\infty} C_n \sin\frac{n\pi x}{2L} = 0$$

that is, $C_n = 0.$

Using the initial condition again, $\frac{\partial u_e(x,0)}{\partial t} = V_0$, then

$$\frac{\partial u_e(x,0)}{\partial t} = \sum_{n=1}^{\infty} (-\frac{n\pi a}{2L} C_n \sin\frac{n\pi at}{2L} + \frac{n\pi}{2L} D_n \cos\frac{n\pi at}{2L})\sin\frac{n\pi x}{2L}$$

$$= \sum_{n=1}^{\infty} \frac{n\pi a}{2L} D_n \sin\frac{n\pi x}{2L} = V_0$$

that is, $D_n = \frac{4V_0}{n\pi a}\int_0^L \sin\frac{n\pi x}{2L}dx = \frac{8LV_0}{n^2\pi^2 a}(1 - \cos\frac{n\pi}{2})$

The solution of the elastic wave can be written as

$$u_e(x,t) = \sum_{n=1}^{\infty} D_n \sin\frac{n\pi at}{2L}\sin\frac{n\pi}{2L}x \qquad (\text{I-14})$$

Take D_n into Equation (I-14), then

$$u_e(x,t) = \sum_{n=1}^{\infty} \frac{8LV_0}{n^2\pi^2 a}(1-\cos\frac{n\pi}{2})\sin\frac{n\pi at}{2L}\sin\frac{n\pi x}{2L} \qquad (I\text{-}15)$$

From this equation, at any time the velocity of the particle, the strain and the stress can be obtained:

The strain: $$\varepsilon_e = \sum_{n=1}^{\infty} \frac{4V_0}{n\pi a}(1-\cos\frac{n\pi}{2})\sin\frac{n\pi at}{2L}\cos\frac{n\pi x}{2L}$$

The stress: $$\sigma_e = E\sum_{n=1}^{\infty} \frac{4V_0}{n\pi a}(1-\cos\frac{n\pi}{2})\sin\frac{n\pi at}{2L}\cos\frac{n\pi x}{2L}$$

The velocity of the particle: $$v_e = \sum_{n=1}^{\infty} \frac{4V_0}{n\pi}(1-\cos\frac{n\pi}{2})\cos\frac{n\pi at}{2L}\sin\frac{n\pi}{2L}x$$

5. The Propagation of the Reflective Elastic Wave in the Rod

As we known, when the elastic wave is reflected at the free end, it propagates toward the plastic wave. The reflected elastic wave collides with the ongoing plastic wave somewhere in the rod. When they meet, the tensile elastic wave reflects from the plastic wave front again as a compressive wave and moves toward the free end of the rod. This back and forth process continues until the propagation of the elastic wave stops as the effect of interior material friction force. Here, the simplest case is considered, that is, when the plastic wave stops propagating, the elastic wave come back from the free end and is reflected at the elasto-plastic boundary. That is to say, the elastic wave is only reflected once during the propagation of the plastic wave. So, the equation of the reflection elastic wave with boundary conditions and the initial conditions can be given as follows

$$E\frac{\partial^2 u_{er}}{\partial x^2} = \rho_0 \frac{\partial^2 u_{er}}{\partial t^2}, \qquad L - l \le x \le L,\ t \ge 0; \tag{I-16}$$

B.C: $u_{er}(L-l,t) = 0, \quad \dfrac{\partial u_{er}(L,t)}{\partial x} = 0,$

I.C: $$\frac{\partial u_{er}(x,0)}{\partial t} = C_p - \frac{\rho_p}{\rho_e}(C_p - v_p),$$

$$\frac{\partial u_{er}(x,0)}{\partial x} = \frac{\sigma - \rho_e(C_p - v_e)(v_p - v_e)}{E}.$$

where x is the coordinate, t is the time, $u_{er}(x,t)$ is the reflective elastic displacement.

Set $u_{er}(x,t) = X_r(x)T_r(t)$ and take it back the equation of the elastic wave, it yields

$$\frac{X_r"(x)}{X_r(x)} = \frac{T_r"(t)}{a^2 T_r(t)}, \qquad \text{where } a = \sqrt{\frac{\rho_e}{E}}$$

The right side and the left side is equal each other, if and only if the above equation is equal to a constant $-\alpha$. Then

$$\frac{X_r"(x)}{X_r(x)} = \frac{T_r"(t)}{a^2 T_r(t)} = -\alpha$$

From the above equation, it yields

$$X_r"(x) + \alpha X_r(x) = 0 \tag{I-17}$$

$$T_r"(x) + \alpha a^2 T_r(t) = 0 \tag{I-18}$$

From the boundary conditions, it gives

$$u_{er}(L-l,t) = X_r(L-l)T_r(t) = 0$$

and $$\frac{\partial u_r(L,t)}{\partial x} = X_r'(L)T_r(t) = 0$$

From the above two equations, one has

$$X_r(L-l)=0 \qquad (I-19)$$

$$X_r'(L)=0 \qquad (I-20)$$

Combine Equation (I-17) and Equation (I-20), it gives

$$\begin{cases} X_r''(x)+\alpha X_r(x)=0 \\ X_r(L-l)=0 \\ X'_r(L)=0 \end{cases} \qquad (I-21)$$

Assume the solution is

$$X_r(x)=A_r\cos\beta_r[x-(L-l)]+B_r\sin\beta_r[x-(L-l)]$$

where $\beta_r^2=\alpha$

Using the boundary condition, it gives

$$A_r=0$$

and $$B_r\beta_r\cos\beta l=0$$

So $$\beta_r=\frac{n\pi}{2l},\ n=1,2,3\cdots$$

or $$\alpha=(\frac{n\pi}{2l})^2,\ n=1,2,3\cdots \qquad (I-22)$$

Equation (I-22) gives a series of eigenvalues, α_n, and the responding function, X_{rn}

$$\alpha_n=(\frac{n\pi}{2l})^2,\ n=1,2,3\cdots$$

$$X_{rn}(x)=B_{rn}\sin\frac{n\pi}{2l}[x-(L-l)],\ n=1,2,3\cdots \qquad (I-23)$$

Combine Equation (I-18) and Equation (I- 22), an equation about the time-dependent part can be obtained

$$T_{rn}''(t) + \frac{a^2 n^2 \pi^2}{4l^2} T_{rn}(t) = 0$$

Apparently, the solution of the above equation is that

$$T_{rn}(t) = C_{rn}' \cos\frac{n\pi at}{2l} + D_{rn}' \sin\frac{n\pi at}{2l} \qquad \text{(I-24)}$$

From $u_{er}(x,t) = X_r(x)T_r(t)$, Equation (I-23) and (I-24), a solution can be obtained

$$u_{rn}(x,t) = (C_{rn} \cos\frac{n\pi at}{2l} + D_{rn} \sin\frac{n\pi at}{2l}) \sin\frac{n\pi}{2l}[x - (L-l)]$$

According to the principle of superposition, the solution is given

$$u_{er}(x,t) = \sum_{n=1}^{\infty} (C_{rn} \cos\frac{n\pi at}{2l} + D_{rn} \sin\frac{n\pi at}{2l}) \sin\frac{n\pi}{2l}[x - (L-l)]$$

Using the initial conditions,

$$\frac{\partial u_{er}(x,0)}{\partial t} = C_p - \frac{\rho_p}{\rho_e}(C_p - v_p)$$

and

$$\frac{\partial u_{er}(x,0)}{\partial x} = \frac{\sigma - \rho_e(C_p - v_e)(v_p - v_e)}{E}$$

then

$$\frac{\partial u_{er}(x,0)}{\partial t} = \sum_{n=1}^{\infty} (-\frac{n\pi a}{2l} C_{rn} \sin\frac{n\pi at}{2l} + \frac{n\pi a}{2l} D_{rn} \cos\frac{n\pi at}{2l}) \sin\frac{n\pi}{2l}[x - (L-l)]$$

$$= \sum_{n=1}^{\infty} \frac{n\pi a}{2l} D_{rn} \sin\frac{n\pi}{2l}[x - (L-l)] = C_p - \frac{\rho_p}{\rho_e}(C_p - v_p)$$

$$\Rightarrow \quad D_{rn} = \frac{4[C_p - \frac{\rho_p}{\rho_e}(C_p - v_p)]}{n\pi a} \int_{L-l}^{L} \sin\frac{n\pi[x - (L-l)]}{2l} dx\,;$$

$$= \frac{8l[C_p - \frac{\rho_p}{\rho_e}(C_p - v_p)]}{n^2\pi^2 a}(1 - \cos\frac{n\pi}{2}) \qquad \text{(I-25)}$$

$$\frac{\partial u_{er}(x,0)}{\partial x} = \sum_{n=1}^{\infty}(C_{rn}\cos\frac{n\pi at}{2l} + D_{rn}\sin\frac{n\pi at}{2l})\frac{n\pi}{2l}\cos\frac{n\pi}{2l}[x-(L-l)]$$

$$= \sum_{n=1}^{\infty} C_{rn}\frac{n\pi}{2l}\cos\frac{n\pi}{2l}x = \frac{\sigma - \rho_e(C_p - v_e)(v_p - v_e)}{E}$$

$$\Rightarrow \qquad C_{rn} = \frac{4}{n\pi E}[\sigma - \rho_e(C_p - v_e)(v_p - v_e)]\int_{L-l}^{L}\cos\frac{n\pi[x-(L-l)]}{2l}dx$$

$$C_{rn} = \frac{8l}{n^2\pi^2 E}[\sigma - \rho_e(C_p - v_e)(v_p - v_e)]\sin\frac{n\pi}{2} \qquad \text{(I-26)}$$

Now assume that $\rho_p = \rho_e$ and $v_e = 0$, then

$$C_{rn} = \frac{8l}{n^2\pi^2 E}(\sigma - \rho_e C_p v_p)\sin\frac{n\pi}{2} \qquad \text{(I-27)}$$

$$D_{rn} = \frac{8lv_p}{n^2\pi^2 a}(1 - \cos\frac{n\pi}{2}) \qquad \text{(I-28)}$$

The solution of the reflective elastic wave can be written as

$$u_{er}(x,t) = \sum_{n=1}^{\infty}(C_{rn}\cos\frac{n\pi at}{2l} + D_{rn}\sin\frac{n\pi at}{2l})\sin\frac{n\pi}{2l}[x-(L-l)] \qquad \text{(I-29)}$$

From Equation (I-29), the strain, the stress and the velocity of the particle can be obtained:

Strain:

$$\varepsilon_{er} = \frac{\partial u_{er}(x,t)}{\partial x} = \sum_{n=1}^{\infty}\frac{n\pi}{2l}(C_{rn}\cos\frac{n\pi at}{2l} + D_{rn}\sin\frac{n\pi at}{2l})\cos\frac{n\pi}{2l}[x-(L-l)]$$

Stress:

$$\sigma_{er} = E \sum_{n=1}^{\infty} \frac{n\pi}{2l}(C_{rn}\cos\frac{n\pi at}{2l} + D_{rn}\sin\frac{n\pi at}{2l})\cos\frac{n\pi}{2l}[x-(L-l)]$$

The velocity of the particle:

$$v_{er} = \sum_{n=1}^{\infty} \frac{n\pi a}{2l}(-C_{rn}\sin\frac{n\pi at}{2l} + D_{rn}\cos\frac{n\pi at}{2l})\sin\frac{n\pi}{2l}[x-(L-l)]$$

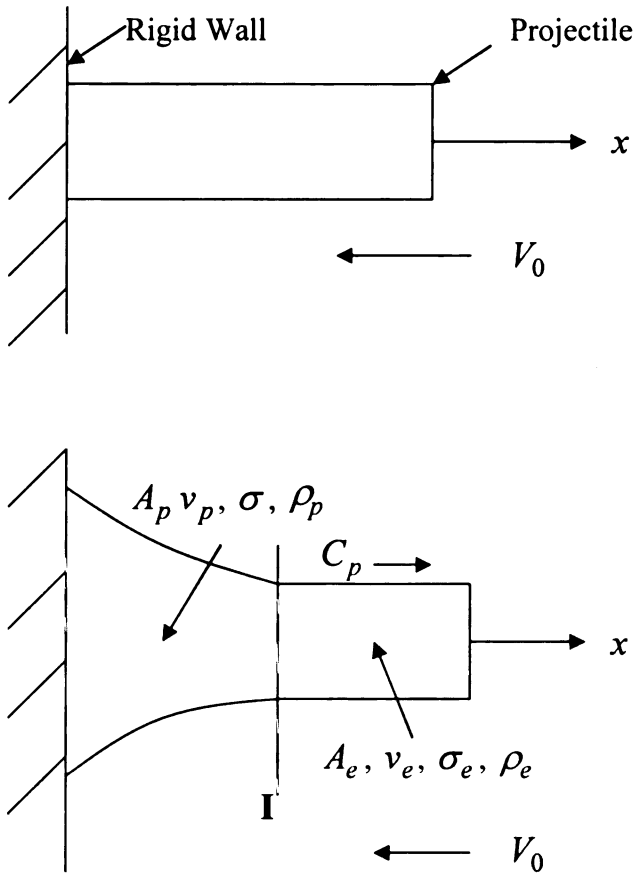

Figure I-1

Appendix J

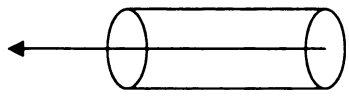

The volume of the element can be written as

$$V = \pi r^2 x$$

Take derivative for both sides of the above equation, then

$$dV = 2x\pi r dr + \pi r^2 dx$$

Consider the incomprehensibility of plasticity, it gives

$$dV = 2x\pi r dr + \pi r^2 dx = 0$$

$$\Rightarrow \quad 2x\pi r dr + \pi r^2 dx = 0$$

$$\Rightarrow \quad \frac{2x\pi r dr}{\pi r^2 x} + \frac{\pi r^2 dx}{\pi r^2 x} = 0$$

$$\Rightarrow \quad \frac{2dr}{r} + \frac{dx}{x} = 0$$

$$\Rightarrow \quad 2\varepsilon_r + \varepsilon_x = 0$$

$$\Rightarrow \quad d\varepsilon_r = -\frac{1}{2} d\varepsilon_x$$

$$\because \quad d\varepsilon_r + d\varepsilon_x + d\varepsilon_\theta = 0$$

$$d\varepsilon_r - 2\varepsilon_r + d\varepsilon_\theta = 0$$

$$\therefore \quad -d\varepsilon_r + d\varepsilon_\theta = 0$$

$$\therefore \quad d\varepsilon_r = d\varepsilon_\theta$$

Appendix K Other Models' Shape Curve

Name	Model	$\frac{\partial\sigma}{\partial\varepsilon}$	$\frac{\partial\sigma}{\partial\dot{\varepsilon}}$	Material	Constants	Shape of Projectile
Hartig	$\sigma = \frac{E}{b}(1-e^{-b\varepsilon})$	$Ee^{-b\varepsilon}$	0	X	$b > 0$	Concave
Logarithmic Law	$\sigma = \sigma_1(\varepsilon) + k\ln\dot{\varepsilon}$	$\frac{\partial\sigma_1}{\partial\varepsilon}$	$\frac{k}{\dot{\varepsilon}}$	X	X	Undefined
Power Law	$\sigma = \sigma_1(\varepsilon)\dot{\varepsilon}^n$	$\dot{\varepsilon}^n\frac{\partial\sigma_1}{\partial\varepsilon}$	$n\sigma_1\dot{\varepsilon}^{n-1}$	X	X	Undefined
Malvern Model $k = 10^6 1/s$	$\sigma = (20000 - \frac{10}{\varepsilon}) + 1000000\dot{\varepsilon}$	$\frac{\partial\sigma_1}{\partial\varepsilon}$	k	Alumi-num		Concave
Power Law Plasticity	$\sigma = k(\varepsilon_e + \varepsilon)^n$	$nk(\varepsilon_e+\varepsilon)^{n-1}$	0	Alumi-num 1100	$k = 0.598$, $n = 0.216$	Concave
Strain Rate Dependent Plasticity	$\sigma = E_p\varepsilon + \sigma_0(\dot{\varepsilon})$	$\frac{\partial E_p}{\partial\varepsilon}$	$\frac{\partial\sigma_0}{\partial\dot{\varepsilon}}$	4140 Steel	X	Straight Line
Johnson-Cook Model	$\sigma = (A + B\varepsilon^n)^* (1 + C\ln\dot{\varepsilon})$	$B\varepsilon^{n-1}(1+C\ln\dot{\varepsilon})$	$\frac{A+B\varepsilon^n}{\dot{\varepsilon}}$	X	X	Concave
Rate Sensitive Power Law Plasticity	$\sigma = k\varepsilon^m\dot{\varepsilon}^n$	$mk\dot{\varepsilon}^n\varepsilon^{m-1}$	$nk\varepsilon^m\dot{\varepsilon}^{n-}$	A356 Alumi-num	$k = 0.002$, $m = 0.7$, $n = 0.32$	Concave

Johnson – Cook Model

Material	A(MPa)	B(MPa)	C	n	Shape of Projectile
OFHC	89	292	0.0025	0.31	Concave
Catridge Brass	117	505	0.009	0.42	Concave
Nickle 200	163	648	0.006	0.33	Concave
Armco Iron	175	380	0.06	0.32	Concave
Carpenter Elertrc Iron	290	336	0.055	0.4	Concave
1006 Steel	350	275	0.022	0.36	Concave
2024-T351 Aluminum	265	426	0.015	0.34	Concave
7038 Aluminum	336	343	0.01	0.41	Concave
4340 Steel	792	510	0.014	0.26	Concave
S-7 Tool Steel	154	476	0.012	0.18	Concave
Tungsten	1056	176	0.016	0.12	Concave
Depleted Uranium	1079	1119	0.007	0.25	Concave
Tantalum	140	300	X	0.3	Concave

Appendix L Computations of Dynamic Yielding Stress, Plastic Wave Velocity and Taylor Formula Computation Results

I. Computations of Dynamic Yielding Stress

Consider that a cylindrical projectile with length L and radius r_0 impacts a rigid wall at a constant velocity V_0, shown in Figure 1,Figure 2 and Figure 3.

Plastic Region:

a. First Phase: In this phase, the density is ρ_{p1}. **The shape of the projectile is concave** in transverse direction after impact. Before impact, the length is h. After impact, the length is h_d. The plastic dispersive wave would be inaugurated at $x = h$.

b. Second Phase: In this phase, the density is ρ. **The shape of the projectile is convex** in transverse direction after impact. Physically, that is the so-called shape of a mushroom. Before impact, the length is $L - L_e - h$. After impact, the length is L_p.

Elastic Region:

c. Third Phase: In this phase, the elastic wave oscillates and disappears after impact as friction in the material. The density is ρ_e. Before impact, the length is L_e. After impact, the length is still L_e. The shape of the projectile remains a straight line.

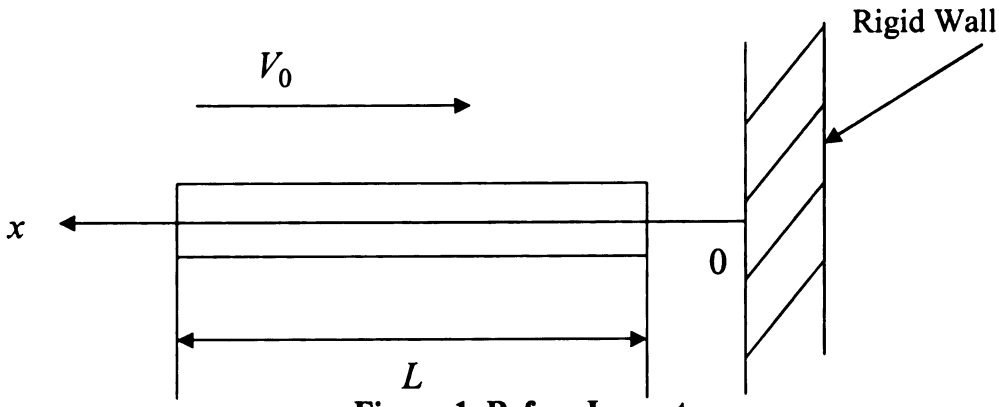

Figure 1 Before Impact

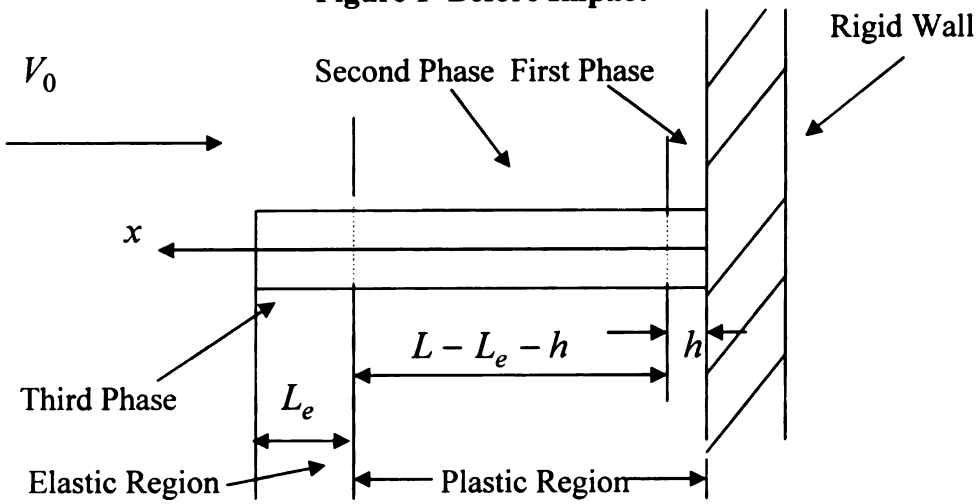

Figure 2 At the Moment of Impact

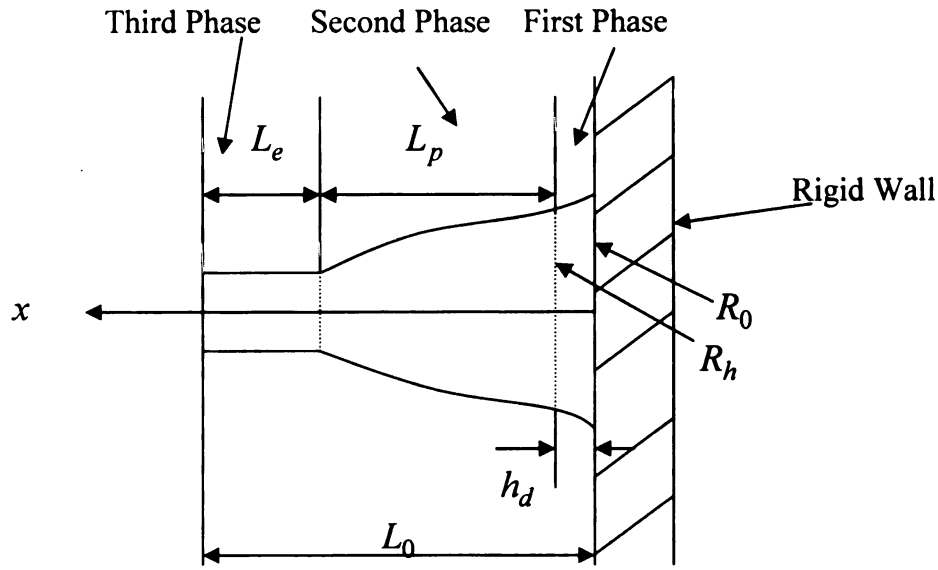

Figure 3 After Impact

1. Computation Steps

1.1 V_0, E, ρ, L should be known.

V_0----- Impact Velocity; ρ---- Density of Material; E --- Young Modulus; L --- The Length of Projectile Before Impact.

1.2 Measure $L_0, L_e, h_d, 2R_h$ and $2R_0$ very precisely.

L_0 ----- The Length of Projectile After Impact; L_e---- The Length of the Third Phase;

h_d---- The Length of the First Phase After Impact; $2R_h$----- The Small End Diameter of the First Phase After Impact; $2R_0$---- The large End Diameter of the First Phase After Impact.

1.3 Calculating h from h_d:

$$h = -\frac{2\ln\frac{R_h}{R_0}}{\ln[1-\frac{2r_0^2}{R_0^2}\ln(\frac{R_h}{R_0})]}h_d$$

h---- The Length of the First Phase Before Impact.

1.4 t_h can be calculated as follows:

$$t_h = \frac{h}{V_0}$$

t_h ---- The Time of Plastic Wave Propagation in the First Phase.

1.5 t_p can be calculated as follows

$$t_p = \frac{L + L_e}{\sqrt{\frac{E}{\rho}}}$$

t_p ---- The Time of Plastic Wave Propagation in the Second Phase.

1.6 Using the following matrix to find C_1, C_2, C_3:

$$\begin{bmatrix} h & h(\ln\frac{h}{t_h} - 1) & t_h \\ 0 & -\frac{h}{t_h} & 1 \\ L - L_e & (L - L_e)(\ln\frac{L - L_e}{t_p} - 1) & t_p \end{bmatrix} \begin{bmatrix} C_1 \\ C_2 \\ C_3 \end{bmatrix} = \begin{bmatrix} h_d \\ V_0 \\ (L - L_0) - (h - h_d) \end{bmatrix}$$

1.7 The dynamic yielding strength of the material can be obtained:

$$\sigma = \frac{\rho C_2}{2} e^{\frac{2|C_1|}{C_2}}$$

See Explanation of Dynamic Model in Figure 5.

2. Example Aluminum 6061-T6511

Density: ρ=2700 kg/m^3
Static Yield Stress: $\sigma_s = 275MPa$
Young Modulus: $E = 69 \times 10^9 N/m^2$
Elastic Wave Velocity: $C_e = 5055m/s$
Impact Velocity: $V_0 = 93m/s$
Original Length: $L = 7.8232cm$
Final Length: $L_0 = 7.512cm$
$L_p = 3.4282cm$
$L_e = 4.12cm$
Projectile Diameter: $D_1 = 1.22936cm$
Measured $h = 0.275cm$, Computed $h = 0.299cm$
$h_d = 0.2565cm$
$2R_h = 1.3195cm$
$2R_0 = .1335cm$
$\Delta L = (L - L_0) - (h - h_d) = 0.927cm$
$t_p = (L + L_e)/C_e = 23.63 \times 10^{-6} s$
$t_h = h/V_0 = 29.55 \times 10^{-6} s$

1. $h = 0.26cm$

$$h(\ln V_0 - 1) = -1.476cm$$

$$t_h = \frac{h}{V_0} = \frac{0.26}{0.0093} = 27.9\mu\sec$$

$$L - L_e = 3.7032cm$$

$$t_p = 23.63\mu s$$

$$(L - L_e)[\ln(\frac{L - L_e}{t_p} - 1)] = -10.56cm$$

$$(L - L_0) - (h - h_d) = 0.5447 - 0.26 = 0.2847cm$$

$$\begin{bmatrix} 0.26 & -1.476 & 27.95 \\ 0 & -0.0093 & 1 \\ 3.7032 & -10.56 & 23.63 \end{bmatrix} \begin{bmatrix} C_1 \\ C_2 \\ C_3 \end{bmatrix} = \begin{bmatrix} 0.2565 \\ 0.0093 \\ 0.2847 \end{bmatrix}$$

$$C_1 = 0.0631,\ C_2 = 0.0163,\ C_3 = 0.0095 cm/\mu s$$

Dynamic Yielding Stress σ:

$$\sigma = \frac{2700 \times 0.0163}{2} e^{\frac{2\times(0.0631)}{0.0163}} \times 10^4 = 499 Mpa$$

2. $h = 0.265 cm$

$$h(\ln V_0 - 1) = -1.505 cm/\mu\sec$$

$$t_h = \frac{h}{V_0} = 28.49 \mu\sec$$

$$L - L_e = 3.7032 cm$$

$$t_p = 23.63 \mu s$$

$$(L - L_e)[\ln(\frac{L - L_e}{t_p} - 1)] = -10.56 cm$$

$$(L - L_0) - (h - h_d) = 0.5447 - 0.265 = 0.2797 cm$$

$$\begin{bmatrix} 0.265 & -1.505 & 28.49 \\ 0 & -0.0093 & 1 \\ 3.7032 & -10.56 & 23.63 \end{bmatrix} \begin{bmatrix} C_1 \\ C_2 \\ C_3 \end{bmatrix} = \begin{bmatrix} 0.2565 \\ 0.0093 \\ 0.2797 \end{bmatrix}$$

$$C_1 = 0.0874,\ C_2 = 0.0255,\ C_3 = 0.0095 cm/\mu s$$

Dynamic Yielding Stress σ:

$$\sigma = \frac{2700 \times 0.0255}{2} e^{\frac{2\times(0.0874)}{0.0255}} \times 10^4 = 326 Mpa$$

3. $h = 0.27cm$

$h(\ln V_0 - 1) = -1.533cm/\mu\sec$

$t_h = \frac{h}{V_0} = 29.03\mu\sec$

$L - L_e = 3.7032cm$

$t_p = 23.63\mu s$

$(L - L_e)[\ln(\frac{L - L_e}{t_p} - 1)] = -10.56cm$

$(L - L_0) - (h - h_d) = 0.5447 - 0.27 = 0.2747cm$

$$\begin{bmatrix} 0.27 & -1.533 & 29.03 \\ 0 & -0.0093 & 1 \\ 3.7032 & -10.56 & 23.63 \end{bmatrix} \begin{bmatrix} C_1 \\ C_2 \\ C_3 \end{bmatrix} = \begin{bmatrix} 0.2565 \\ 0.0093 \\ 0.2747 \end{bmatrix}$$

$C_1 = 0.1107,\ C_2 = 0.0343,\ C_3 = 0.0096cm/\mu s$

Dynamic Yielding Stress σ:

$$\sigma = \frac{2700 \times 0.0343}{2} e^{\frac{2\times(0.1107)}{0.0343}} \times 10^4 = 294Mpa$$

4. $h = 0.275cm$

$h(\ln V_0 - 1) = -1.5613cm/\mu\sec$

$t_h = \frac{h}{V_0} = 29.56\mu\sec$

$L - L_e = 3.7032cm$

$t_p = 23.63\mu s$

$(L - L_e)[\ln(\frac{L - L_e}{t_p} - 1)] = -10.56cm$

$(L - L_0) - (h - h_d) = 0.5447 - 0.275 = 0.269cm$

$$\begin{bmatrix} 0.275 & -1.5613 & 29.56 \\ 0 & -0.0093 & 1 \\ 3.7032 & -10.56 & 23.63 \end{bmatrix} \begin{bmatrix} C_1 \\ C_2 \\ C_3 \end{bmatrix} = \begin{bmatrix} 0.2565 \\ 0.0093 \\ 0.269 \end{bmatrix}$$

$C_1 = 0.1321,\ C_2 = 0.0426,\ C_3 = 0.00101 cm/\mu s$

Dynamic Yielding Stress σ:

$$\sigma = \frac{2700 \times 0.0426}{2} e^{\frac{2\times(0.1321)}{0.0426}} \times 10^4 = 283 Mpa$$

5. $h = 0.28cm$

$h(\ln V_0 - 1) = -1.589 cm/\mu\sec$

$t_h = \frac{h}{V_0} = 30.101\mu\sec$

$L - L_e = 3.7032 cm$

$t_p = 23.63\mu s$

$(L - L_e)[\ln(\frac{L - L_e}{t_p} - 1)] = -10.56 cm$

$(L - L_0) - (h - h_d) = 0.5447 - 0.28 = 0.2647 cm$

$$\begin{bmatrix} 0.28 & -1.589 & 30.101 \\ 0 & -0.0093 & 1 \\ 3.7032 & -10.56 & 23.63 \end{bmatrix} \begin{bmatrix} C_1 \\ C_2 \\ C_3 \end{bmatrix} = \begin{bmatrix} 0.2565 \\ 0.0093 \\ 0.2647 \end{bmatrix}$$

$C_1 = 0.1543,\ C_2 = 0.0509,\ C_3 = 0.0098 cm/\mu s$

Dynamic Yielding Stress σ:

$$\sigma = \frac{2700 \times 0.0509}{2} e^{\frac{2\times(0.1543)}{0.0509}} \times 10^4 = 295 Mpa$$

6. $h = 0.29cm$

$h(\ln V_0 - 1) = -1.6465cm/\mu\sec$

$t_h = \frac{h}{V_0} = 31.182\mu\sec$

$L - L_e = 3.7032cm$

$t_p = 23.63\mu s$

$(L - L_e)[\ln(\frac{L - L_e}{t_p} - 1)] = -10.56cm$

$(L - L_0) - (h - h_d) = 0.5447 - 0.29 = 0.2547cm$

$$\begin{bmatrix} 0.29 & -1.6465 & 31.182 \\ 0 & -0.0093 & 1 \\ 3.7032 & -10.56 & 23.63 \end{bmatrix} \begin{bmatrix} C_1 \\ C_2 \\ C_3 \end{bmatrix} = \begin{bmatrix} 0.2565 \\ 0.0093 \\ 0.2547 \end{bmatrix}$$

$C_1 = 0.1945,\ C_2 = 0.0663,\ C_3 = 0.0099cm/\mu s$

Dynamic Yielding Stress σ:

$$\sigma = \frac{2700 \times 0.0663}{2} e^{\frac{2\times(0.1945)}{0.0663}} \times 10^4 = 316Mpa$$

7. $h = 0.30cm$

$h(\ln V_0 - 1) = -1.703cm/\mu\sec$

$t_h = \frac{h}{V_0} = 32.25\mu\sec$

$L - L_e = 3.7032cm$

$t_p = 23.63\mu s$

$(L - L_e)[\ln(\frac{L - L_e}{t_p} - 1)] = -10.56cm$

$(L - L_0) - (h - h_d) = 0.5447 - 0.23 = 0.2447cm$

$$\begin{bmatrix} 0.30 & -1.703 & 32.25 \\ 0 & -0.0093 & 1 \\ 3.7032 & -10.56 & 23.63 \end{bmatrix} \begin{bmatrix} C_1 \\ C_2 \\ C_3 \end{bmatrix} = \begin{bmatrix} 0.2565 \\ 0.0093 \\ 0.2447 \end{bmatrix}$$

$C_1 = 0.2312,\ C_2 = 0.0804,\ C_3 = 0.0100 cm/\mu s$

Dynamic Yielding Stress σ:

$$\sigma = \frac{2700 \times 0.0804}{2} e^{\frac{2\times(0.2312)}{0.0804}} \times 10^4 = 341 Mpa$$

8. $h = 0.32cm$

$h(\ln V_0 - 1) = -1.8168 cm/\mu\sec$

$t_h = \frac{h}{V_0} = 34.41\mu\sec$

$L - L_e = 3.7032cm$

$t_p = 23.63\mu s$

$(L - L_e)[\ln(\frac{L - L_e}{t_p} - 1)] = -10.56cm$

$(L - L_0) - (h - h_d) = 0.5447 - 0.32 = 0.2247cm$

$$\begin{bmatrix} 0.32 & -1.8168 & 34.41 \\ 0 & -0.0093 & 1 \\ 3.7032 & -10.56 & 23.63 \end{bmatrix} \begin{bmatrix} C_1 \\ C_2 \\ C_3 \end{bmatrix} = \begin{bmatrix} 0.2565 \\ 0.0093 \\ 0.2247 \end{bmatrix}$$

$C_1 = 0.2973,\ C_2 = 0.1060,\ C_3 = 0.0103 cm/\mu s$

Dynamic Yielding Stress σ:

$$\sigma = \frac{2700 \times 0.1060}{2} e^{\frac{2\times(0.2973)}{0.1060}} \times 10^4 = 390 Mpa$$

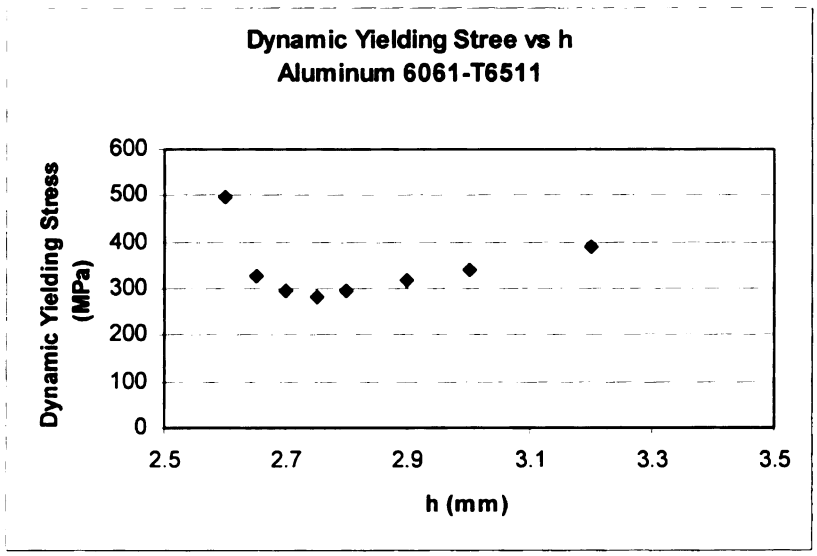
Dynamic Yielding Stree vs h
Aluminum 6061-T6511
Dynamic Yielding Stress (MPa)
600
500
400
300
200
100
0
2.5
2.7
2.9
3.1
3.3
3.5
h (mm)

Figure 4

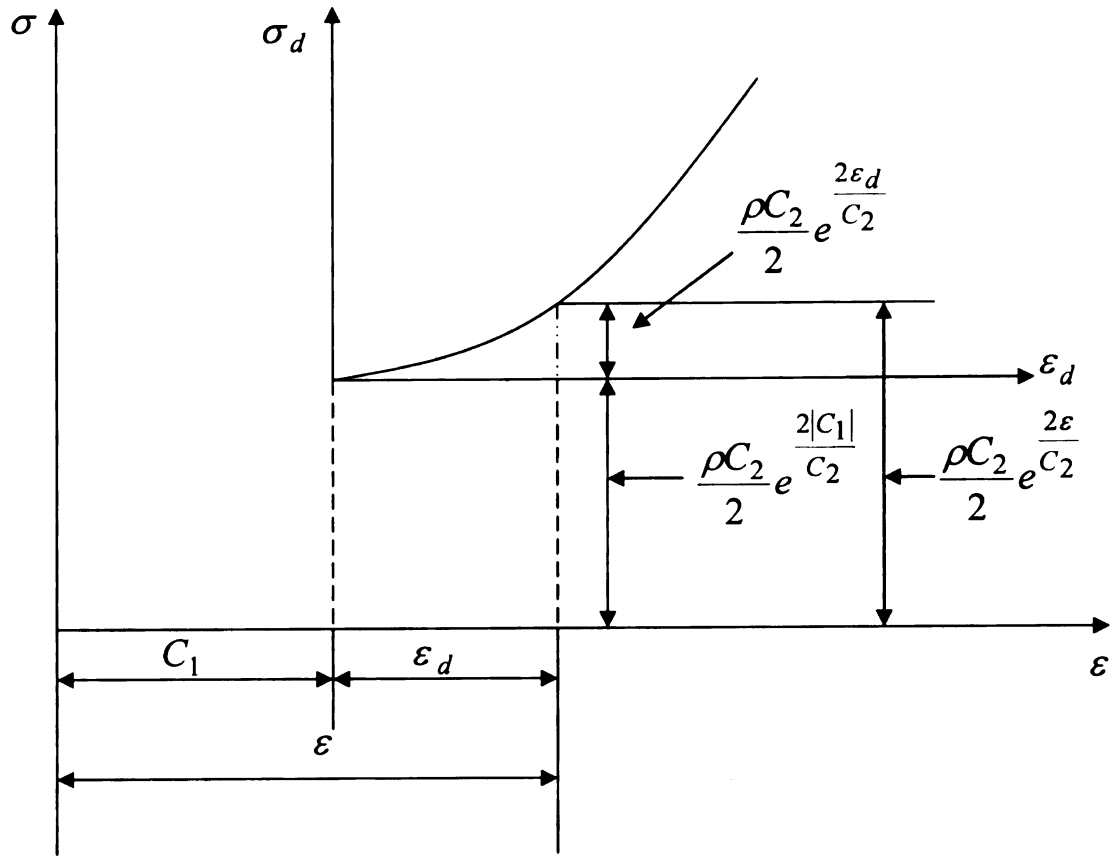

Figure 5 Explanation of Dynamic Model

Dynamic Stress Computation:

$$\sigma = \frac{\rho C_2}{2} e^{\frac{2(\varepsilon - C_1)}{C_2}} = \frac{\rho C_2}{2} e^{\frac{2\varepsilon_d}{C_2}}$$

Dynamic Yielding Stress:

$$\sigma = \frac{\rho C_2}{2} e^{\frac{2|C_1|}{C_2}}$$

ε_d is measured strain.

II. **Computations of Plastic Wave Velocity**

Plastic Wave Velocity:

$$C_p = e^{\frac{(\varepsilon - C_1)}{C_2}}$$

$$\Rightarrow \quad C_p = e^{\frac{\varepsilon}{C_2} - \frac{C_1}{C_2}} = \frac{e^{\frac{\varepsilon}{C_2}}}{e^{\frac{C_1}{C_2}}}$$

$$\Rightarrow \quad e^{\frac{C_1}{C_2}} \times C_p = e^{\frac{\varepsilon}{C_2}}$$

$$\because \quad \varepsilon = \varepsilon_d + C_1$$

$$\therefore \quad e^{\frac{C_1}{C_2}} \times C_p = e^{\frac{\varepsilon_d + C_1}{C_2}}$$

$$\Rightarrow \quad C_p = e^{\frac{\varepsilon_d}{C_2}}$$

If $\varepsilon_d = 0$, then $C_p(\varepsilon_d = 0) = 1$

If $\varepsilon = 0$, then $C_p(\varepsilon = 0) = e^{-\frac{C_1}{C_2}}$

$$\because \quad \frac{C_p(\varepsilon_d = 0)}{C_p(\varepsilon = 0)} = \frac{e^{\frac{\varepsilon_d}{C_2}}}{e^{\frac{\varepsilon - C_1}{C_2}}}$$

$$\therefore \quad e^{\frac{\varepsilon - C_1}{C_2}} = \frac{e^{\frac{\varepsilon_d}{C_2}} \times C_p(\varepsilon = 0)}{C_p(\varepsilon_d = 0)} = \frac{e^{\frac{\varepsilon_d}{C_2}} \times e^{-\frac{C_1}{C_2}}}{1} = e^{\frac{\varepsilon_d - C_1}{C_2}}$$

III. **Taylor Formula Computation Results**

$$\sigma_d = \frac{\rho V_0^2 (L - L_e)}{2(L - L_0)\ln(\frac{L}{L_e})}$$

Gong Song's Calculated Results

Material	Static Yield Stress(MPa)	Computed Dynamic Yielding Stress (MPa)	Discrepancies
Aluminum 6061-T6511	275	283	3.24%
Copper 145-Hard-H02	32	33	3.125%
Steel C1045	585	604	3.25%

Taylor's Calculated Results

Material	Static Yield Stress(MPa)	Computed Dynamic Yielding Stress (MPa)	Discrepancies
Aluminum 6061-T6511	275	225	-18%
Copper 145-Hard-H02	32	1099	3200%
Steel C1045	585	628	7.3%

Bibliography

1. L. H. Donnell, " Longitudinal Wave Transmission and Impact " Trans. ASME, Vol.52, 1930, pp. 153 – 167.

2. T. von Karman and P. Duwez, " The Propagation of Plastic Deformation In Solids ", J.Appl. Physics, Vol.21, 1950, pp. 987 – 994.

3. G. I. Taylor, " The Plastic Wave In A Wire Extended By An Impact Load ". The Scientific Papers of Sir Geoffrey Taylor, Cambridge University Press, 1958, pp. 467 – 479.

4. J. Bell, MECHANICS OF SOLIDS, Volume I, " The Experimental Foundation of Solid Mechanics ", Springer _Verlag, 1984.

5. P. Duwez and D. S. Clark, " An Experiment Study of the Propagation of Plastic Deformation Under Condition of Longitudinal Impact ", Proc.Am.Soc.Test.Mat., Vol.47, 1949, pp. 502 – 532.

6. J. D. Campell, " An Investigation of the Plastic Behavior of Metal Rods Subjected to Longitudinal Impact ", Journal of the Mechanics and Physics of Solids, Vol.1, 1953, pp.113.

7. J. E. Johnson, D. S. Wood and D. S. Clark, " Dynamic Stress-Strain Relations for Annealed 2S Aluminum under Compression Impact ".

8. L.Efron, " Longitudinal Plastic Wave Propagation in Annealed Aluminum Bars ", main Library/ 107242 THS, Michigan State University.

9. V.V. Sokolovsky, " The Propagation of Elastic-Viscous-Plastic Waves In Bars ",

Prikl. Mat. i Mek., Vol. 12, pp. 261 – 286, 1948 (Russian). Translation All – T6, Brown University, 1949.

10. L. E. Malvern, " Plastic Wave Propagation In a Bar of Material Exhibiting a Strain Rate Effect", Quart. Appl. Math., Vol. 8, 1950, pp. 405 – 11.

11. J.F. Bell, " Diffraction Grating Strain Gauge ", Proc. SESA, Vol. 1, 1959, pp. 51-64.

12. J. F. Bell, " Propagation of Large Amplitude Waves in Annealed Aluminum ", J. Appl. Phys. Vol.31, No.1, 1960, pp. 277 – 282.

13. J. F. Bell, " Study of Initial Conditions in Constant Velocity Impact ", J. Appl. Phys., Vol. 31, No2, 1960, pp. 2188 – 2195.

14. H. Kolsky and L. S. Dough, " Experimental Studies in Plastic Wave Propagation ", J. Mech. Phys. Solids, Vol. 10, July/Sept. 1962, pp. 195 – 223.

15. U.S. Lindholm, " Some Experiments With the Split Hopkinson Pressure Bar ", Technical Report No.1, Contact No. DA-23-072-ORD-1674, Sw RI Project No. 02 – 1102, Southwest Research Institute, San Antonio, Texas, March 1964.

16. Malvern, L.E. (1965), in N.J.Huffington, Jr(Ed.), Behaviour of Materilas Under Dnamic Loading, ASME, New York, p.81.

17. W.J.Gillich and W.O.Ewing, " Mechanics of Solids ", Volume I, The Experimental Foundations of Solid Mechanics, pp. 630, Author: James Bell, 1984.

18. J. A. Simmons, F. Hauser and J.E. Dorn, " Mathematical Theories of Plastic Deformation Under Impulsive Loading ", University. Calif. Pub. Engng 5, 177 – 230 (1962).

19. J. Lubliner and M. Valathur, " Some Wave-Propagation Problems In Plastic-Viscoplastic Materials." Int.J. Solids Structure, 1969, Vol.5, pp.1275 – 1298, Pergamon Press. Printed In Great Britain.

20. J. Bell, " An Experimental Study of Instability Phenomena In the Initial of Plastic Waves In Long Rods." Symposium, Held in San Antonia, Texas, Septmber 6 – 8, 1967., Printed by Springer – Verlay New York Inc, 1968.

21. R. J. Clifton, " Plastic Waves: Theory and Experiment." in Nemeat- Nasser, 5., (ed), Mechanics Today, 1, Pergamon, New York.

22. R.J. Clifton, " Some recent Developments in Plate Impact Experiments." in Varley, E., (ed.), Propagation of Shock Waves in Solids, ASME, New York, 27 – 40. 2000.

23. C. H. Karnes, (1968) " The Plate Impact Configuration for Determining Mechanical properties of materials at High Strain rates." in Lindholm, U.S., (ed), Mechanical Behavior of material Under Dynamic Loads, Spring- Verlay, Berlin, 270 – 293.

24. L.D. Bertholf and C.H. Karnes, (1970) " Two-Dimensional Analysis of the Split Hopkinson Pressure Bar System." J. Mech.Phys. Solids, 23, 1.

25. J. A. Zukas, T. Nicholas, H.F. Swift, L. B. Greszczuk and D. R. Curran, " IMPACT DYNAMICS ", A Wiley-Interscience Publication, JOHN WILEY & SONS, 1982.

26. S.E. Jones, P.P. Gillis , J.C. Foster, JR., and L. L. Wilson, " A One Dimensional, Two-Phase Flow Model for Taylor Impact Specimens." Recent Advances In Impact Dynamics of Engineering Structures, ASME, AMD – Vol. 105, AD – Vol.17. 1989.

27. S.E. Jones, P.J. Maudlin and J.C. Foster, JR., " An Engineering Analysis of Plastic Wave Propagation in the Taylor Test." Int. J. Engng. Vol. 19, No.2, pp. 95-106,1997.

28. A.S. Khan and C. Hsiao, " Behavior of Fully Annealed and As-Received Polycrystalline 1100 Aluminum During Propagation of Small and large Amplitude Plastic Waves." International Journal of Plasticity, Vol.7, pp. 773 – 748, 1991.

29. P.J. Maudlin, J.C. Foster, JR., and S.E. Jones, " A Continuum Mechanics Code Analysis of Steady Plastic Wave Propagation in the Taylor Test." Int. J. Impact Engng Vol. 19, No.3.

30. T.W. Wright, " Axial Plastic Waves In A Rod." International Journal of Plasticity, 14: (1 – 3) 25 – 42, 1998.

31. A. Rusinek and Klepaczko JR., " A Numerical Study on the Wave Propagation in Tensile and Performance Test." Journal De Physique IV, 10: (p9) 653 – 658, Sept. 2000.

32. G.I.Taylor, " The testing of materials at high rates of loading" J.Inst.Civi Eng.26 (1946) 486-519.

33. G.I.Taylor, " The use of flat ended projectiles for determining yield stress. I: Theoretical considerations " Proc.R.Soc.Lond.A194 (1948) 289-299.

34. M.L.Wilkins and Michael W. Guinan, " Impact of Cylinders on a Rigid Boundary ", J.Appl.Phys., Vol.44, No.3, Marcg 1973.

35. Kuscher, G. (1985), " Nicht-lineare Ausbreitung elasto-plastischer Wellen in Staben," Ernst-Mach-Inst. (EMI), Berjcht 2/85, Freigurg, West germany. English see Reference [25].

36. William F.Ames, " Numerical Methods For partial Differential Equation", Academic Press, New York, 1997.

37. G.Thomas Mase and George.E.Mase, " CONTINUUM MECHANICS for ENGINEER", Secong Edition, CRC Press LLC, 1999.

38. R.C.Batra and J.B.Stenens, " Adiabatic Shear Banding in Axisymmetric Impact and Penetration Problems", Computer Methods in Applied Mechanics and Engineering, 151 3-4): 325 – 342, Jan 20, 1998.